Structural and Dynamic Studies Of Amino Acids, Proteins and Nucleic Acids By Chemical-Hyperspectral Imaging, FT-IR/NIR, Vibro-Rotational Spectroscopy, Plasma, Microwave and Neutron Spectroscopy

03/31/2012

I.C. Baianu

AFC-NMR & NIR Microspectroscopy Facility,
College of ACES, FSHN & NPRE Departments,
University of Illinois at Urbana,
Urbana, IL. 61801, USA
Email address: **ibaianu @illinois.edu**

Table of Contents

Spectroscopy

Spectroscopy was originally the study of the interaction between radiation and matter as a function of wavelength (λ). In fact, historically, spectroscopy referred to the use of visible light dispersed according to its wavelength, e.g. by a prism. Later the concept was expanded greatly to comprise any measurement of a quantity as function of either wavelength or frequency. Thus it also can refer to a response to an alternating field or varying frequency (ν). A further extension of the scope of the definition added energy (E) as a variable, once the very close relationship $E = h\nu$ for photons was realized (h is the Planck constant). A plot of the response as a function of wavelength—or more commonly frequency—is referred to as a spectrum; see also spectral linewidth.

Spectrometry is the spectroscopic technique used to assess the concentration or amount of a given species. In this case, the instrument that performs such measurements is a spectrometer or spectrograph.

Spectroscopy/spectrometry is often used in physical and analytical chemistry for the identification of substances through the spectrum emitted from or absorbed by them.

Spectroscopy/spectrometry is also heavily used in astronomy and remote sensing. Most large telescopes have spectrometers, which are used either to measure the chemical composition and physical properties of astronomical objects or to measure their velocities from the Doppler shift of their spectral lines.

Classification of methods

Nature of excitation measured

The type of spectroscopy depends on the physical quantity measured. Normally, the quantity that is measured is an intensity, either of energy absorbed or produced.

- Electromagnetic spectroscopy involves interactions of matter with electromagnetic radiation, such as light.
- Electron spectroscopy involves interactions with electron beams. Auger spectroscopy involves inducing the Auger effect with an electron beam. In this case the measurement typically involves the kinetic energy of the electron as variable.
- Acoustic spectroscopy involves the frequency of sound.
- Dielectric spectroscopy involves the frequency of an external electrical field
- Mechanical spectroscopy involves the frequency of an external mechanical stress, e.g. a torsion applied to a piece of material.

Measurement process

Most spectroscopic methods are differentiated as either atomic or molecular based on whether or not they apply to atoms or molecules. Along with that distinction, they can be classified on the nature of their interaction:

- Absorption spectroscopy uses the range of the electromagnetic spectra in which a substance absorbs. This includes atomic absorption spectroscopy and various molecular techniques, such as → infrared, ultraviolet-visible and → microwave spectroscopy.
- Emission spectroscopy uses the range of electromagnetic spectra in which a substance radiates (emits). The substance first must absorb energy. This energy can be from a variety of sources, which determines the name of the subsequent emission, like luminescence. Molecular luminescence techniques include spectrofluorimetry.

• Scattering spectroscopy measures the amount of light that a substance scatters at certain wavelengths, incident angles, and polarization angles. One of the most useful applications of light scattering spectroscopy is → Raman spectroscopy.

Common types

Absorption

Absorption spectroscopy is a technique in which the power of a beam of light measured before and after interaction with a sample is compared. Specific absorption techniques tend to be referred to by the wavelength of radiation measured such as ultraviolet, infrared or microwave absorption spectroscopy. Absorption occurs when the energy of the photons matches the energy difference between two states of the material.

Fluorescence

Fluorescence spectroscopy uses higher energy photons to excite a sample, which will then emit lower energy photons. This technique has become popular for its biochemical and medical applications, and can be used for confocal microscopy, fluorescence resonance energy transfer, and fluorescence lifetime imaging.

Spectrum of light from a fluorescent lamp showing prominent mercury peaks

X-ray

When X-rays of sufficient frequency (energy) interact with a substance, inner shell electrons in the atom are excited to outer empty orbitals, or they may be removed completely, ionizing the atom. The inner shell "hole" will then be filled by electrons from outer orbitals. The energy available in this de-excitation process is emitted as radiation (fluorescence) or will remove other less-bound electrons from the atom (Auger effect). The absorption or emission frequencies (energies) are characteristic of the specific atom. In addition, for a specific atom small frequency (energy) variations occur which are characteristic of the chemical bonding. With a suitable apparatus, these characteristic X-ray frequencies or Auger electron energies can be measured. X-ray absorption and emission spectroscopy is used in chemistry and material sciences to determine elemental composition and chemical bonding.

X-ray crystallography is a scattering process; crystalline materials scatter X-rays at well-defined angles. If the wavelength of the incident X-rays is known, this allows calculation of the distances between planes of atoms within the crystal. The intensities of the scattered X-rays give information about the atomic positions and allow the arrangement of the atoms within the crystal structure to be calculated.
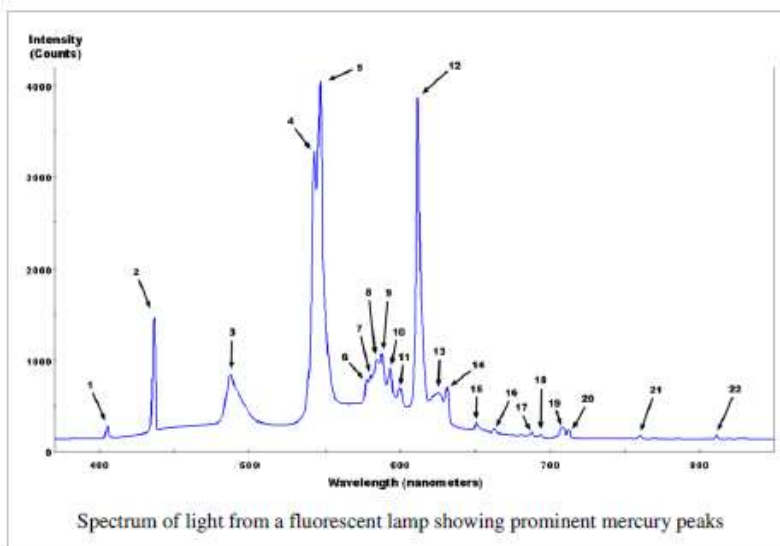
Flame

Liquid solution samples are aspirated into a burner or nebulizer/burner combination, desolvated, atomized, and sometimes excited to a higher energy electronic state. The use of a flame during analysis requires fuel and oxidant, typically in the form of gases. Common fuel gases used are acetylene (ethyne) or hydrogen. Common oxidant gases used are oxygen, air, or nitrous oxide. These methods are often capable of analyzing metallic element analytes in the part per million, billion, or possibly lower concentration ranges. Light detectors are needed to detect light with the analysis information coming from the flame.

- **Atomic Emission Spectroscopy** - This method uses flame excitation; atoms are excited from the heat of the flame to emit light. This method commonly uses a total consumption burner with a round burning outlet. A higher temperature flame than atomic absorption spectroscopy (AA) is typically used to produce excitation of analyte atoms. Since analyte atoms are excited by the heat of the flame, no special elemental lamps to shine into the flame are needed. A high resolution polychromator can be used to produce an emission intensity vs. wavelength spectrum over a range of wavelengths showing multiple element excitation lines, meaning multiple elements can be detected in one run. Alternatively, a monochromator can be set at one wavelength to concentrate on analysis of a single element at a certain emission line. Plasma emission spectroscopy is a more modern version of this method. See Flame emission spectroscopy for more details.
- **Atomic absorption spectroscopy** (often called AA) - This method commonly uses a pre-burner nebulizer (or nebulizing chamber) to create a sample mist and a slot-shaped burner which gives a longer pathlength flame. The temperature of the flame is low enough that the flame itself does not excite sample atoms from their ground state. The nebulizer and flame are used to desolvate and atomize the sample, but the excitation of the analyte atoms is done by the use of lamps shining through the flame at various wavelengths for each type of analyte. In AA, the amount of light absorbed after going through the flame determines the amount of analyte in the sample. A graphite furnace for heating the sample to desolvate and atomize is commonly used for greater sensitivity. The graphite furnace method can also analyze some solid or slurry samples. Because of its good sensitivity and selectivity, it is still a commonly used method of analysis for certain trace elements in aqueous (and other liquid) samples.
- **Atomic Fluorescence Spectroscopy** - This method commonly uses a burner with a round burning outlet. The flame is used to solvate and atomize the sample, but a lamp shines light at a specific wavelength into the flame to excite the analyte atoms in the flame. The atoms of certain elements can then fluoresce emitting light in a different direction. The intensity of this fluorescing light is used for quantifying the amount of analyte element in the sample. A graphite furnace can also be used for atomic fluorescence spectroscopy. This method is not as commonly used as atomic absorption or plasma emission spectroscopy.

Plasma Emission Spectroscopy In some ways similar to flame atomic emission spectroscopy, it has largely replaced it.

- Direct-current plasma (DCP)

A direct-current plasma (DCP) is created by an electrical discharge between two electrodes. A plasma support gas is necessary, and Ar is common. Samples can be deposited on one of the electrodes, or if conducting can make up one electrode.

- Glow discharge-optical emission spectrometry (GD-OES)
- Inductively coupled plasma-atomic emission spectrometry (ICP-AES)
- Laser Induced Breakdown Spectroscopy (LIBS) (LIBS), also called Laser-induced plasma spectrometry (LIPS)
- Microwave-induced plasma (MIP)

Spark or arc (emission) spectroscopy - is used for the analysis of metallic elements in solid samples. For non-conductive materials, a sample is ground with graphite powder to make it conductive. In traditional arc spectroscopy methods, a sample of the solid was commonly ground up and destroyed during analysis. An electric arc or spark is passed through the sample, heating the sample to a high temperature to excite the atoms in it. The excited analyte atoms glow emitting light at various wavelengths which could be detected by common spectroscopic methods. Since the conditions producing the arc emission typically are not controlled quantitatively, the analysis for the elements is qualitative. Nowadays, the spark sources with controlled discharges under an argon atmosphere allow that this method can be considered eminently quantitative, and its use is widely expanded worldwide through production control laboratories of foundries and steel mills.

Visible

Many atoms emit or absorb visible light. In order to obtain a fine line spectrum, the atoms must be in a gas phase. This means that the substance has to be vaporised. The spectrum is studied in absorption or emission. Visible absorption spectroscopy is often combined with UV absorption spectroscopy in UV/Vis spectroscopy. Although this form may be uncommon as the human eye is a similar indicator, it still proves useful when distinguishing colours.

Ultraviolet

All atoms absorb in the Ultraviolet (UV) region because these photons are energetic enough to excite outer electrons. If the frequency is high enough, photoionization takes place. UV spectroscopy is also used in quantifying protein and DNA concentration as well as the ratio of protein to DNA concentration in a solution. Several amino acids usually found in protein, such as tryptophan, absorb light in the 280 nm range and DNA absorbs light in the 260 nm range. For this reason, the ratio of 260/280 nm absorbance is a good general indicator of the relative purity of a solution in terms of these two macromolecules. Reasonable estimates of protein or DNA concentration can also be made this way using Beer's law.

Infrared

Infrared spectroscopy offers the possibility to measure different types of inter atomic bond vibrations at different frequencies. Especially in organic chemistry the analysis of IR absorption spectra shows what type of bonds are present in the sample. It is also an important method for analysing polymers and constituents like fillers, pigments and plasticizers.

Near Infrared (NIR)

The near infrared NIR range, immediately beyond the visible wavelength range, is especially important for practical applications because of the much greater penetration depth of NIR radiation into the sample than in the case of mid IR spectroscopy range. This allows also large samples to be measured in each scan by → NIR spectroscopy, and is currently employed for many practical applications such as: rapid grain analysis, medical diagnosis pharmaceuticals/medicines[1] , biotechnology, genomics analysis, proteomic analysis, interactomics research, inline textile monitoring, food analysis and → chemical imaging/hyperspectral imaging of intact organisms[2] [3] [4] , plastics, textiles, insect detection, forensic lab application, crime detection, various military applications, and so on.

Raman

Raman spectroscopy uses the inelastic scattering of light to analyse vibrational and rotational modes of molecules. The resulting 'fingerprints' are an aid to analysis.

Coherent anti-Stokes Raman spectroscopy (CARS)

CARS is a recent technique that has high sensitivity and powerful applications for *in vivo* spectroscopy and imaging[5] .

Nuclear magnetic resonance

Nuclear magnetic resonance spectroscopy analyzes the magnetic properties of certain atomic nuclei to determine different electronic local environments of hydrogen, carbon, or other atoms in an organic compound or other compound. This is used to help determine the structure of the compound.

Mössbauer

Transmission or conversion-electron (CEMS) modes of Mössbauer spectroscopy probe the properties of specific isotope nuclei in different atomic environments by analyzing the resonant absorption of characteristic energy gamma-rays known as the Mössbauer effect.

Other types

There are many different types of materials analysis techniques under the broad heading of "spectroscopy", utilizing a wide variety of different approaches to probing material properties, such as absorbance, reflection, emission, scattering, thermal conductivity, and refractive index.

- Acoustic spectroscopy
- Auger Spectroscopy is a method used to study surfaces of materials on a micro-scale. It is often used in connection with electron microscopy.
- Cavity ring down spectroscopy
- Circular Dichroism spectroscopy
- Deep-level transient spectroscopy measures concentration and analyzes parameters of electrically active defects in semiconducting materials
- Dielectric spectroscopy
- Dual polarisation interferometry measures the real and imaginary components of the complex refractive index
- Force spectroscopy
- → Fourier transform spectroscopy is an efficient method for processing spectra data obtained using interferometers. Nearly all infrared spectroscopy techniques (such as FTIR) and nuclear magnetic resonance (NMR) are based on Fourier transforms.
- Fourier transform infrared spectroscopy (FTIR)
- Hadron spectroscopy studies the energy/mass spectrum of hadrons according to spin, parity, and other particle properties. Baryon spectroscopy and meson spectroscopy are both types of hadron spectroscopy.
- Inelastic electron tunnelling spectroscopy (IETS) uses the changes in current due to inelastic electron-vibration interaction at specific energies which can also measure optically forbidden transitions.
- → Inelastic neutron scattering is similar to Raman spectroscopy, but uses neutrons instead of photons.
- Laser spectroscopy uses lasers[6] and other types of coherent emission sources, such as optical parametric oscillators,[7] for selective excitation of atomic or molecular species.
  - Ultra fast laser spectroscopy
- Mechanical spectroscopy involves interactions with macroscopic vibrations, such as phonons. An example is acoustic spectroscopy, involving sound waves.
- → Neutron spin echo spectroscopy measures internal dynamics in proteins and other soft matter systems
- Nuclear magnetic resonance (NMR)
- Photoacoustic spectroscopy measures the sound waves produced upon the absorption of radiation.
- Photothermal spectroscopy measures heat evolved upon absorption of radiation.
- Raman optical activity spectroscopy exploits Raman scattering and optical activity effects to reveal detailed information on chiral centers in molecules.
- Terahertz spectroscopy uses wavelengths above infrared spectroscopy and below microwave or millimeter wave measurements.

Related Topics:

- Absorption cross section
- Astronomical spectroscopy
- Atomic spectroscopy
- Nuclear magnetic resonance
- → 2D-FT NMRI and Spectroscopy
- → Near infrared spectroscopy
- Coherent spectroscopy
- Cold vapour atomic fluorescence spectroscopy
- Deep-level transient spectroscopy
- EPR spectroscopy
- Gamma spectroscopy
- Kelvin probe force microscope
- Metamerism (color)
- Rigid rotor
- Rotational spectroscopy
- Saturated spectroscopy
- Scanning tunneling spectroscopy
- Scattering theory
- Spectral power distributions
- Spectral reflectance
- Spectrophotometry
- Spectroscopic notation
- Spectrum analysis
- The Unscrambler (CAMO Software)
- Vibrational spectroscopy
- → Vibrational circular dichroism spectroscopy
- Joseph von Fraunhofer
- Robert Bunsen
- Gustav Kirchhoff

- Spectroscopy links [9] at the Open Directory Project
- Amateur spectroscopy links [10] at the Open Directory Project
- History of Spectroscopy [11]
- Chemometric Analysis for Spectroscopy [12]
- The Science of Spectroscopy [13] - supported by NASA, includes OpenSpectrum, a Wiki-based learning tool for spectroscopy that anyone can edit
- A Short Study of the Characteristics of two Lab Spectroscopes [14]
- NIST government spectroscopy data [15]
- Potentiodynamic Electrochemical Impedance Spectroscopy [16]

References

[1] J. Dubois, G. Sando, E. N. Lewis, Near-Infrared Chemical Imaging, A Valuable Tool for the Pharmaceutical Industry, G.I.T. Laboratory Journal Europe, No. 1-2, 2007

[2] http://www.malvern.com/LabEng/products/sdi/bibliography/sdi_bibliography.htm E. N. Lewis, E. Lee and L. H. Kidder, Combining Imaging and Spectroscopy: Solving Problems with Near-Infrared Chemical Imaging. Microscopy Today, Volume 12, No. 6, 11/2004.

[3] Near Infrared Microspectroscopy, Fluorescence Microspectroscopy,Infrared Chemical Imaging and High Resolution Nuclear Magnetic Resonance Analysis of Soybean Seeds, Somatic Embryos and Single Cells., Baianu, I.C. et al. 2004., In *Oil Extraction and Analysis.*, D. Luthria, Editor pp.241-273, AOCS Press., Champaign, IL.

[4] Single Cancer Cell Detection by Near Infrared Microspectroscopy, Infrared Chemical Imaging and Fluorescence Microspectroscopy.2004.I. C. Baianu, D. Costescu, N. E. Hofmann and S. S. Korban, q-bio/0407006 (July 2004) (http://arxiv.org/abs/q-bio/0407006)

[5] C.L. Evans and X.S. Xie.2008. Coherent Anti-Stokes Raman Scattering Microscopy: Chemical Imaging for Biology and Medicine., doi:10.1146/annurev.anchem.1.031207.112754 *Annual Review of Analytical Chemistry*, **1**: 883-909.

[6] W. Demtroder, *Laser Spectroscopy*, 3rd Ed. (Springer, 2003).

[7] F. J. Duarte (Ed.),*Tunable Laser Applications*, 2nd Ed. (CRC, 2009) Chapter 2.

[8] " Using NIR Spectroscopy to Predict Weathered Wood Exposure Times (http://www.fpl.fs.fed.us/documnts/pdf2006/fpl_2006_wang002.pdf)". .

[9] http://www.dmoz.org//Science/Physics/Optics/Spectroscopy//

[10] http://www.dmoz.org//Science/Astronomy/Amateur/Spectroscopy//

[11] http://www.cofc.edu/~deavorj/521/History%20of%20Spectroscopy.htm

[12] http://www.laboratoryequipment.com/article-chemometric-analysis-for-spectroscopy.aspx

[13] http://www.scienceofspectroscopy.info

[14] http://ioannis.virtualcomposer2000.com/spectroscope/

[15] http://physics.nist.gov/Pubs/AtSpec/index.html

[16] http://www.abc.chemistry.bsu.by/vi/

Fourier transform spectroscopy

Fourier transform spectroscopy is a measurement technique whereby spectra are collected based on measurements of the coherence of a radiative source, using time-domain or space-domain measurements of the electromagnetic radiation or other type of radiation. It can be applied to a variety of types of spectroscopy including optical spectroscopy, → infrared spectroscopy (FT IR, FT-NIRS), → Fourier transform (FT) nuclear magnetic resonance[1] , mass spectrometry and electron spin resonance spectroscopy. There are several methods for measuring the temporal coherence of the light, including the continuous wave *Michelson* or *Fourier transform* spectrometer and the pulsed Fourier transform spectrograph (which is more sensitive and has a much shorter sampling time than conventional spectroscopic techniques, but is only applicable in a laboratory environment).

Conceptual introduction (for FTIR and other absorption spectroscopy)

The goal of any absorption spectroscopy (FTIR, Ultraviolet-visible ("UV-Vis") spectroscopy, etc.) is to measure how well a sample absorbs or transmits light at each different wavelength. The most straightforward way to do this is to shine a monochromatic light beam through a sample, measure how much of the light is absorbed, and repeat for each different wavelength. (This is how UV-Vis spectrometers work, for example.)

Fourier transform spectroscopy is a less intuitive way to get the same information. Rather than passing a *monochromatic* beam of light through the sample, this technique passes a beam containing many different frequencies of light at once, and measures how much of that beam is absorbed by the sample. Next, the beam is modified to contain a different combination of frequencies, giving a second data point. This process is repeated many times. Afterwards, a computer takes all this data and works backwards to infer what the absorption is at each wavelength.

The beam described above is generated by starting with a broadband light source—one containing the full spectrum of wavelengths to be measured. The light shines into a certain configuration of mirrors that allows some wavelengths to pass through but blocks others (due to wave interference). The beam is modified for each new data point by moving one of the mirrors; this changes the set of wavelengths that pass through.

As mentioned, computer processing is required to turn the raw data (light absorption for each mirror position) into the desired result (light absorption for each wavelength). The processing required turns out to be a common algorithm called the Fourier transform (hence the name, "Fourier transform spectroscopy"). The raw data is sometimes called an "interferogram".

Continuous wave *Michelson* or *Fourier transform* spectrograph

The Michelson spectrograph is similar to the instrument used in the Michelson-Morley experiment. Light from the source is split into two beams by a half-silvered mirror, one is reflected off a fixed mirror and one off a moving mirror which introduces a time delay -- the Fourier transform spectrometer is just a Michelson interferometer with a movable mirror. The beams interfere, allowing the temporal coherence of the light to be measured at each different time delay setting, effectively converting the time domain into a spatial coordinate. By making measurements of the signal at many discrete positions of the moving mirror, the spectrum can be reconstructed using a Fourier transform of the temporal coherence of the light. Michelson spectrographs are capable of very high spectral resolution observations of very bright sources. The Michelson or Fourier transform spectrograph was popular for infra-red applications at a time when infra-red astronomy only had single pixel detectors.

The Fourier transform spectrometer is just a Michelson interferometer but one of the two fully-reflecting mirrors is movable, allowing a variable delay (in the travel-time of the light) to be included in one of the beams.

Imaging Michelson spectrometers are a possibility, but in general have been supplanted by imaging Fabry-Perot instruments which are easier to construct.
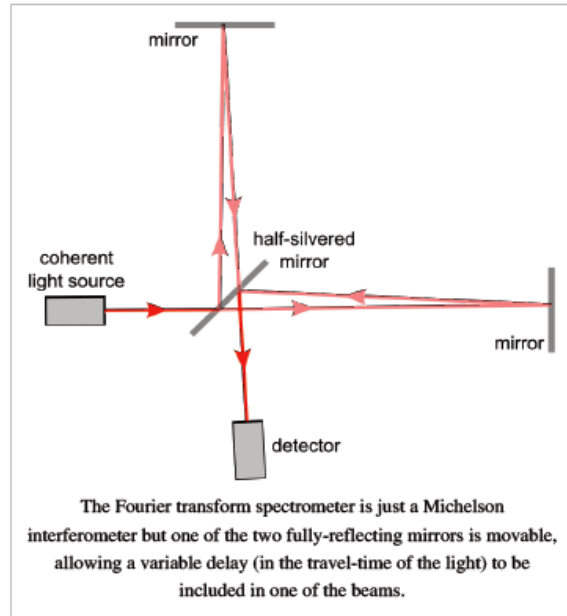
Extracting the spectrum

The intensity as a function of the path length difference in the interferometer p and wavenumber $\tilde{\nu} = 1/\lambda$ is [2]

$$I(p, \tilde{\nu}) = I(\tilde{\nu})[1 + \cos(2\pi\tilde{\nu}p)],$$

where $I(\tilde{\nu})$ is the spectrum to be determined. Note that it is not necessary for $I(\tilde{\nu})$ to be modulated by the sample before the interferometer. In fact, most FTIR spectrometers place the sample after the interferometer in the optical path. The total intensity at the detector is

$$I(p) = \int_0^\infty I(p, \tilde{\nu})d\tilde{\nu} = \int_0^\infty I(\tilde{\nu})[1 + \cos(2\pi\tilde{\nu}p)]d\tilde{\nu}.$$

This is just a Fourier cosine transform. The inverse gives us our desired result in terms of the measured quantity $I(p)$:

$$I(\tilde{\nu}) = 4 \int_0^\infty \left[I(p) - \tfrac{1}{2}I(p = 0)\right]\cos(2\pi\tilde{\nu}p)dp.$$

Pulsed *Fourier transform* spectrometer

A pulsed *Fourier transform* spectrometer does not employ transmittance techniques. In the most general description of pulsed FT spectrometry, a sample is exposed to an energizing event which causes a periodic response. The frequency of the periodic response, as governed by the field conditions in the spectrometer, is indicative of the measured properties of the analyte.

Examples of Pulsed Fourier transform spectrometry

In magnetic spectroscopy (EPR, NMR), an RF pulse in a strong ambient magnetic field is used as the energizing event. This turns the magnetic particles at an angle to the ambient field, resulting in gyration. The gyrating spins then induce a periodic current in a detector coil. Each spin exhibits a characteristic frequency of gyration (relative to the field strength) which reveals information about the analyte.

In FT-mass spectrometry, the energizing event is the injection of the charged sample into the strong electromagnetic field of a cyclotron. These particles travel in circles, inducing a current in a fixed coil on one point in their circle. Each traveling particle exhibits a characteristic cyclotron frequency-field ratio revealing the masses in the sample.

The Free Induction Decay

Pulsed FT spectrometry gives the advantage of requiring a single, time-dependent measurement which can easily deconvolute a set of similar but distinct signals. The resulting composite signal, is called a *free induction decay,* because typically the signal will decay due to inhomogeneities in sample frequency, or simply unrecoverable loss of signal due to entropic loss of the property being measured.

Fellgett Advantage

One of the most important advantages of Fourier transform spectroscopy was shown by P.B. Fellgett, an early advocate of the method. The Fellgett advantage, also known as the multiplex principle, states that a multiplex spectrometer such as the Fourier transform spectroscopy will produce a gain of the order of the square root of m in the signal-to-noise ratio of the resulting spectrum, when compared with an equivalent scanning monochromator, where m is the number of elements comprising the resulting spectrum when the measurement noise is dominated by detector noise.

Converting spectra from time domain to frequency domain

$$S(t) = \int_{-\infty}^{\infty} I(\nu)e^{-i\nu 2\pi t}\, d\nu$$

The sum is performed over all contributing frequencies to give a signal S(t) in the time domain.

$$I(\nu) = 2Re \int_{-\infty}^{\infty} S(t)e^{2i\pi\nu t} dt$$

gives non-zero value when S(t) contains a component that matches the oscillating function.
Remember that

$$e^{ix} = \cos x + i\sin x$$

References

[1] Antoine Abragam. 1968. *Principles of Nuclear Magnetic Resonance.*, 895 pp., Cambridge University Press: Cambridge, UK.

[2] Peter Atkins, Julio De Paula. 2006. *Physical Chemistry.*, 8th ed. Oxford University Press: Oxford, UK.

[3] http://dx.doi.org/10.1039%2Fb602376m

[4] http://scienceworld.wolfram.com/physics/FourierTransformSpectrometer.html

[5] http://www.astro.livjm.ac.uk/courses/phys362/notes/

[6] http://www.ijvs.com/volume5/edition5/section1.html#Feature

[7] http://www.osa.org/meetings/topicalmeetings/fts/default.aspx

Infrared spectroscopy

Infrared spectroscopy (IR spectroscopy) is the subset of → spectroscopy that deals with the infrared region of the electromagnetic spectrum. It covers a range of techniques, the most common being a form of absorption spectroscopy. As with → all spectroscopic techniques, it can be used to identify compounds or investigate sample composition. Infrared spectroscopy correlation tables are tabulated in the literature. A common laboratory instrument that uses this technique is an infrared spectrophotometer.

Background and theory

The infrared portion of the electromagnetic spectrum is divided into three regions; the near-, mid- and far- infrared, named for their relation to the visible spectrum. The far-infrared, approximately $400–10 \ cm^{-1}$ ($1000–30 \ \mu m$), lying adjacent to the microwave region, has low energy and may be used for rotational spectroscopy. The mid-infrared, approximately $4000–400 \ cm^{-1}$ ($30–2.5 \ \mu m$) may be used to study the fundamental vibrations and associated rotational-vibrational structure. The higher energy near-IR, approximately $14000–4000 \ cm^{-1}$ ($2.5–0.8 \ \mu m$) can excite overtone or harmonic vibrations. The names and classifications of these subregions are merely conventions. They are neither strict divisions nor based on exact molecular or electromagnetic properties.

Infrared spectroscopy exploits the fact that molecules have specific frequencies at which they rotate or vibrate corresponding to discrete energy levels (vibrational modes). These resonant frequencies are determined by the shape of the molecular potential energy surfaces, the masses of the atoms and, by the associated vibronic coupling. In order for a vibrational mode in a molecule to be IR active, it must be associated with changes in the permanent dipole. In particular, in the Born–Oppenheimer and harmonic approximations, i.e. when the molecular Hamiltonian corresponding to the electronic ground state can be approximated by a harmonic oscillator in the neighborhood of the equilibrium molecular geometry, the resonant frequencies are determined by the normal modes corresponding to the molecular electronic ground state potential energy surface. Nevertheless, the resonant frequencies can be in a first approach related to the strength of the bond, and the mass of the atoms at either end of it. Thus, the frequency of the vibrations can be associated with a particular bond type.

Simple diatomic molecules have only one bond, which may stretch. More complex molecules have many bonds, and vibrations can be conjugated, leading to infrared absorptions at characteristic frequencies that may be related to chemical groups. For example, the atoms in a CH_2 group, commonly found in organic compounds can vibrate in six different ways: **symmetrical and antisymmetrical stretching, scissoring, rocking, wagging and twisting:**

Symmetrical stretching	Antisymmetrical stretching	Scissoring	Rocking	Wagging	Twisting

The infrared spectrum of a sample is collected by passing a beam of infrared light through the sample. Examination of the transmitted light reveals how much energy was absorbed at each wavelength. This can be done with a monochromatic beam, which changes in wavelength over time, or by using a Fourier transform instrument to measure all wavelengths at once. From this, a transmittance or absorbance spectrum can be produced, showing at which IR wavelengths the sample absorbs. Analysis of these absorption characteristics reveals details about the molecular structure of the sample. When the frequency of the IR is the same as the vibrational frequency of a bond, absorption occurs.

This technique works almost exclusively on samples with covalent bonds. Simple spectra are obtained from samples with few IR active bonds and high levels of purity. More complex molecular structures lead to more absorption bands and more complex spectra. The technique has been used for the characterization of very complex mixtures.

Conventional method

A beam of infrared light is produced and split into two separate beams. One is passed through the sample, the other passed through a reference which is often the substance the sample is dissolved in. The beams are both reflected back towards a detector, however first they pass through a splitter which quickly alternates which of the two beams enters the detector. The two signals are then compared and a printout is obtained.

Typical apparatus
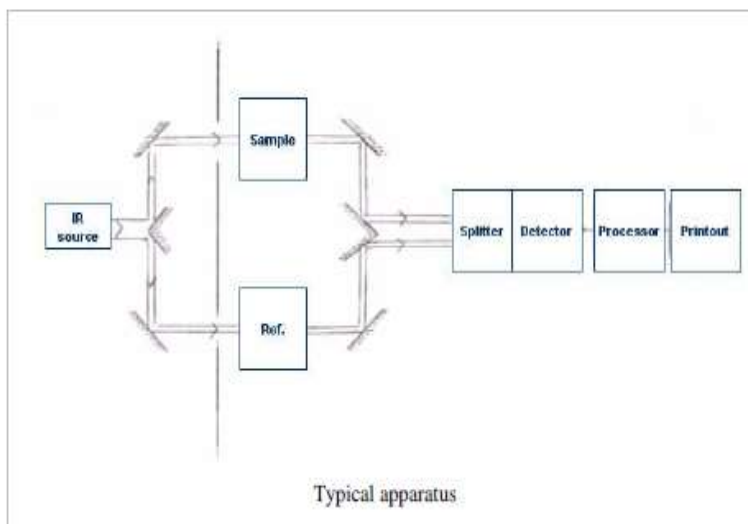
A reference is used for two reasons:

- This prevents fluctuations in the output of the source affecting the data
- This allows the effects of the solvent to be cancelled out (the reference is usually a pure form of the solvent the sample is in)

Fourier transform infrared spectroscopy

Fourier transform infrared (FTIR) spectroscopy is a measurement technique for collecting infrared spectra. Instead of recording the amount of energy absorbed when the frequency of the infra-red light is varied (monochromator), the IR light is guided through an interferometer. After passing through the sample, the measured signal is the interferogram. Performing a Fourier transform on this signal data results in a spectrum identical to that from conventional (dispersive) infrared spectroscopy.

FTIR spectrometers are cheaper than conventional spectrometers because building an interferometer is easier than the fabrication of a monochromator. In addition, measurement of a single spectrum is faster for the FTIR technique because the information at all frequencies is collected simultaneously. This allows multiple samples to be collected and averaged together resulting in an improvement in sensitivity. Virtually all modern infrared spectrometers are FTIR instruments.

Summary of absorptions of bonds in organic molecules
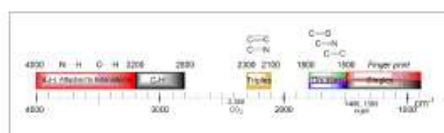
Wavenumbers listed in cm^{-1}.

Uses and applications

Infrared spectroscopy is widely used in both research and industry as a simple and reliable technique for measurement, quality control and dynamic measurement. It is of especial use in forensic analysis in both criminal and civil cases, enabling identification of polymer degradation for example. It is perhaps the most widely used method of applied spectroscopy.

The instruments are now small, and can be transported, even for use in field trials. With increasing technology in computer filtering and manipulation of the results, samples in solution can now be measured accurately (water produces a broad absorbance across the range of interest, and thus renders the spectra unreadable without this computer treatment). Some instruments will also automatically tell you what substance is being measured from a store of thousands of reference spectra held in storage.

By measuring at a specific frequency over time, changes in the character or quantity of a particular bond can be measured. This is especially useful in measuring the degree of polymerization in polymer manufacture. Modern research instruments can take infrared measurements across the whole range of interest as frequently as 32 times a second. This can be done whilst simultaneous measurements are made using other techniques. This makes the observations of chemical reactions and processes quicker and more accurate.

Techniques have been developed to assess the quality of tea-leaves using infrared spectroscopy. This will mean that highly trained experts (also called 'noses') can be used more sparingly, at a significant cost saving.[4]

Infrared spectroscopy has been highly successful for applications in both organic and inorganic chemistry. Infrared spectroscopy has also been successfully utilized in the field of semiconductor microelectronics[5] : for example, infrared spectroscopy can be applied to semiconductors like silicon, gallium arsenide, gallium nitride, zinc selenide, amorphous silicon, silicon nitride, etc.

Isotope effects

The different isotopes in a particular species may give fine detail in infrared spectroscopy. For example, the O-O stretching frequency (in reciprocal centimeters) of oxyhemocyanin is experimentally determined to be 832 and 788 cm^{-1} for $\nu(^{16}O-^{16}O)$ and $\nu(^{18}O-^{18}O)$ respectively.

By considering the O-O as a spring, the wavenumber of absorbance, ν can be calculated:

$$\nu = \frac{1}{2\pi c}\sqrt{\frac{k}{\mu}}$$

where k is the spring constant for the bond, c is the speed of light, and μ is the reduced mass of the A-B system:

$$\mu = \frac{m_A m_B}{m_A + m_B}$$

(m_i is the mass of atom i).

The reduced masses for $^{16}O-^{16}O$ and $^{18}O-^{18}O$ can be approximated as 8 and 9 respectively. Thus

$$\frac{\nu_{16O}}{\nu_{18O}} = \sqrt{\frac{9}{8}} \approx \frac{832}{788}.$$

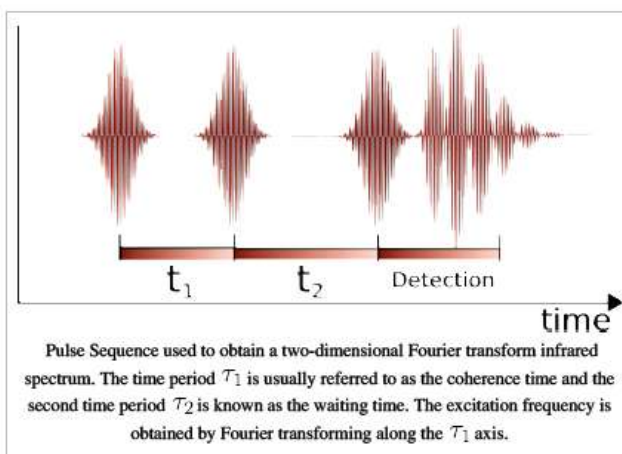Where ν is the wavenumber [wavenumber = frequency/(speed of light)]

The effect of isotopes, both on the vibration and the decay dynamics, has been found to be stronger than previously thought. In some systems, such as silicon and germanium, the decay of the anti-symmetric stretch mode of interstitial oxygen involves the symmetric stretch mode with a strong isotope dependence. For example, it was shown that for a natural silicon sample, the lifetime of the anti-symmetric vibration is 11.4 ps. When the isotope of one of the silicon atoms is increased to 29Si, the lifetime increases to 19 ps, similarly, when the silicon atom is changed to 30Si, the lifetime becomes 27 ps.[6]

Two-dimensional infrared spectroscopy

Two-dimensional infrared correlation spectroscopy analysis is the application of 2D correlation analysis on infrared spectra. By extending the spectral information of a perturbed sample, spectral analysis is simplified and resolution is enhanced. The 2D synchronous and 2D asynchronous spectra represent a graphical overview of the spectral changes due to a perturbation (such as a changing concentration or changing temperature) as well as the relationship between the spectral changes at two different wavenumbers.

Nonlinear two-dimensional infrared spectroscopy[7] [8] is the infrared version of correlation spectroscopy. Nonlinear two-dimensional infrared spectroscopy is a technique that has become available with the development of femtosecond infrared laser pulses. In this experiment first a set of pump pulses are applied to the sample. This is followed by a waiting time, where the system is allowed to relax. The waiting time typically lasts from zero to several picoseconds and the duration can be controlled with a resolution of tens of femtoseconds. A probe pulse is then applied

Pulse Sequence used to obtain a two-dimensional Fourier transform infrared spectrum. The time period τ_1 is usually referred to as the coherence time and the second time period τ_2 is known as the waiting time. The excitation frequency is obtained by Fourier transforming along the τ_1 axis.

resulting in the emission of a signal from the sample. The nonlinear two-dimensional infrared spectrum is a two-dimensional correlation plot of the frequency ω_1 that was excited by the initial pump pulses and the frequency ω_3

excited by the probe pulse after the waiting time. This allows the observation of coupling between different vibrational modes; because of its extremely high time resolution it can be used to monitor molecular dynamics on a picosecond timescale. It is still a largely unexplored technique and is becoming increasingly popular for fundamental research.

Like in two-dimensional nuclear magnetic resonance (2DNMR) spectroscopy this technique spreads the spectrum in two dimensions and allow for the observation of cross peaks that contain information on the coupling between different modes. In contrast to 2DNMR nonlinear two-dimensional infrared spectroscopy also involve the excitation to overtones. These excitations result in excited state absorption peaks located below the diagonal and cross peaks. In 2DNMR two distinct techniques, COSY and NOESY, are frequently used. The cross peaks in the first are related to the scalar coupling, while in the later they are related to the spin transfer between different nuclei. In nonlinear two-dimensional infrared spectroscopy analogs have been drawn to these 2DNMR techniques. Nonlinear two-dimensional infrared spectroscopy with zero waiting time corresponds to COSY and nonlinear two-dimensional infrared spectroscopy with finite waiting time allowing vibrational population transfer corresponds to NOESY. The COSY variant of nonlinear two-dimensional infrared spectroscopy has been used for determination of the secondary structure content proteins.[9]

References

[1] Laurence M. Harwood, Christopher J. Moody. *Experimental organic chemistry: Principles and Practice* (Illustrated edition ed.). pp. 289-292.

[2] Laurence M. Harwood, Christopher J. Moody. *Experimental organic chemistry: Principles and Practice* (Illustrated edition ed.). pp. 292.

[3] Laurence M. Harwood, Christopher J. Moody. *Experimental organic chemistry: Principles and Practice* (Illustrated edition ed.). pp. 295-296.

[4] Luypaert, J.; Zhang, M.H.; Massart, D.L. (2003), "Feasibility study for the use of near infrared spectroscopy in the qualitative and quantitative analysis of green tea, Camellia sinensis (L.)", *Analytica Chimica Acta*, **478(2)**, Elsevier, pp. 303–312

[5] Lau, W.S. (1999). *Infrared characterization for microelectronics*. World Scientific.

[6] Isotope Dependence of the Lifetime of the 1136-cm[sup -1] Vibration of Oxygen in Silicon K. K. Kohli, Gordon Davies, N. Q. Vinh, D. West, S. K. Estreicher, T. Gregorkiewicz, I. Izeddin, and K. M. Itoh, Phys. Rev. Lett. 96, 225503 (2006), DOI:10.1103/PhysRevLett.96.225503

[7] P. Hamm, M. H. Lim, R. M. Hochstrasser (1998). "Structure of the amide I band of peptides measured by femtosecond nonlinear-infrared spectroscopy". *J. Phys. Chem. B* **102**: 6123. doi: 10.1021/jp9813286 (http://dx.doi.org/10.1021/jp9813286).

[8] S. Mukamel (2000). "Multidimensional Fentosecond Correlation Spectroscopies of Electronic and Vibrational Excitations". *Annual Review of Physics and Chemistry* **51**: 691. doi: 10.1146/annurev.physchem.51.1.691 (http://dx.doi.org/10.1146/annurev.physchem.51.1.691).

[9] N. Demirdöven, C. M. Cheatum, H. S. Chung, M. Khalil, J. Knoester, A. Tokmakoff (2004). "Two-dimensional infrared spectroscopy of antiparallel beta-sheet secondary structure". *Journal of the American Chemical Society* **126**: 7981. doi: 10.1021/ja049811j (http://dx.doi.org/

10.1021/ja049811j).

[10] http://www.shu.ac.uk/schools/sci/chem/tutorials/molspec/irspec1.htm

[11] http://www.organicworldwide.net/infrared

[12] http://riodb01.ibase.aist.go.jp/sdbs/cgi-bin/cre_index.cgi?lang=eng
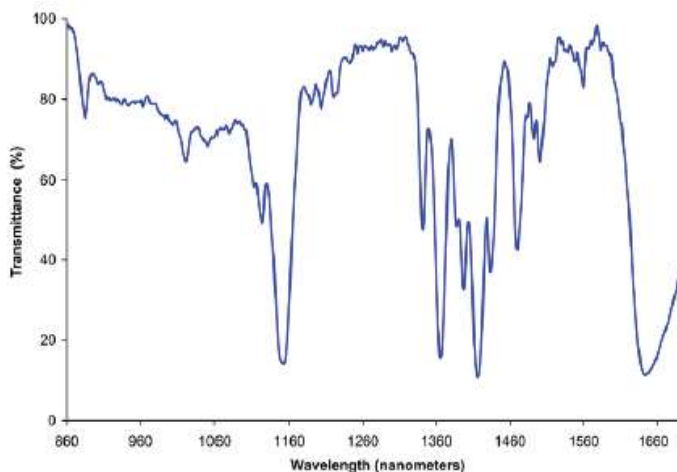
Near infrared spectroscopy

Near infrared spectroscopy (NIRS) is a spectroscopic method which uses the near infrared region of the electromagnetic spectrum (from about 800 nm to 2500 nm). Typical applications include pharmaceutical, medical diagnostics (including blood sugar and oximetry), food and agrochemical quality control, as well as combustion research.

Theory

Near infrared spectroscopy is based on molecular overtone and combination vibrations. Such transitions are forbidden by the selection rules of

Near IR absorption spectrum of dichloromethane showing complicated overlapping overtones of mid IR absorption features.

quantum mechanics. As a result, the molar absorptivity in the near IR region is typically quite small. One advantage is that NIR can typically penetrate much farther into a sample than → mid infrared radiation. Near infrared spectroscopy is therefore not a particularly sensitive technique, but it can be very useful in probing bulk material with little or no sample preparation.

The molecular overtone and combination bands seen in the near IR are typically very broad, leading to complex spectra; it can be difficult to assign specific features to specific chemical components. Multivariate (multiple wavelength) calibration techniques (e.g., principal components analysis or partial least squares) are often employed to extract the desired chemical information. Careful development of a set of calibration samples and application of multivariate calibration techniques is essential for near infrared analytical methods.

History

The discovery of near-infrared energy is ascribed to Herschel in the 19th century, but the first industrial application began in the 1950s. In the first applications, NIRS was used only as an add-on unit to other optical devices that used other wavelengths such as ultraviolet (UV), visible (Vis), or mid-infrared (MIR) spectrometers. In the 1980s, a single unit, stand-alone NIRS system was made available, but the application of NIRS was focused more on chemical analysis. With the introduction of light-fiber optics in the mid 80s and the monochromator-detector developments in early nineties, NIRS became a more powerful tool for scientific research.

Near infrared spectrum of liquid ethanol.
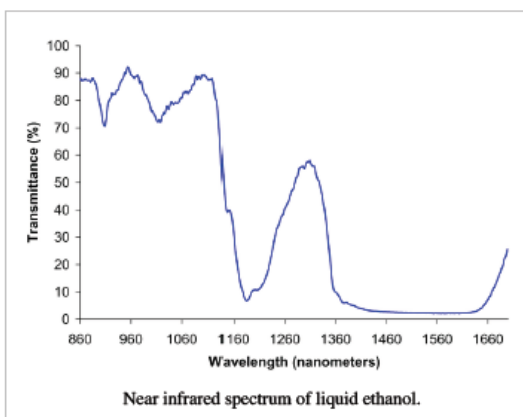
This optical method can be used in a number of fields of science including physics, physiology, or medicine. It was only in the last few decades that NIRS began to be used as a medical tool for monitoring patients.

Instrumentation

Instrumentation for near-IR (NIR) spectroscopy is partially similar to instruments for the visible and mid-IR ranges. There is a source, a detector, and a dispersive element (such as a prism, or more commonly a diffraction grating) to allow the intensity at different wavelengths to be recorded. → Fourier transform NIR instruments using an interferometer are also common, especially for wavelengths above ~1000 nm. Depending on the sample, the spectrum can be measured in either in reflection or transmission.

Common incandescent or quartz halogen light bulbs are most often used as broadband sources of near infrared radiation for analytical applications. Light-emitting diodes (LEDs) are also used; they offer greater lifetime and spectral stability and reduced power requirements.[1] .

The type of detector used depends primarily on the range of wavelengths to be measured. Silicon-based CCDs are suitable for the shorter end of the NIR range, but are not sufficiently sensitive over most of the range. InGaAs and PbS devices are more suitable. In certain diode array (DA) NIRS instruments, both silicon-based and InGaAs detectors are employed in the same instrument. Such instruments can record both visible and NIR spectra 'simultaneously'.

Instruments intended for → chemical imaging in the NIR may use a 2D array detector with a acousto-optic tunable filter. Multiple images may be recorded sequentially at different narrow wavelength bands.[2]

Many commercial instruments for UV/vis spectroscopy are capable of recording spectra in the NIR range (to perhaps ~900 nm). In the same way, the range of some mid-IR instruments may extend into the NIR. In these instruments the detector used for the NIR wavelengths is often the same detector used for the instrument's "main" range of interest.

Applications

The primary application of NIRS to the human body uses the fact that the transmission and absorption of NIR light in human body tissues contains information about haemoglobin concentration changes. When a specific area of the brain is activated, the localized blood volume in that area changes quickly. Optical imaging can measure the location and activity of specific regions of the brain by continuously monitoring blood haemoglobin levels through the determination of optical absorption coefficients.

Typical applications of NIR spectroscopy include the analysis of foodstuffs, pharmaceuticals, combustion products and a major branch of astronomical spectroscopy.

NIR sensor for moisture measurement installed on a belt conveyor

Astronomical spectroscopy

Near-infrared → spectroscopy is used in astronomy for studying the atmospheres of cool stars where molecules can form. The vibrational and rotational signatures of molecules such as titanium oxide, cyanide and carbon monoxide can be seen in this wavelength range and can give a clue towards the star's spectral type. It is additionally used for studying molecules in other astronomical contexts, such as in molecular clouds where new stars are formed. The astronomical phenomenon known as reddening means that near-infrared wavelengths are less affected by dust in the interstellar medium, such that regions inaccessible by optical spectroscopy can be studied in the near-infrared. Since dust and gas are strongly associated, these dusty regions are exactly those where infrared spectroscopy is most useful. The near-infrared spectra of very young stars provide important information about their ages and masses, which is important for understanding star formation in general.

Remote monitoring

Techniques have been developed for NIR spectroscopic imaging. These have been used for a wide range of uses, including the remote investigation of plants and soils. Data can be collected from instruments on airplanes or satellites to assess ground cover and soil chemistry.

Medical uses

Medical applications of NIRS center on the non-invasive measurement of the amount and oxygen content of haemoglobin, as well as the use of exogenous optical tracers in conjunction with flow kinetics.

NIRS can be used for non-invasive assessment of brain function through the intact skull in human subjects by detecting changes in blood haemoglobin concentrations associated with neural activity, e.g. in branches of Cognitive psychology as a partial replacement for fMRI techniques. NIRS can be used on infants, where fMRI cannot (at least in the United States), and NIRS is much more portable than fMRI machines, even wireless instrumentation is available, which enables investigations in freely moving subjects[3]). However, NIRS cannot fully replace fMRI because it can only be used to scan cortical tissue, where fMRI can be used to measure activation throughout the brain.

The application in functional mapping of the human cortex is called optical topography (OT), near infrared imaging (NIRI) or functional NIRS (fNIRS). The term optical tomography is used for three-dimensional NIRS. The terms NIRS, NIRI and OT are often used interchangeably, but they have some distinctions. The most important difference between NIRS and OT/NIRI is that OT/NIRI is mainly used to detect changes in optical properties of tissue simultaneously from multiple measurement points and display the results in the form of a map or image over a specific area, whereas NIRS provides quantitative data in absolute terms on up to a few specific points. The latter is

also used to investigate other tissues such as e.g. muscle, breast, and tumors.

By employing several wavelengths and time resolved (frequency or time domain) and/or spatially resolved methods blood flow, volume and oxygenation can be quantified[4] . These measurements are a form of oximetry. Applications of oximetry by NIRS methods include the detection of illnesses which affect the blood circulation (e.g. peripheral vascular disease), the detection and assessment of breast tumors, and the optimization of training in sports medicine. These techniques can also be used for industry or agro processes in order to predict particle size/density.[5]

The use of NIRS in conjunction with a bolus injection of indocyanine green (ICG) has been used to measure cerebral blood flow[6] and cererbral metabolic rate of oxygen consumption[7] in neonatal models.

NIRS is starting to be used in pediatric critical care, to help deal with cardiac surgery post-op. Indeed, NIRS is able to measure venous oxygen saturation (SVO2), which is determined by the cardiac output, as well as other parameters (FiO2, haemoglobin, oxygen uptake). Therefore, following the NIRS gives critical care physicians a notion of the cardiac output. NIRS is liked by patients, because it is non-invasive, painless and uses non-ionizing radiation.

The instrumental development of NIRS/NIRI/OT has proceeded tremendously during the last years and in particular in terms of quantification, imaging and miniaturisation[8] .

Particle measurement

NIR is often used in particle sizing in a range of different fields, including studying pharmaceutical and agricultural powders.

Industrial uses

As opposed to NIRS used in optical topography, general NIRS used in chemical assays does not provide imaging by mapping. For example, a clinical carbon dioxide analyzer requires reference techniques and calibration routines to be able to get accurate CO_2 content change. In this case, calibration is performed by adjusting the zero control of the sample being tested after purposefully supplying 0% CO_2 or another known amount of CO_2 in the sample. Normal compressed gas from distributors contains about 95% O_2 and 5% CO_2 which can also be used to adjust %CO_2 meter reading to be exactly 5% at initial calibration.

Related Topics:

- fNIR
- → Fourier transform spectroscopy
- → FT-NIRS
- → Infrared spectroscopy
- Vibrational spectroscopy
- Rotational spectroscopy
- → Spectroscopy
- Chemical Imaging
- Optical imaging

2D-FT NMR Imaging/NMRI and FT-NMR Spectrsocopy

2D-FT Nuclear magnetic resonance imaging (2D-FT NMRI), or Two-dimensional Fourier transform nuclear magnetic resonance imaging (NMRI), is primarily a non-invasive imaging technique most commonly used in biomedical research and medical radiology/nuclear medicine/MRI to visualize structures and functions of the living systems and single cells. For example it can provide fairly detailed images of a human body in any selected cross-sectional plane, such as longitudinal, transversal, sagital, etc. The basic NMR phenomenon or physical principle[1] is essentially the same in N(MRI), nuclear magnetic resonance/→ FT (NMR) spectroscopy, topical NMR, or even in Electron Spin Resonance /EPR; however, the details are significantly different at present for EPR, as only in the early days of NMR the static magnetic field was scanned for obtaining spectra, as it is still the case in many EPR or ESR spectrometers. NMRI, on the other hand, often utilizes a linear magnetic field gradient to obtain an image that combines the visualization of molecular structure and dynamics. It is this dynamic aspect of NMRI, as well as its highest sensitivity for the ^{1}H nucleus that distinguishes it very dramatically from X-ray CAT scanning that 'misses' hydrogens because of their very low X-ray scattering factor.

Thus, NMRI provides much greater contrast especially for the different soft tissues of the body than computed tomography (CT) as its most sensitive option observes the nuclear spin distribution and dynamics of highly mobile molecules that contain the naturally abundant, stable hydrogen isotope ^{1}H as in plasma water molecules, blood, dissolved metabolites and fats. This approach makes it most useful in cardiovascular, oncological (cancer), neurological (brain), musculoskeletal, and cartilage imaging. Unlike CT, it uses no ionizing radiation, and also unlike nuclear imaging it does not employ any radioactive isotopes. Some of the first MRI images reported were published in 1973[2] and the first study performed on a human took place on July 3, 1977.[3] Earlier papers were also published by Sir Peter Mansfield[4] in UK (Nobel Laureate in 2003), and R. Damadian in the USA[5], (together with an approved patent for 'fonar', or magnetic imaging). The detailed physical theory of NMRI was published by Peter Mansfield in 1973[6]. Unpublished 'high-resolution' (50 micron resolution) images of other living systems, such as hydrated wheat grains, were also obtained and communicated in UK in 1977-1979, and were subsequently confirmed by articles published in *Nature* by Peter Callaghan.

NMR Principle

Certain nuclei such as ^{1}H nuclei, or `fermions' have spin-1/2, because there are two spin states, referred to as "up" and "down" states. The nuclear magnetic resonance absorption phenomenon occurs when samples containing such nuclear spins are placed in a static magnetic field and a very short radiofrequency pulse is applied with a center, or carrier, frequency matching that of the transition between the up and down states of the spin-1/2 ^{1}H nuclei that were polarized by the static magnetic field. [1] Very low field schemes have also been recently reported.[7]

Advanced 3 T clinical diagnostics and biomedical research NMR Imaging instrument.

Chemical Shifts

NMR is a very useful family of techniques for chemical and biochemical research because of the chemical shift; this effect consists in a frequency shift of the nuclear magnetic resonance for specific chemical groups or atoms as a result of the partial shielding of the corresponding nuclei from the applied, static external magnetic field by the electron orbitals (or molecular orbitals) surrounding such nuclei present in the chemical groups. Thus, the higher the electron density surrounding a specific nucleus the larger the chemical shift will be. The resulting magnetic field at the nucleus is thus lower than the applied external magnetic field and the resonance frequencies observed as a result of such shielding are lower than the value that would be observed in the absence of any electronic orbital shielding. Furthermore, in order to obtain a chemical shift value independent of the strength of the applied magnetic field and allow for the direct comparison of spectra obtained at different magnetic field values, the chemical shift is defined by the ratio of the strength of the local magnetic field value at the observed (electron orbital-shielded) nucleus by the external magnetic field strength, H_{loc} / H_0. The first NMR observations of the chemical shift, with the correct physical chemistry interpretation, were reported for ^{19}F containing compounds in the early 1950s by Herbert S. Gutowsky and Charles P. Slichter from the University of Illinois at Urbana (USA).

A related effect in metals is called the Knight shift, which is due only to the conduction electrons. Such conduction electrons present in metals induce an "additional" local field at the nuclear site, due to the spin re-orientation of the conduction electrons in the presence of the applied (constant), external magnetic field. This is only broadly `similar' to the chemical shift in either solutions or diamagnetic solids.

NMR Imaging Principles

A number of methods have been devised for combining magnetic field gradients and radiofrequency pulsed excitation to obtain an image. Two major methods involve either 2D -FT or 3D-FT[8] reconstruction from projections, somewhat similar to Computed Tomography, with the exception of the image interpretation that in the former case must include dynamic and relaxation/contrast enhancement information as well. Other schemes involve building the NMR image either point-by-point or line-by-line. Some schemes use instead gradients in the rf field

rather than in the static magnetic field. The majority of NMR images routinely obtained are either by the Two-Dimensional Fourier Transform (2D-FT) technique [9] (with slice selection), or by the Three-Dimensional Fourier Transform (3D—FT) techniques that are however much more time consuming at present. 2D-FT NMRI is sometime called in common parlance a "spin-warp". An NMR image corresponds to a spectrum consisting of a number of `spatial frequencies' at different locations in the sample investigated, or in a patient.[10] A two—dimensional Fourier transformation of such a "real" image may be considered as a representation of such "real waves" by a matrix of spatial frequencies known as the k—space. We shall see next in some mathematical detail how the 2D-FT computation works to obtain 2D-FT NMR images.

Two-dimensional Fourier transform imaging and spectroscopy

A two-dimensional Fourier transform (2D-FT) is computed numerically or carried out in two stages, both involving `standard', one-dimensional Fourier transforms. However, the second stage Fourier transform is not the inverse Fourier transform (which would result in the original function that was transformed at the first stage), but a Fourier transform in a second variable—which is `shifted' in value—relative to that involved in the result of the first Fourier transform. Such 2D-FT analysis is a very powerful method for both NMRI and two-dimensional nuclear magnetic resonance spectroscopy (2D-FT NMRS)[11] that allows the three-dimensional reconstruction of polymer and biopolymer structures at atomic resolution[12] for molecular weights (Mw) of dissolved biopolymers in aqueous solutions (for example) up to about 50,000 MW. For larger biopolymers or polymers, more complex methods have been developed to obtain limited structural resolution needed for partial 3D-reconstructions of higher molecular structures, e.g. for up 900,000 MW or even oriented microcrystals in aqueous suspensions or single crystals; such methods have also been reported for *in vivo* 2D-FT NMR spectroscopic studies of algae, bacteria, yeast and certain mammalian cells, including human ones. The 2D-FT method is also widely utilized in optical spectroscopy, such as *2D-FT NIR hyperspectral imaging* (2D-FT NIR-HS), or in MRI imaging for research and clinical, diagnostic applications in Medicine. In the latter case, 2D-FT $\rightarrow$ NIR-HS has recently allowed the identification of single, malignant cancer cells surrounded by healthy human breast tissue at about 1 micron resolution, well-beyond the resolution obtainable by 2D-FT NMRI for such systems in the limited time available for such diagnostic investigations (and also in magnetic fields up to the FDA approved magnetic field strength H_0 of 4.7 T, as shown in the top image of the state-of-the-art NMRI instrument). A more precise mathematical definition of the `double' (2D) Fourier transform involved in both 2D NMRI and 2D-FT NMRS is specified next, and a precise example follows this generally accepted definition.

2D-FT Definition

A *2D-FT, or two-dimensional Fourier transform*, is a standard Fourier transformation of a function of two variables, $f(x_1, x_2)$, carried first in the first variable x_1, followed by the Fourier transform in the second variable x_2 of the resulting function $F(s_1, x_2)$. Note that in the case of both 2D-FT NMRI and 2D-FT NMRS the two independent variables in this definition are in the time domain, whereas the results of the two successive Fourier transforms have, of course, frequencies as the independent variable in the NMRS, and ultimately spatial coordinates for both 2D NMRI and 2D-FT NMRS following computer structural reconstructions based on special algorithms that are different from FT or 2D-FT. Moreover, such structural algorithms are different for 2D NMRI and 2D-FT NMRS: in the former case they involve macroscopic, or anatomical structure determination, whereas in the latter case of 2D-FT NMRS the atomic structure reconstruction algorithms are based on the quantum theory of a microphysical (quantum) process such as nuclear Overhauser enhancement NOE, or specific magnetic dipole-dipole interactions[13] between neighbor nuclei.

Example 1

A 2D Fourier transformation and phase correction is applied to a set of 2D NMR (FID) signals: $s(t_1, t_2)$ yielding a real 2D-FT NMR `spectrum' (collection of 1D FT-NMR spectra) represented by a matrix $\mathbf{S}$ whose elements are

$$\mathbf{S}\,(\nu_1, \nu_2) = \mathrm{Re} \int \int cos(\nu_1 t_1) exp^{(-i\nu_2 t_2)} s(t_1, t_2) dt_1 dt_2$$

where : ν_1 and : ν_2 denote the discrete indirect double-quantum and single-quantum(detection) axes, respectively, in the 2D NMR experiments. Next, the *covariance matrix* is calculated in the frequency domain according to the following equation

$$\mathbf{C}\ (\nu_2', \nu_2) = S^T S = \sum_{\nu'} S(\nu_1, \nu_2') S(\nu_1, \nu_2)],$$ with : ν_2, ν_2' taking all possible single-quantum

frequency values and with the summation carried out over all discrete, double quantum frequencies : ν_1.

Example 2

Atomic Structure from 2D-FT STEM Images [14] of electron distributions in a high-temperature cuprate superconductor `paracrystal' reveal both the domains (or `location') and the local symmetry of the 'pseudo-gap' in the electron-pair correlation band responsible for the high—temperature superconductivity effect (obtained at Cornell University). So far there have been three Nobel prizes awarded for 2D-FT NMR/MRI during 1992-2003, and an additional, earlier Nobel prize for 2D-FT of X-ray data (`CAT scans'); recently the advanced possibilities of 2D-FT techniques in Chemistry, Physiology and Medicine [15] received very significant recognition.[16]

Brief explanation of NMRI diagnostic uses in Pathology

As an example, a diseased tissue such as a malignant tumor, can be detected by 2D-FT NMRI because the hydrogen nuclei of molecules in different tissues return to their equilibrium spin state at different relaxation rates, and also because of the manner in which a malignant tumor spreads and grows rapidly along the blood vessels adjacent to the tumor, also inducing further vascularization to occur. By changing the pulse delays in the RF pulse sequence employed, and/or the RF pulse sequence itself, one may obtain a `relaxation—based contrast', or contrast enhancement between different types of body tissue, such as normal vs. diseased tissue cells for example. Excluded from such diagnostic observations by NMRI are all patients with ferromagnetic metal implants, (e.g., cochlear implants), and all cardiac pacemaker patients who cannot undergo any NMRI scan because of the very intense magnetic and RF fields employed in NMRI which would strongly interfere with the correct functioning of such pacemakers. It is, however, conceivable that future developments may also include along with the NMRI diagnostic treatments with special techniques involving applied magnetic fields and very high frequency RF. Already, surgery with special tools is being experimented on in the presence of NMR imaging of subjects.Thus, NMRI is used to image almost every part of the body, and is especially useful for diagnosis in neurological conditions, disorders of the muscles and joints, for evaluating tumors, such as in lung or skin cancers, abnormalities in the heart (especially in children with hereditary disorders), blood vessels, CAD, atherosclerosis and cardiac infarcts [17] (courtesy of Dr. Robert R. Edelman)

Related Topics:

- Nuclear magnetic resonance (NMR)
- Edward Mills Purcell
- Felix Bloch
- Medical imaging
- Paul C. Lauterbur
- Magnetic resonance microscopy
- Peter Mansfield
- Computed tomography (CT)

- Solid-state NMR
- Knight shift
- John Hasbrouck Van Vleck
- Chemical shift
- Herbert S. Gutowsky
- John S. Waugh
- Charles Pence Slichter
- Protein nuclear magnetic resonance spectroscopy
- Kurt Wüthrich
- Nuclear Overhauser effect
- → Fourier transform spectroscopy(FTS)
- Jean Jeneer
- Richard R. Ernst

- → FT-NIRS (NIR)
- Magnetic resonance elastography

- Relaxation
- Earth's field NMR (EFNMR)
- Robinson oscillator

References

- Antoine Abragam. 1968. *Principles of Nuclear Magnetic Resonance.*, 895 pp., Cambridge University Press: Cambridge, UK.
- Charles P. Slichter.1996. *Principles of Magnetic Resonance.* Springer: Berlin and New York, Third Edition., 651pp. ISBN 0-387-50157-6.
- Kurt Wüthrich. 1986, *NMR of Proteins and Nucleic Acids.*, J. Wiley and Sons: New York, Chichester, Brisbane, Toronto, Singapore. (Nobel Laureate in 2002 for 2D-FT NMR Studies of Structure and Function of Biological Macromolecules [18]
- Protein structure determination in solution by NMR spectroscopy [19] Kurt Wüthrich. J Biol Chem. 1990 December 25;265(36):22059-62
- 2D-FT NMRI Instrument image: A JPG color image of a 2D-FT NMRI `monster' Instrument [20].
- Richard R. Ernst. 1992. Nuclear Magnetic Resonance Fourier Transform (2D-FT) Spectroscopy. Nobel Lecture [15], on December 9, 1992.
- Peter Mansfield. 2003.Nobel Laureate in Physiology and Medicine for (2D and 3D) MRI [21]
- D. Benett. 2007. PhD Thesis. Worcester Polytechnic Institute. PDF of 2D-FT Imaging Applications to NMRI in Medical Research. [22] Worcester Polytechnic Institute. (Includes many 2D-FT NMR images of human brains.)
- Paul Lauterbur. 2003.Nobel Laureate in Physiology and Medicine for (2D and 3D) MRI. [23]
- Jean Jeener. 1971. Two-dimensional Fourier Transform NMR, presented at an Ampere International Summer School, Basko Polje, unpublished. A verbatim quote follows from Richard R. Ernst's Nobel Laureate Lecture delivered on December 2, 1992, "A new approach to measure two-dimensional (2D) spectra." has been proposed by Jean Jeener at an Ampere Summer School in Basko Polje, Yugoslavia, 1971 (Jean Jeneer,1971)). He suggested a 2D Fourier transform experiment consisting of two $\pi/2$ pulses with a variable time t_1 between the pulses and the time variable t_2 measuring the time elapsed after the second pulse as shown in Fig. 6 that expands the principles of Fig. 1. Measuring the response $s(t_1,t_2)$ of the two-pulse sequence and Fourier-transformation with respect to both time variables produces a two-dimensional spectrum $S(O_1,O_2)$ of the desired form. This two-pulse experiment by Jean Jeener is the forefather of a whole class of $2D$ experiments that can also easily be expanded to multidimensional spectroscopy.

- Dudley, Robert, L (1993). "High-Field NMR Instrumentation". *Ch. 10 in Physical Chemistry of Food Processes* (New York: Van Nostrand-Reinhold) **2**: 421-30. ISBN 0-442-00582-2.

- Baianu, I.C.; Kumosinski, Thomas (August 1993). "NMR Principles and Applications to Structure and Hydration,". *Ch.9 in Physical Chemistry of Food Processes* (New York: Van Nostrand-Reinhold) **2**: 338-420. ISBN 0-442-00582-2.

- Haacke, E Mark; Brown, Robert F; Thompson, Michael; Venkatesan, Ramesh (1999). *Magnetic resonance imaging: physical principles and sequence design.* New York: J. Wiley & Sons. ISBN 0-471-35128-8.

- Raftery D (August 2006). "MRI without the magnet [24]". *Proc Natl Acad Sci USA.* **103** (34): 12657−8. doi:10.1073/pnas.0605625103 [25]. PMID 16912110 [26].

- Wu Y, Chesler DA, Glimcher MJ, *et al.* (February 1999). "Multinuclear solid-state three-dimensional MRI of bone and synthetic calcium phosphates [27]". *Proc. Natl. Acad. Sci. U.S.A.* **96** (4): 1574−8. doi:10.1073/pnas.96.4.1574 [28]. PMID 9990066 [29]. PMC 15521 [30].

Related Topics:

- Medical imaging
- Computed tomography
- Magnetic resonance microscopy
- → Fourier transform spectroscopy
- → FT-NIRS
- → Chemical imaging
- Magnetic resonance elastography
- Nuclear magnetic resonance (NMR)
- Chemical shift
- Relaxation
- Robinson oscillator
- Earth's field NMR (EFNMR)
- Rabi cycle

This article incorporates material by the original author from 2D-FT MR- Imaging and related Nobel awards [37] *on* PlanetPhysics [38], *which is licensed under the GFDL.*

References

[1] Antoine Abragam. 1968. *Principles of Nuclear Magnetic Resonance.*, 895 pp., Cambridge University Press: Cambridge, UK.

[2] Lauterbur, P.C., Nobel Laureate in 2003 (1973). "Image Formation by Induced Local Interactions: Examples of Employing Nuclear Magnetic Resonance". *Nature* **242**: 190–1. doi: 10.1038/242190a0 (http://dx.doi.org/10.1038/242190a0).

[3] Howstuffworks "How MRI Works" (http://www.howstuffworks.com/mri.htm/printable)

[4] Peter Mansfield. 2003. Nobel Laureate in Physiology and Medicine for (2D and 3D) MRI (http://www.parteqinnovations.com/pdf-doc/fandr-Gaz1006.pdf)

[5] Damadian, R. V. "Tumor Detection by Nuclear Magnetic Resonance," Science, 171 (March 19, 1971): 1151-1153 (http://www.sciencemag.org/cgi/content/abstract/171/3976/1151)

[6] NMR 'diffraction' in solids? P. Mansfield et al. 1973 J. Phys. C: Solid State Phys. 6 L422-L426 doi: 10.1088/0022-3719 (http://www.iop.org/EJ/article/0022-3719/6/22/007/jcv6i22pL422.pdf)

[7] Raftery D (August 2006). " MRI without the magnet (http://www.pubmedcentral.nih.gov/articlerender.fcgi?tool=pmcentrez&artid=1568902)". *Proc Natl Acad Sci USA*. **103** (34): 12657–8. doi: 10.1073/pnas.0605625103 (http://dx.doi.org/10.1073/pnas.0605625103). PMID 16912110 (http://www.ncbi.nlm.nih.gov/pubmed/16912110).

[8] Wu Y, Chesler DA, Glimcher MJ, *et al.* (February 1999). " Multinuclear solid-state three-dimensional MRI of bone and synthetic calcium phosphates (http://www.pnas.org/cgi/pmidlookup?view=long&pmid=9990066)". *Proc. Natl. Acad. Sci. U.S.A.* **96** (4): 1574–8. doi: 10.1073/pnas.96.4.1574 (http://dx.doi.org/10.1073/pnas.96.4.1574). PMID 9990066 (http://www.ncbi.nlm.nih.gov/pubmed/9990066). PMC 15521 (http://www.pubmedcentral.nih.gov/articlerender.fcgi?tool=pmcentrez&artid=15521). .

[9] http://www.math.cuhk.edu.hk/course/mat2071a/lec1_08.ppt

[10] *Haacke, E Mark; Brown, Robert F; Thompson, Michael; Venkatesan, Ramesh (1999). *Magnetic resonance imaging: physical principles and sequence design*. New York: J. Wiley & Sons. ISBN 0-471-35128-8.

[11] Richard R. Ernst. 1992. Nuclear Magnetic Resonance Fourier Transform (2D-FT) Spectroscopy. Nobel Lecture (http://nobelprize.org/nobel_prizes/chemistry/laureates/1991/ernst-lecture.pdf), on December 9, 1992.

[12] http://en.wikipedia.org/wiki/Nuclear_magnetic_resonance#Nuclear_spin_and_magnets Kurt Wüthrich in 1982-1986 : 2D-FT NMR of solutions

[13] Charles P. Slichter.1996. *Principles of Magnetic Resonance*. Springer: Berlin and New York, Third Edition., 651pp. ISBN 0-387-50157-6.

[14] http://www.physorg.com/news129395045.html

[15] http://nobelprize.org/nobel_prizes/chemistry/laureates/1991/ernst-lecture.pdf

[16] Protein structure determination in solution by NMR spectroscopy (http://www.ncbi.nlm.nih.gov/entrez/query.fcgi?cmd=Retrieve&db=pubmed&dopt=Abstract&list_uids=2266107&query_hl=33&itool=pubmed_docsum) Kurt Wüthrich. J Biol Chem. 1990 December 25;265(36):22059-62.

[17] http://www.mr-tip.com/serv1.php?type=img&img=Cardiac%20Infarct%20Short%20Axis%20Cine%204

[18] http://nobelprize.org/nobel_prizes/chemistry/laureates/2002/wutrich-lecture.pdf

[19] http://www.ncbi.nlm.nih.gov/entrez/query.fcgi?cmd=Retrieve&db=pubmed&dopt=Abstract&list_uids=2266107&query_hl=33&itool=pubmed_docsum

[20] http://upload.wikimedia.org/wikipedia/en/b/bf/HWB-NMRv900.jpg

[21] http://www.parteqinnovations.com/pdf-doc/fandr-Gaz1006.pdf

[22] http://www.wpi.edu/Pubs/ETD/Available/etd-081707-080430/unrestricted/dbennett.pdf

[23] http://nobelprize.org/nobel_prizes/medicine/laureates/2003/

[24] http://www.pubmedcentral.nih.gov/articlerender.fcgi?tool=pmcentrez&artid=1568902

[25] http://dx.doi.org/10.1073%2Fpnas.0605625103

[26] http://www.ncbi.nlm.nih.gov/pubmed/16912110

[27] http://www.pnas.org/cgi/pmidlookup?view=long&pmid=9990066

[28] http://dx.doi.org/10.1073%2Fpnas.96.4.1574

[29] http://www.ncbi.nlm.nih.gov/pubmed/9990066

[30] http://www.pubmedcentral.nih.gov/articlerender.fcgi?tool=pmcentrez&artid=15521

[31] http://www.mr-tip.com/exam_gifs/cardiac_infarct_short_axis_cine_6.gif

[32] http://www.e-mri.org

[33] http://books.nap.edu/html/biomems/hgutowsky.pdf

[34] http://www.patiencys.com/MRI/

[35] http://www.ismrm.org

[36] http://www.simplyphysics.com/flying_objects.html

[37] http://planetphysics.org/encyclopedia/2DFTImaging.html

[38] http://planetphysics.org/

Chemical imaging

Chemical imaging is the analytical capability (as quantitative - mapping) to create a visual image from simultaneous measurement of spectra (as quantitative - chemical) and spatial, time informations. [1] [2] The technique is most often applied to either solid or gel samples, and has applications in chemistry, biology[3] [4] [5] [6] [7] [8] , medicine[9] [10] , pharmacy[11] (see also for example: Chemical Imaging Without Dyeing [12]), food science, biotechnology[13] [14] , agriculture and industry (see for example:NIR Chemical Imaging in Pharmaceutical Industry [15] and Pharmaceutical Process Analytical Technology: [16]). NIR, IR and Raman chemical imaging is also referred to as hyperspectral, spectroscopic, spectral or multispectral imaging (also see microspectroscopy). However, other ultra-sensitive and selective, chemical imaging techniques are also in use that involve either UV-visible or fluorescence microspectroscopy. Chemical imaging techniques can be used to analyze samples of all sizes, from the single molecule[17] [18] to the cellular level in biology and medicine[19] [20] [21] , and to images of planetary systems in astronomy, but different instrumentation is employed for making observations on such widely different systems.

Chemical imaging instrumentation is composed of three components: a radiation source to illuminate the sample, a spectrally selective element, and usually a detector array (the camera) to collect the images. When many stacked spectral channels (wavelengths) are collected for different locations of the microspectrometer focus on a line or planar array in the focal plane, the data is called hyperspectral; fewer wavelength data sets are called multispectral. The data format is called a hypercube. The data set may be visualized as a three-dimensional block of data spanning two spatial dimensions (x and y), with a series of wavelengths (lambda) making up the third (spectral) axis. The hypercube can be visually and mathematically treated as a series of spectrally resolved images (each image plane corresponding to the image at one wavelength) or a series of spatially resolved spectra. The analyst may choose to view the spectrum measured at a particular spatial location; this is useful for chemical identification. Alternatively, selecting an image plane at a particular wavelength can highlight the spatial distribution of sample components, provided that their spectral signatures are different at the selected wavelength.

Many materials, both manufactured and naturally occurring, derive their functionality from the spatial distribution of sample components. For example, extended release pharmaceutical formulations can be achieved by using a coating that acts as a barrier layer. The release of active ingredient is controlled by the presence of this barrier, and imperfections in the coating, such as discontinuities, may result in altered performance. In the semi-conductor industry, irregularities or contaminants in silicon wafers or printed micro-circuits can lead to failure of these components. The functionality of biological systems is also dependent upon chemical gradients – a single cell, tissue, and even whole organs function because of the very specific arrangement of components. It has been shown that even small changes in chemical composition and distribution may be an early indicator of disease.

Any material that depends on chemical gradients for functionality may be amenable to study by an analytical technique that couples spatial and chemical characterization. To efficiently and effectively design and manufacture such materials, the 'what' and the 'where' must both be measured. The demand for this type of analysis is increasing as manufactured materials become more complex. Chemical imaging techniques not only permit visualization of the spatially resolved chemical information that is critical to understanding modern manufactured products, but it is also a non-destructive technique so that samples are preserved for further testing.

History

Commercially available laboratory-based chemical imaging systems emerged in the early 1990s (ref. 1-5). In addition to economic factors, such as the need for sophisticated electronics and extremely high-end computers, a significant barrier to commercialization of infrared imaging was that the focal plane array (FPA) needed to read IR images were not readily available as commercial items. As high-speed electronics and sophisticated computers became more commonplace, and infrared cameras became readily commercially available, laboratory chemical imaging systems were introduced.

Initially used for novel research in specialized laboratories, chemical imaging became a more commonplace analytical technique used for general R&D, quality assurance (QA) and quality control (QC) in less than a decade. The rapid acceptance of the technology in a variety of industries (pharmaceutical, polymers, semiconductors, security, forensics and agriculture) rests in the wealth of information characterizing both chemical composition and morphology. The parallel nature of chemical imaging data makes it possible to analyze multiple samples simultaneously for applications that require high throughput analysis in addition to characterizing a single sample.

Principles

Chemical imaging shares the fundamentals of vibrational spectroscopic techniques, but provides additional information by way of the simultaneous acquisition of spatially resolved spectra. It combines the advantages of digital imaging with the attributes of spectroscopic measurements. Briefly, vibrational spectroscopy measures the interaction of light with matter. Photons that interact with a sample are either absorbed or scattered; photons of specific energy are absorbed, and the pattern of absorption provides information, or a fingerprint, on the molecules that are present in the sample.

On the other hand, in terms of the observation setup, chemical imaging can be carried out in one of the following modes: (optical) absorption, emission (fluorescence), (optical) transmission or scattering (Raman). A consensus currently exists that the fluorescence (emission) and Raman scattering modes are the most sensitive and powerful, but also the most expensive.

In a transmission measurement, the radiation goes through a sample and is measured by a detector placed on the far side of the sample. The energy transferred from the incoming radiation to the molecule(s) can be calculated as the difference between the quantity of photons that were emitted by the source and the quantity that is measured by the detector. In a diffuse reflectance measurement, the same energy difference measurement is made, but the source and detector are located on the same side of the sample, and the photons that are measured have re-emerged from the illuminated side of the sample rather than passed through it. The energy may be measured at one or multiple wavelengths; when a series of measurements are made, the response curve is called a spectrum.

A key element in acquiring spectra is that the radiation must somehow be energy selected – either before or after interacting with the sample. Wavelength selection can be accomplished with a fixed filter, tunable filter, spectrograph, an interferometer, or other devices. For a fixed filter approach, it is not efficient to collect a significant number of wavelengths, and multispectral data are usually collected. Interferometer-based chemical imaging requires that entire spectral ranges be collected, and therefore results in hyperspectral data. Tunable filters have the flexibility to provide either multi- or hyperspectral data, depending on analytical requirements.

Spectra may be measured one point at a time using a single element detector (single-point mapping), as a line-image using a linear array detector (typically 16 to 28 pixels) (linear array mapping), or as a two-dimensional image using a Focal Plane Array (FPA)(typically 256 to 16,384 pixels) (FPA imaging). For single-point the sample is moved in the x and y directions point-by-point using a computer-controlled stage. With linear array mapping, the sample is moved line-by-line with a computer-controlled stage. FPA imaging data are collected with a two-dimensional FPA detector, hence capturing the full desired field-of-view at one time for each individual wavelength, without having to move the sample. FPA imaging, with its ability to collected tens of thousands of spectra simultaneously is orders of magnitude faster than linear arrays which are can typically collect 16 to 28 spectra simultaneously, which are in turn much faster than single-point mapping.

Terminology

Some words common in spectroscopy, optical microscopy and photography have been adapted or their scope modified for their use in chemical imaging. They include: resolution, field of view and magnification. There are two types of resolution in chemical imaging. The spectral resolution refers to the ability to resolve small energy differences; it applies to the spectral axis. The spatial resolution is the minimum distance between two objects that is required for them to be detected as distinct objects. The spatial resolution is influenced by the field of view, a physical measure of the size of the area probed by the analysis. In imaging, the field of view is a product of the magnification and the number of pixels in the detector array. The magnification is a ratio of the physical area of the detector array divided by the area of the sample field of view. Higher magnifications for the same detector image a smaller area of the sample.

Types of vibrational chemical imaging instruments

Chemical imaging has been implemented for mid-infrared, near-→ infrared spectroscopy and → Raman spectroscopy. As with their bulk spectroscopy counterparts, each imaging technique has particular strengths and weaknesses, and are best suited to fulfill different needs.

Mid-infrared chemical imaging

Mid-infrared (MIR) spectroscopy probes fundamental molecular vibrations, which arise in the spectral range 2,500-25,000 nm. Commercial imaging implementations in the MIR region typically employ Fourier Transform Infrared (FT-IR) interferometers and the range is more commonly presented in wavenumber, $4,000 - 400 \text{ cm}^{-1}$. The MIR absorption bands tend to be relatively narrow and well-resolved; direct spectral interpretation is often possible by an experienced spectroscopist. MIR spectroscopy can distinguish subtle changes in chemistry and structure, and is often used for the identification of unknown materials. The absorptions in this spectral range are relatively strong; for this reason, sample presentation is important to limit the amount of material interacting with the incoming radiation in the MIR region. Most data collected in this range is collected in transmission mode through thin sections (~10 micrometres) of material. Water is a very strong absorber of MIR radiation and wet samples often require advanced sampling procedures (such as attenuated total reflectance). Commercial instruments include point and line mapping, and imaging. All employ an FT-IR interferometer as wavelength selective element and light source.

For types of MIR microscope, see Microscopy#infrared microscopy.

Atmospheric windows in the infrared spectrum are also employed to perform chemical imaging remotely. In these spectral regions the atmospheric gases (mainly water and CO_2) present low absorption and allow infrared viewing over kilometer distances. Target molecules can then be viewed using the selective absorption/emission processes

Remote chemical imaging of a simultaneous release of SF_6 and NH_3 at 1.5km using the FIRST imaging spectrometer[22]

described above. An example of the chemical imaging of a simultaneous release of SF_6 and NH_3 is shown in the image.

Near-infrared chemical imaging

The analytical near infrared (NIR) region spans the range from approximately 700-2,500 nm. The absorption bands seen in this spectral range arise from overtones and combination bands of O-H, N-H, C-H and S-H stretching and bending vibrations. Absorption is one to two orders of magnitude smaller in the NIR compared to the MIR; this phenomenon eliminates the need for extensive sample preparation. Thick and thin samples can be analyzed without any sample preparation, it is possible to acquire NIR chemical images through some packaging materials, and the technique can be used to examine hydrated samples, within limits. Intact samples can be imaged in transmittance or diffuse reflectance.

The lineshapes for overtone and combination bands tend to be much broader and more overlapped than for the fundamental bands seen in the MIR. Often, multivariate methods are used to separate spectral signatures of sample components. NIR chemical imaging is particularly useful for performing rapid, reproducible and non-destructive analyses of known materials[23] [24] . NIR imaging instruments are typically based on one of two platforms: imaging using a tunable filter and broad band illumination, and line mapping employing an FT-IR interferometer as the wavelength filter and light source.

Raman chemical imaging

The Raman shift chemical imaging spectral range spans from approximately 50 to 4,000 cm^{-1}; the actual spectral range over which a particular Raman measurement is made is a function of the laser excitation frequency. The basic principle behind → Raman spectroscopy differs from the MIR and NIR in that the x-axis of the Raman spectrum is measured as a function of energy shift (in cm^{-1}) relative to the frequency of the laser used as the source of radiation. Briefly, the Raman spectrum arises from inelastic scattering of incident photons, which requires a change in polarizability with vibration, as opposed to infrared absorption, which requires a change in dipole moment with vibration. The end result is spectral information that is similar and in many cases complementary to the MIR. The Raman effect is weak - only about one in 10^7 photons incident to the sample undergoes Raman scattering. Both organic and inorganic materials possess a Raman spectrum; they generally produce sharp bands that are chemically specific. Fluorescence is a competing phenomenon and, depending on the sample, can overwhelm the Raman signal, for both bulk spectroscopy and imaging implementations.

Raman chemical imaging requires little or no sample preparation. However, physical sample sectioning may be used to expose the surface of interest, with care taken to obtain a surface that is as flat as possible. The conditions required for a particular measurement dictate the level of invasiveness of the technique, and samples that are sensitive to high power laser radiation may be damaged during analysis. It is relatively insensitive to the presence of water in the sample and is therefore useful for imaging samples that contain water such as biological material.

Fluorescence imaging (visible and NIR)

This emission microspectroscopy mode is the most sensitive in both visible and FT-NIR microspectroscopy, and has therefore numerous biomedical, biotechnological and agricultural applications. There are several powerful, highly specific and sensitive fluorescence techniques that are currently in use, or still being developed; among the former are FLIM, FRAP, FRET and FLIM-FRET; among the latter are NIR fluorescence and probe-sensitivity enhanced NIR fluorescence microspectroscopy and nanospectroscopy techniques (see "Further reading" section).

Sampling and samples

The value of imaging lies in the ability to resolve spatial heterogeneities in solid-state or gel/gel-like samples. Imaging a liquid or even a suspension has limited use as constant sample motion serves to average spatial information, unless ultra-fast recording techniques are employed as in fluorescence correlation microspectroscopy or FLIM obsevations where a single molecule may be monitored at extremely high (photon) detection speed. High-throughput experiments (such as imaging multi-well plates) of liquid samples can however provide valuable

information. In this case, the parallel acquisition of thousands of spectra can be used to compare differences between samples, rather than the more common implementation of exploring spatial heterogeneity within a single sample.

Similarly, there is no benefit in imaging a truly homogeneous sample, as a single point spectrometer will generate the same spectral information. Of course the definition of homogeneity is dependent on the spatial resolution of the imaging system employed. For MIR imaging, where wavelengths span from 3-10 micrometres, objects on the order of 5 micrometres may theoretically be resolved. The sampled areas are limited by current experimental implementations because illumination is provided by the interferometer. Raman imaging may be able to resolve particles less than 1 micrometre in size, but the sample area that can be illuminated is severely limited. With Raman imaging, it is considered impractical to image large areas and, consequently, large samples. FT-NIR chemical/hyperspectral imaging usually resolves only larger objects (>10 micrometres), and is better suited for large samples because illumination sources are readily available. However, FT-NIR microspectroscopy was recently reported to be capable of about 1.2 micron (micrometer) resolution in biological samples[25] Furthermore, two-photon excitation FCS experiments were reported to have attained 15 nanometer resolution on biomembrane thin films with a special coincidence photon-counting setup.

Detection limit

The concept of the detection limit for chemical imaging is quite different than for bulk spectroscopy, as it depends on the sample itself. Because a bulk spectrum represents an average of the materials present, the spectral signatures of trace components are simply overwhelmed by dilution. In imaging however, each pixel has a corresponding spectrum. If the physical size of the trace contaminant is on the order of the pixel size imaged on the sample, its spectral signature will likely be detectable. If however, the trace component is dispersed homogeneously (relative to pixel image size) throughout a sample, it will not be detectable. Therefore, detection limits of chemical imaging techniques are strongly influenced by particle size, the chemical and spatial heterogeneity of the sample, and the spatial resolution of the image.

Data analysis

Data analysis methods for chemical imaging data sets typically employ mathematical algorithms common to single point spectroscopy or to image analysis. The reasoning is that the spectrum acquired by each detector is equivalent to a single point spectrum; therefore pre-processing, chemometrics and pattern recognition techniques are utilized with the similar goal to separate chemical and physical effects and perform a qualitative or quantitative characterization of individual sample components. In the spatial dimension, each chemical image is equivalent to a digital image and standard image analysis and robust statistical analysis can be used for feature extraction.

Related Topics:

- chemical mapping
- Multispectral image
- Microspectroscopy
- Imaging spectroscopy

Further reading

1. E. N. Lewis, P. J. Treado, I. W. Levin, Near-Infrared and Raman Spectroscopic Imaging, American Laboratory, 06/1994:16 (1994)
2. E. N. Lewis, P. J. Treado, R. C. Reeder, G. M. Story, A. E. Dowrey, C. Marcott, I. W. Levin, FTIR spectroscopic imaging using an infrared focal-plane array detector, Analytical Chemistry, 67:3377 (1995)

3. P. Colarusso, L. H. Kidder, I. W. Levin, J. C. Fraser, E. N. Lewis Infrared Spectroscopic Imaging: from Planetary to Cellular Systems, Applied Spectroscopy, 52 (3):106A (1998)

4. P. J. Treado I. W. Levin, E. N. Lewis, Near-Infrared Spectroscopic Imaging Microscopy of Biological Materials Using an Infrared Focal-Plane Array and an Acousto-Optic Tunable Filter (AOTF), Applied Spectroscopy, 48:5 (1994)

5. Hammond, S.V., Clarke, F. C., Near-infrared microspectroscopy. In: Handbook of Vibrational Spectroscopy, Vol. 2, J.M. Chalmers and P.R. Griffiths Eds. John Wiley and Sons, West Sussex, UK, 2002, p.1405-1418

6. L.H. Kidder, A.S. Haka, E.N. Lewis, Instrumentation for FT-IR Imaging. In: Handbook of Vibrational Spectroscopy, Vol. 2, J.M. Chalmers and P.R. Griffiths Eds. John Wiley and Sons, West Sussex, UK, 2002, pp.1386-1404

7. J. Zhang; A. O'Connor; J. F. Turner II, Cosine Histogram Analysis for Spectral Image Data Classification,Applied Spectroscopy, Volume 58, Number 11, November 2004, pp. 1318-1324(7)

8. J. F. Turner II; J. Zhang; A. O'Connor, A Spectral Identity Mapper for Chemical Image Analysis, Applied Spectroscopy, Volume 58, Number 11, November 2004, pp. 1308-1317(10)

9. H. R. MORRIS, J. F. TURNER II, B. MUNRO, R. A. RYNTZ, P. J. TREADO, Chemical imaging of thermoplastic olefin (TPO) surface architecture, Langmuir, 1999, vol. 15, no8, pp. 2961-2972

10. J. F. Turner II, Chemical imaging and spectroscopy using tunable filters: Instrumentation, methodology, and multivariate analysis, Thesis (PhD). UNIVERSITY OF PITTSBURGH, Source DAI-B 59/09, p. 4782, Mar 1999, 286 pages.

11. P. Schwille.(2001). in *Fluorescence Correlation Spectroscopy. Theory and applications.* R. Rigler & E.S. Elson, eds., p. 360. Springer Verlag: Berlin.

12. Schwille P., Oehlenschläger F. and Walter N. (1996). Analysis of RNA-DNA hybridization kinetics by fluorescence correlation spectroscopy, *Biochemistry* 35:10182.

13. FLIM | Fluorescence Lifetime Imaging Microscopy: Fluorescence, fluorophore chemical imaging, confocal emission microspectroscopy, FRET, cross-correlation fluorescence microspectroscopy [26].

14. FLIM Applications: [26] "FLIM is able to discriminate between fluorescence emanating from different fluorophores and autofloresing molecules in a specimen, even if their emission spectra are similar. It is, therefore, ideal for identifying fluorophores in multi-label studies. FLIM can also be used to measure intracellular ion concentrations without extensive calibration procedures (for example, Calcium Green) and to obtain information about the local environment of a fluorophore based on changes in its lifetime." FLIM is also often used in microspectroscopic/chemical imaging, or microscopic, studies to monitor spatial and temporal protein-protein interactions, properties of membranes and interactions with nucleic acids in living cells.

15. Gadella TW Jr., *FRET and FLIM techniques*, 33. Imprint: Elsevier, ISBN 978-0-08-054958-3. (2008) 560 pages

16. Langel FD, et al., Multiple protein domains mediate interaction between Bcl10 and Malt1, *J. Biol. Chem.*, (2008) 283(47):32419-31

17. Clayton AH., The polarized AB plot for the frequency-domain analysis and representation of fluorophore rotation and resonance energy homotransfer. J *Microscopy*. (2008) 232(2):306-12

18. Clayton AH, et al., Predominance of activated EGFR higher-order oligomers on the cell surface. *Growth Factors* (2008) 20:1

19. Plowman et al., Electrostatic Interactions Positively Regulate K-Ras Nanocluster Formation and Function. *Molecular and Cellular Biology* (2008) 4377–4385

20. Belanis L, et al., Galectin-1 Is a Novel Structural Component and a Major Regulator of H-Ras Nanoclusters. *Molecular Biology of the Cell* (2008) 19:1404–1414

21. Van Manen HJ, Refractive index sensing of green fluorescent proteins in living cells using fluorescence lifetime imaging microscopy. Biophys J. (2008) 94(8):L67-9

22. Van der Krogt GNM, et al., A Comparison of Donor-Acceptor Pairs for Genetically Encoded FRET Sensors: Application to the Epac cAMP Sensor as an Example, PLoS ONE, (2008) 3(4):e1916

23. Dai X, et al., Fluorescence intensity and lifetime imaging of free and micellar-encapsulated doxorubicin in living cells. *Nanomedicine*. (2008) 4(1):49-56.

References

[1] http://www.imaging.net/chemical-imaging/Chemical imaging

[2] http://www.malvern.com/LabEng/products/sdi/bibliography/sdi_bibliography.htm E. N. Lewis, E. Lee and L. H. Kidder, Combining Imaging and Spectroscopy: Solving Problems with Near-Infrared Chemical Imaging. Microscopy Today, Volume 12, No. 6, 11/2004.

[3] C.L. Evans and X.S. Xie.2008. Coherent Anti-Stokes Raman Scattering Microscopy: Chemical Imaging for Biology and Medicine., doi:10.1146/annurev.anchem.1.031207.112754 *Annual Review of Analytical Chemistry*, **1**: 883-909.

[4] Diaspro, A., and Robello, M. (1999). Multi-photon Excitation Microscopy to Study Biosystems. European Microscopy and Analysis., 5:5-7.

[5] D.S. Mantus and G. H. Morrison. 1991. Chemical imaging in biology and medicine using ion microscopy., *Microchimica Acta*, **104**, (1-6) January 1991, doi: 10.1007/BF01245536

[6] Bagatolli, L.A., and Gratton, E. (2000). Two-photon fluorescence microscopy of coexisting lipid domains in giant unilamellar vesicles of binary phospholipid mixtures. Biophys J., 78:290-305.

[7] Schwille, P., Haupts, U., Maiti, S., and Webb. W.(1999). Molecular dynamics in living cells observed by fluorescence correlation spectroscopy with one- and two-photon excitation. Biophysical Journal, 77(10):2251-2265.

[8] 1.Lee, S. C. et al., (2001). One Micrometer Resolution NMR Microscopy. J. Magn. Res., 150: 207-213.

[9] Near Infrared Microspectroscopy, Fluorescence Microspectroscopy,Infrared Chemical Imaging and High Resolution Nuclear Magnetic Resonance Analysis of Soybean Seeds, Somatic Embryos and Single Cells., Baianu, I.C. et al. 2004., In *Oil Extraction and Analysis.*, D. Luthria, Editor pp.241-273, AOCS Press., Champaign, IL.

[10] Single Cancer Cell Detection by Near Infrared Microspectroscopy, Infrared Chemical Imaging and Fluorescence Microspectroscopy.2004.I. C. Baianu, D. Costescu, N. E. Hofmann and S. S. Korban, q-bio/0407006 (July 2004) (http://arxiv.org/abs/q-bio/0407006)

[11] J. Dubois, G. Sando, E. N. Lewis, Near-Infrared Chemical Imaging, A Valuable Tool for the Pharmaceutical Industry, G.I.T. Laboratory Journal Europe, No. 1-2, 2007.

[12] http://witec.de/en/download/Raman/ImagingMicroscopy04.pdf

[13] Raghavachari, R., Editor. 2001. *Near-Infrared Applications in Biotechnology*, Marcel-Dekker, New York, NY.

[14] Applications of Novel Techniques to Health Foods, Medical and Agricultural Biotechnology.(June 2004) I. C. Baianu, P. R. Lozano, V. I. Prisecaru and H. C. Lin q-bio/0406047 (http://arxiv.org/abs/q-bio/0406047)

[15] http://www.spectroscopyeurope.com/NIR_14_3.pdf

[16] http://www.fda.gov/cder/OPS/PAT.htm

[17] Eigen, M., and Rigler, R. (1994). Sorting single molecules: Applications to diagnostics and evolutionary biotechnology, Proc. Natl. Acad. Sci. USA 91:5740.

[18] Rigler R. and Widengren J. (1990). Ultrasensitive detection of single molecules by fluorescence correlation spectroscopy, *BioScience* (Ed. Klinge & Owman) p.180.

[19] Single Cancer Cell Detection by Near Infrared Microspectroscopy, Infrared Chemical Imaging and Fluorescence Microspectroscopy.2004.I. C. Baianu, D. Costescu, N. E. Hofmann, S. S. Korban and et al., q-bio/0407006 (July 2004) (http://arxiv.org/abs/q-bio/0407006)

[20] Oehlenschläger F., Schwille P. and Eigen M. (1996). Detection of HIV-1 RNA by nucleic acid sequence-based amplification combined with fluorescence correlation spectroscopy, *Proc. Natl. Acad. Sci. USA* **93**:1281.

[21] Near Infrared Microspectroscopy, Fluorescence Microspectroscopy,Infrared Chemical Imaging and High Resolution Nuclear Magnetic Resonance Analysis of Soybean Seeds, Somatic Embryos and Single Cells., Baianu, I.C. et al. 2004., In *Oil Extraction and Analysis.*, D. Luthria, Editor pp.241-273, AOCS Press., Champaign, IL.

[22] M. Chamberland, V. Farley, A. Vallières, L. Belhumeur, A. Villemaire, J. Giroux et J. Legault, High-Performance Field-Portable Imaging Radiometric Spectrometer Technology For Hyperspectral imaging Applications, Proc. SPIE 5994, 59940N, September 2005.

[23] Novel Techniques for Microspectroscopy and Chemical Imaging Analysis of Soybean Seeds and Embryos.(2002). Baianu, I.C., Costescu, D.M., and You, T. *Soy2002 Conference*, Urbana, Illinois.

[24] Near Infrared Microspectroscopy, Chemical Imaging and NMR Analysis of Oil in Developing and Mutagenized Soybean Embryos in Culture. (2003). Baianu, I.C., Costescu, D.M., Hofmann, N., and Korban, S.S. *AOCS Meeting, Analytical Division*.

[25] Near Infrared Microspectroscopy, Fluorescence Microspectroscopy,Infrared Chemical Imaging and High Resolution Nuclear Magnetic Resonance Analysis of Soybean Seeds, Somatic Embryos and Single Cells., Baianu, I.C. et al. 2004., In *Oil Extraction and Analysis.*, D.

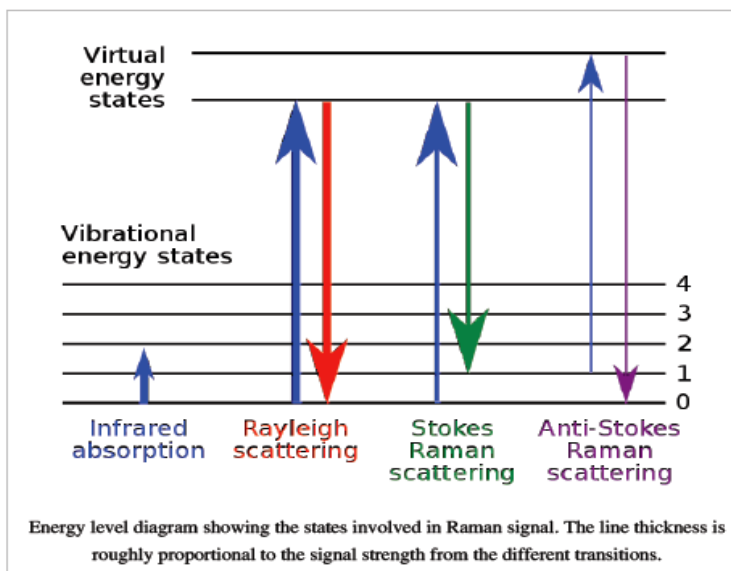Luthria, Editor pp.241-273, AOCS Press., Champaign, IL.

[26] http://www.nikoninstruments.com/infocenter.php?n=FLIM

[27] http://www.spectroscopymag.com/spectroscopy/Near-IR+Spectroscopy/NIR-Chemical-Imaging-for-Counterfeit-Pharmaceutica/
      ArticleStandard/Article/detail/406629

[28] http://www.sciencedaily.com/releases/2007/08/070802103435.htm

Raman spectroscopy

Raman spectroscopy (named after C. V. Raman, pronounced /ˈrɑːmən/) is a → spectroscopic technique used to study vibrational, rotational, and other low-frequency modes in a system.[1] It relies on inelastic scattering, or Raman scattering, of monochromatic light, usually from a laser in the visible, near infrared, or near ultraviolet range. The laser light interacts with phonons or other excitations in the system, resulting in the energy of the laser photons being shifted up or down. The shift in energy gives information about the phonon modes in the system. → Infrared spectroscopy yields similar, but complementary, information.

Energy level diagram showing the states involved in Raman signal. The line thickness is roughly proportional to the signal strength from the different transitions.

Typically, a sample is illuminated with a laser beam. Light from the illuminated spot is collected with a lens and sent through a monochromator. Wavelengths close to the laser line, due to elastic Rayleigh scattering, are filtered out while the rest of the collected light is dispersed onto a detector.

Spontaneous Raman scattering is typically very weak, and as a result the main difficulty of Raman spectroscopy is separating the weak inelastically scattered light from the intense Rayleigh scattered laser light. Historically, Raman spectrometers used holographic gratings and multiple dispersion stages to achieve a high degree of laser rejection. In the past, photomultipliers were the detectors of choice for dispersive Raman setups, which resulted in long acquisition times. However, modern instrumentation almost universally employs notch or edge filters for laser rejection and spectrographs (either axial transmissive (AT), Czerny-Turner (CT) monochromator) or FT (→ Fourier transform spectroscopy based), and CCD detectors.

There are a number of advanced types of Raman spectroscopy, including surface-enhanced Raman, tip-enhanced Raman, polarised Raman, stimulated Raman (analogous to stimulated emission), transmission Raman, spatially-offset Raman, and hyper Raman.

Basic theory

The Raman effect occurs when light impinges upon a molecule and interacts with the electron cloud and the bonds of that molecule. For the spontaneous Raman effect, a photon excites the molecule from the ground state to a virtual energy state. When the molecule emits a photon and returns to the ground state, it returns to a different rotational or vibrational state. The difference in energy between the original state and this new state leads to a shift in the emitted photon's frequency away from the excitation frequency.

If the final state of the molecule is more energetic than the initial state, then the emitted photon will be shifted to a lower frequency in order for the total energy of the system to remain balanced. This shift in frequency is designated as a Stokes shift. If the final state is less energetic than the initial state, then the emitted photon will be shifted to a higher frequency, and this is designated as an anti-Stokes shift. Raman scattering is an example of inelastic scattering because of the energy transfer between the photons and the molecules during their interaction.

A change in the molecular polarization potential — or amount of deformation of the electron cloud — with respect to the vibrational coordinate is required for a molecule to exhibit a Raman effect. The amount of the polarizability change will determine the Raman scattering intensity. The pattern of shifted frequencies is determined by the rotational and vibrational states of the sample.

History

Although the inelastic scattering of light was predicted by Adolf Smekal in 1923, it was not until 1928 that it was observed in practice. The Raman effect was named after one of its discoverers, the Indian scientist Sir C. V. Raman who observed the effect by means of sunlight (1928, together with K. S. Krishnan and independently by Grigory Landsberg and Leonid Mandelstam).[1] Raman won the Nobel Prize in Physics in 1930 for this discovery accomplished using sunlight, a narrow band photographic filter to create monochromatic light and a "crossed" filter to block this monochromatic light. He found that light of changed frequency passed through the "crossed" filter.

Systematic pioneering theory of the Raman effect was developed by Czechoslovak physicist George Placzek between 1930 and 1934.[2] The mercury arc became the principal light source, first with photographic detection and then with spectrophotometric detection. Currently lasers are used as light sources.

Applications

Raman spectroscopy is commonly used in chemistry, since vibrational information is specific to the chemical bonds and symmetry of molecules. It therefore provides a fingerprint by which the molecule can be identified. For instance, the vibrational frequencies of SiO, Si_2O_2, and Si_3O_3 were identified and assigned on the basis of normal coordinate analyses using infrared and Raman spectra.[3] The fingerprint region of organic molecules is in the (wavenumber) range 500-2000 cm^{-1}. Another way that the technique is used is to study changes in chemical bonding, e.g., when a substrate is added to an enzyme.

Raman gas analyzers have many practical applications. For instance, they are used in medicine for real-time monitoring of anaesthetic and respiratory gas mixtures during surgery.

In solid state physics, spontaneous Raman spectroscopy is used to, among other things, characterize materials, measure temperature, and find the crystallographic orientation of a sample. As with single molecules, a given solid material has characteristic phonon modes that can help an experimenter identify it. In addition, Raman spectroscopy can be used to observe other low frequency excitations of the solid, such as plasmons, magnons, and superconducting gap excitations. The spontaneous Raman signal gives information on the population of a given phonon mode in the ratio between the Stokes (downshifted) intensity and anti-Stokes (upshifted) intensity.

Raman scattering by an anisotropic crystal gives information on the crystal orientation. The → polarization of the Raman scattered light with respect to the crystal and the polarization of the laser light can be used to find the orientation of the crystal, if the crystal structure (specifically, its point group) is known.

Raman active fibers, such as aramid and carbon, have vibrational modes that show a shift in Raman frequency with applied stress. Polypropylene fibers also exhibit similar shifts. The radial breathing mode is a commonly used technique to evaluate the diameter of carbon nanotubes. In nanotechnology, a Raman microscope can be used to analyze nanowires to better understand the composition of the structures.

Spatially-offset Raman spectroscopy (SORS), which is less sensitive to surface layers than conventional Raman, can be used to discover counterfeit drugs without opening their internal packaging, and for non-invasive monitoring of biological tissue.[4] Raman spectroscopy can be used to investigate the chemical composition of historical documents such as the Book of Kells and contribute to knowledge of the social and economic conditions at the time the documents were produced.[5] This is especially helpful because Raman spectroscopy offers a non-invasive way to determine the best course of preservation or conservation treatment for such materials.

Raman spectroscopy is being investigated as a means to detect explosives for airport security.[6]

Microspectroscopy

Raman spectroscopy offers several advantages for microscopic analysis. Since it is a scattering technique, specimens do not need to be fixed or sectioned. Raman spectra can be collected from a very small volume (< 1 μm in diameter); these spectra allow the identification of species present in that volume. Water does not generally interfere with Raman spectral analysis. Thus, Raman spectroscopy is suitable for the microscopic examination of minerals, materials such as polymers and ceramics, cells and proteins. A Raman microscope begins with a standard optical microscope, and adds an excitation laser, a monochromator, and a sensitive detector (such as a charge-coupled device (CCD), or photomultiplier tube (PMT)). → FT-Raman has also been used with microscopes.

In *direct imaging*, the whole field of view is examined for scattering over a small range of wavenumbers (Raman shifts). For instance, a wavenumber characteristic for cholesterol could be used to record the distribution of cholesterol within a cell culture.

The other approach is *hyperspectral imaging* or → *chemical imaging*, in which thousands of Raman spectra are acquired from all over the field of view. The data can then be used to generate images showing the location and amount of different components. Taking the cell culture example, a hyperspectral image could show the distribution of cholesterol, as well as proteins, nucleic acids, and fatty acids. Sophisticated signal- and image-processing techniques can be used to ignore the presence of water, culture media, buffers, and other interferents.

Raman microscopy, and in particular confocal microscopy, has very high spatial resolution. For example, the lateral and depth resolutions were 250 nm and 1.7 μm, respectively, using a confocal Raman microspectrometer with the 632.8 nm line from a He-Ne laser with a pinhole of 100 μm diameter. Since the objective lenses of microscopes focus the laser beam to several micrometres in diameter, the resulting photon flux is much higher than achieved in conventional Raman setups. This has the added benefit of enhanced fluorescence quenching. However, the high photon flux can also cause sample degradation, and for this reason some setups require a thermally conducting substrate (which acts as a heat sink) in order to mitigate this process.

By using Raman microspectroscopy, *in vivo* time- and space-resolved Raman spectra of microscopic regions of samples can be measured. As a result, the fluorescence of water, media, and buffers can be removed. Consequently *in vivo* time- and space-resolved Raman spectroscopy is suitable to examine proteins, cells and organs.

Raman microscopy for biological and medical specimens generally uses near-infrared (NIR) lasers (785 nm diodes and 1064 nm Nd:YAG are especially common). This reduces the risk of damaging the specimen by applying higher energy wavelengths. However, the intensity of NIR Raman is low (owing to the ω^4 dependence of Raman scattering intensity), and most detectors required very long collection times. Recently, more sensitive detectors have become available, making the technique better suited to general use. Raman microscopy of inorganic specimens, such as rocks and ceramics and polymers, can use a broader range of excitation wavelengths.[7]

Polarized analysis

The $\rightarrow$ polarization of the Raman scattered light also contains useful information. This property can be measured using (plane) polarized laser excitation and a polarization analyzer. Spectra acquired with the analyzer set at both perpendicular and parallel to the excitation plane can be used to calculate the depolarization ratio. Study of the technique is pedagogically useful in teaching the connections between group theory, symmetry, Raman activity and peaks in the corresponding Raman spectra.

The spectral information arising from this analysis gives insight into molecular orientation and vibrational symmetry. In essence, it allows the user to obtain valuable information relating to the molecular shape, for example in synthetic chemistry or polymorph analysis. It is often used to understand macromolecular orientation in crystal lattices, liquid crystals or polymer samples.[8]

Variations

Several variations of Raman spectroscopy have been developed. The usual purpose is to enhance the sensitivity (e.g., surface-enhanced Raman), to improve the spatial resolution (Raman microscopy), or to acquire very specific information (resonance Raman).

- **Surface Enhanced Raman Spectroscopy (SERS)** - Normally done in a silver or gold colloid or a substrate containing silver or gold. Surface plasmons of silver and gold are excited by the laser, resulting in an increase in the electric fields surrounding the metal. Given that Raman intensities are proportional to the electric field, there is large increase in the measured signal (by up to 10^{11}). This effect was originally observed by Martin Fleischmann but the prevailing explanation was proposed by Van Duyne in 1977.[9]
- **Resonance Raman spectroscopy** - The excitation wavelength is matched to an electronic transition of the molecule or crystal, so that vibrational modes associated with the excited electronic state are greatly enhanced. This is useful for studying large molecules such as polypeptides, which might show hundreds of bands in "conventional" Raman spectra. It is also useful for associating normal modes with their observed frequency shifts.[10]
- **Surface Enhanced Resonance Raman Spectroscopy (SERRS)** - A combination of SERS and resonance Raman spectroscopy which uses proximity to a surface to increase Raman intensity, and excitation wavelength matched to the maximum absorbance of the molecule being analysed.
- **Hyper Raman** - A non-linear effect in which the vibrational modes interact with the second harmonic of the excitation beam. This requires very high power, but allows the observation of vibrational modes which are normally "silent". It frequently relies on SERS-type enhancement to boost the sensitivity.[11]
- **Spontaneous Raman Spectroscopy** - Used to study the temperature dependence of the Raman spectra of molecules.
- **Optical Tweezers Raman Spectroscopy (OTRS)** - Used to study individual particles, and even biochemical processes in single cells trapped by optical tweezers.
- **Stimulated Raman Spectroscopy** - A spatially coincident, two color pulse transfers the population from ground to a rovibrationally excited state, if the difference in energy corresponds to an allowed Raman transition, and if neither frequency corresponds to an electronic resonance. Two photon UV ionization, applied after the population transfer but before relaxation, allows the intra-molecular or inter-molecular Raman spectrum of a gas or molecular cluster (indeed, a given conformation of molecular cluster) to be collected. This is a useful molecular dynamics technique.
- **Spatially Offset Raman Spectroscopy (SORS)** - The Raman scatter is collected from regions laterally offset away from the excitation laser spot, leading to significantly lower contributions from the surface layer than with traditional Raman spectroscopy.[12]
- **Coherent anti-Stokes Raman spectroscopy (CARS)** - Two laser beams are used to generate a coherent anti-Stokes frequency beam, which can be enhanced by resonance.

- **Raman optical activity (ROA)** - Measures vibrational optical activity by means of a small difference in the intensity of Raman scattering from chiral molecules in right- and left-circularly polarized incident light or, equivalently, a small circularly polarized component in the scattered light.[13]
- **Transmission Raman** - Allows probing of a significant bulk of a turbid material, such as powders, capsules, living tissue, etc. It was largely ignored following investigations in the late 1960s[14] but was rediscovered in 2006 as a means of rapid assay of pharmaceutical dosage forms.[15] There are also medical diagnostic applications.[16]
- **Inverse Raman spectroscopy.**
- **Tip-Enhanced Raman Spectroscopy (TERS)** - Uses a silver or gold tip to enhance the Raman signals of molecules situated in its vicinity. The spatial resolution is approximately the size of the tip apex (20-30 nm). TERS has been shown to have sensitivity down to the single molecule level.

Related Topics:

- An introduction to Raman spectroscopy [17]
- Raman Application examples [18]
- A introduction on Raman Scattering [19]
- Chemical Imaging Without Dyeing [12] - Chemical Imaging Without Dyeing
- DoITPoMS Teaching and Learning Package - Raman Spectroscopy [20] - an introduction, aimed at undergraduate level
- Raman Spectroscopy Tutorial [21] - A detailed explanation of Raman Spectroscopy including Resonance-Enhanced Raman Scattering and Surface-Enhanced Raman Scattering.
- The Science Show, ABC Radio National [22] - Interview with Scientist on NASA funded project to build Raman Spectrometer for the 2009 Mars mission: a cellular phone size device to detect almost any substance known, with commercial <USD$5000 commercial spin-off, prototyped by June 2006.
- Raman spectroscopy for medical diagnosis [23] from the June 1, 2007 issue of *Analytical Chemistry* [24]
- Spontaneous Raman Scattering (SRS) [25]

References

[1] Gardiner, D.J. (1989). *Practical Raman spectroscopy*. Springer-Verlag. ISBN 978-0387502540.

[2] Placzek G.: "Rayleigh Streeung und Raman Effekt", In: Hdb. der Radiologie, Vol. VI., 2, 1934, p. 209

[3] Khanna, R.K. (1981). "Raman-spectroscopy of oligomeric SiO species isolated in solid methane". *Journal of Chemical Physics*. doi: 10.1063/1.441393 (http://dx.doi.org/10.1063/1.441393).

[4] . BBC News. 2007-01-31. http://news.bbc.co.uk/2/hi/health/6314287.stm. Retrieved 2008-12-08.

[5] Irish Classic Is Still a Hit (in Calfskin, Not Paperback) - New York Times (http://www.nytimes.com/2007/05/28/world/europe/28kells.html)

[6] Ben Vogel (29 August 2008). " Raman spectroscopy portends well for standoff explosives detection (http://www.janes.com/news/transport/business/jar/jar080829_1_n.shtml)". Jane's. . Retrieved 2008-08-29.

[7] Ellis DI, Goodacre R (August 2006). "Metabolic fingerprinting in disease diagnosis: biomedical applications of infrared and Raman spectroscopy". *Analyst* 131 (8): 875–85. doi: 10.1039/b602376m (http://dx.doi.org/10.1039/b602376m). PMID 17028718 (http://www.ncbi.nlm.nih.gov/pubmed/17028718).

[8] Khanna, R.K. (1957). *Evidence of ion-pairing in the polarized Raman spectra of a Ba2+CrO doped KI single crystal*. John Wiley & Sons, Ltd. doi: 10.1002/jrs.1250040104 (http://dx.doi.org/10.1002/jrs.1250040104).

[9] Jeanmaire DL, van Duyne RP (1977). "Surface Raman Electrochemistry Part I. Heterocyclic, Aromatic and Aliphatic Amines Adsorbed on the Anodized Silver Electrode". *Journal of Electroanalytical Chemistry* (Elsevier Sequouia S.A.) 84: 1–20. doi: 10.1016/S0022-0728(77)80224-6 (http://dx.doi.org/10.1016/S0022-0728(77)80224-6).

[10] Chao RS, Khanna RK, Lippincott ER (1974). "Theoretical and experimental resonance Raman intensities for the manganate ion". *J Raman Spectroscopy* 3: 121. doi: 10.1002/jrs.1250030203 (http://dx.doi.org/10.1002/jrs.1250030203).

[11] Kneipp K, *et al.* (1999). "Surface-Enhanced Non-Linear Raman Scattering at the Single Molecule Level". *Chem. Phys.* 247: 155–162. doi: 10.1016/S0301-0104(99)00165-2 (http://dx.doi.org/10.1016/S0301-0104(99)00165-2).

[12] Matousek P, Clark IP, Draper ERC, *et al.* (2005). "Subsurface Probing in Diffusely Scattering Media using Spatially Offset Raman Spectroscopy". *Applied Spectroscopy* 59: 393. doi: 10.1366/000370205775142548 (http://dx.doi.org/10.1366/000370205775142548).

[13] Barron LD, Hecht L, McColl IH, Blanch EW (2004). "Raman optical activity comes of age". *Molec. Phys.* 102 (8): 731–744. doi: 10.1080/00268970410001704399 (http://dx.doi.org/10.1080/00268970410001704399).

[14] B. Schrader, G. Bergmann, Fresenius. Z. (1967). *Anal. Chem.*: 225–230.

[15] P. Matousek, A. W. Parker (2006). "Bulk Raman Analysis of Pharmaceutical Tablets". *Applied Spectroscopy* 60: 1353–1357. doi: 10.1366/000370206779321463 (http://dx.doi.org/10.1366/000370206779321463).

[16] P. Matousek, N. Stone (2007). "Prospects for the diagnosis of breast cancer by noninvasive probing of calcifications using transmission Raman spectroscopy". *Journal of Biomedical Optics* 12: 024008. doi: 10.1117/1.2718934 (http://dx.doi.org/10.1117/1.2718934).

[17] http://www.horiba.com/us/en/scientific/products/raman-spectroscopy/raman-resource/raman-tutorial/

[18] http://www.horiba.com/scientific/products/raman-spectroscopy/application-notes/

[19] http://www.d3technologies.co.uk/en/10371.aspx

[20] http://www.doitpoms.ac.uk/tlplib/raman/index.php

[21] http://161.58.205.25/Raman_Spectroscopy/rtr-ramantutorial.php?ss=800

[22] http://www.abc.net.au/rn/science/ss/stories/s1581469.htm

[23] http://pubs.acs.org/subscribe/journals/ancham/79/i11/pdf/0607feature_griffiths.pdf

[24] http://pubs3.acs.org/acs/journals/toc.page?incoden=ancham&indecade=0&involume=79&inissue=11

[25] http://www.lavision.de/techniques/mie_raman_rayleigh/raman_imaging.php

FCS

Fluorescence correlation spectroscopy (FCS) is a common technique used by physicists, chemists, and biologists to experimentally characterize the dynamics of fluorescent species (e.g. single fluorescent dye molecules in nanostructured materials, autofluorescent proteins in living cells, etc.). Although the name indicates a specific link to fluorescence, the method is used today also for exploring other forms of luminescence (like reflections, luminescence from gold-beads or quantum dots or phosphorescent species). The "spectroscopy" in the name is not readily found as in common usage a spectrum is generally understood to be a frequency spectrum. The autocorrelation is a genuine form of spectrum, however: It is the time-spectrum generated from the power spectrum (via inverse fourier transform).

Commonly, FCS is employed in the context of optical microscopy, in particular confocal or two photon microscopy. In these techniques light is focused on a sample and the measured fluorescence intensity fluctuations (due to diffusion, physical or chemical reactions, aggregation, etc.) are analyzed using the temporal autocorrelation. Because the measured property is essentially related to the magnitude and/or the amount of fluctuations, there is an optimum measurement regime at the level when individual species enter or exit the observation volume (or turn on and off in the volume). When too many entities are measured at the same time the overall fluctuations are small in comparison to the total signal and may not be resolvable - in the other direction, if the individual fluctuation-events are too sparse in time, one measurement may take prohibitively too long. FCS is in a way the fluorescent counterpart to dynamic light scattering, which uses coherent light scattering, instead of (incoherent) fluorescence.

When an appropriate model is known, FCS can be used to obtain quantitative information such as

- diffusion coefficients
- hydrodynamic radii
- average concentrations
- kinetic chemical reaction rates
- singlet-triplet dynamics

Because fluorescent markers come in a variety of colors and can be specifically bound to a particular molecule (e.g. proteins, polymers, metal-complexes, etc.), it is possible to study the behavior of individual molecules (in rapid succession in composite solutions). With the development of sensitive detectors such as avalanche photodiodes the detection of the fluorescence signal coming from individual molecules in highly dilute samples has become practical. With this emerged the possibility to conduct FCS experiments in a wide variety of specimens, ranging from materials science to biology. The advent of engineered cells with genetically tagged proteins (like green fluorescent protein) has made FCS a common tool for studying molecular dynamics in living cells.

History

Signal-correlation techniques have first been experimentally applied to fluorescence in 1972 by Magde, Elson, and Webb[1] , who are therefore commonly credited as the "inventors" of FCS. The technique was further developed in a group of papers by these and other authors soon after, establishing the theoretical foundations and types of applications.[2] [3] [4] See Thompson (1991)[5] for a review of that period.

Beginning in 1993[6] , a number of improvements in the measurement techniques--notably using confocal microscopy, and then two photon microscopy--to better define the measurement volume and reject background greatly improved the signal-to-noise and allowed single molecule sensitivity.[7] [8] Since then, there has been a renewed interest in FCS, and as of August 2007 there has been over 3,000 papers using FCS found in Web of Science. See Krichevsky and Bonnet[9] for a recent review. In addition, there has been a flurry of activity extending FCS in various ways, for instance to laser scanning and spinning disk confocal microscopy (from a stationary, single point measurement), in using cross-correlation (FCCS) between two fluorescent channels instead of autocorrelation, and in using Förster Resonance Energy Transfer (FRET) instead of fluorescence.

Typical FCS setup

The typical FCS setup consists of a laser line (wavelengths ranging typically from 405 - 633 nm (cw), and from 690 - 1100 nm (pulsed)), which is reflected into a microscope objective by a dichroic mirror. The laser beam is focused in the sample, which contains fluorescent particles (molecules) in such high dilution, that only few are within the focal spot (usually 1 - 100 molecules in one fL). When the particles cross the focal volume, they fluoresce. This light is collected by the same objective and, because it is red-shifted with respect to the excitation light it passes the dichroic reaching a detector, typically a photomultiplier tube or avalanche photodiode detector. The resulting electronic signal can be stored either directly as an intensity versus time trace to be analyzed at a later point, or, computed to generate the autocorrelation directly (which requires special acquisition cards). The FCS curve by itself only represents a time-spectrum. Conclusions on physical phenomena have to be extracted from there with appropriate models. The parameters of interest are found after fitting the autocorrelation curve to modeled functional forms. [10] The setup is shown in Figure 1.

The Measurement Volume

The measurement volume is a convolution of illumination (excitation) and detection geometries, which result from the optical elements involved. The resulting volume is described mathematically by the point spread function (or PSF), it is essentially the image of a point source. The PSF is often described as an ellipsoid (with unsharp boundaries) of few hundred nanometers in focus diameter, and almost one micrometre along the optical axis. The shape varies significantly (and has a large impact on the resulting FCS curves) depending on the quality of the optical elements (it is crucial to avoid astigmatism and to check the real shape of the PSF on the instrument). In the case of confocal microscopy, and for small pinholes (around one Airy unit), the PSF is well approximated by Gaussians:

$$PSF(r,z) = I_0 e^{-2r^2/\omega_{xy}^2} e^{-2z^2/\omega_z^2}$$

where I_0 is the peak intensity, r and z are radial and axial position, and ω_{xy} and ω_z are the radial and axial radii, and $\omega_z > \omega_{xy}$. This Gaussian form is assumed in deriving the functional form of the autocorrelation.

Typically ω_{xy} is 200-300 nm, and ω_z is **2-6** times larger.[11] One common way of calibrating the measurement volume parameters is to perform FCS on a species with known diffusion coefficient and concentration (see below). Diffusion coefficients for common fluorophores in water are given in a later section.

The Gaussian approximation works to varying degrees depending on the optical details, and corrections can sometimes be applied to offset the errors in approximation.[12]

Autocorrelation Function

The (temporal) autocorrelation function is the correlation of a time series with itself shifted by time τ, as a function of τ:

$$G(\tau) = \frac{\langle \delta I(t) \delta I(t+\tau) \rangle}{\langle I(t) \rangle^2} = \frac{\langle I(t) I(t-\tau) \rangle}{\langle I(t) \rangle^2} - 1$$

where $\delta I(t) = I(t) - \langle I(t) \rangle$ is the deviation from the mean intensity. The normalization (denominator) here is the most commonly used for FCS, because then the correlation at $\tau = 0$, $G(0)$, is related to the average number of particles in the measurement volume.

Interpreting the Autocorrelation Function

To extract quantities of interest, the autocorrelation data can be fitted, typically using a nonlinear least squares algorithm. The fit's functional form depends on the type of dynamics (and the optical geometry in question).

Normal Diffusion

The fluorescent particles used in FCS are small and thus experience thermal motions in solution. The simplest FCS experiment is thus normal 3D diffusion, for which the autocorrelation is:

$$G(\tau) = G(0) \frac{1}{(1 + (\tau/\tau_D))(1 + a^{-2}(\tau/\tau_D))^{1/2}} - G(\infty)$$

where $a = \omega_z/\omega_{xy}$ is the ratio of axial to radial e^{-2} radii of the measurement volume, and τ_D is the characteristic residence time. This form was derived assuming a Gaussian measurement volume. Typically, the fit would have three free parameters--G(0), $G(\infty)$, and τ_D --from which the diffusion coefficient and fluorophore concentration can be obtained.

With the normalization used in the previous section, G(0) gives the mean number of diffusers in the volume <N>, or equivalently--with knowledge of the observation volume size--the mean concentration:

$$G(0) = \frac{1}{<N>} = \frac{1}{V_{eff} <C>},$$

where the effective volume is found from integrating the Gaussian form of the measurement volume and is given by:

$$V_{eff} = \pi^{3/2} \omega_{xy}^2 \omega_z.$$

τ_D gives the diffusion coefficient: $D = \omega_{xy}^2/4\tau_D$.

Anomalous diffusion

If the diffusing particles are hindered by obstacles or pushed by a force (molecular motors, flow, etc.) the dynamics is often not sufficiently well-described by the normal diffusion model, where the mean squared displacement (MSD) grows linearly with time. Instead the diffusion may be better described as anomalous diffusion, where the temporal dependenc of the MSD is non-linear as in the power-law:

$$MSD = 6 D_a t^\alpha$$

where D_a is an anomalous diffusion coefficient. "Anomalous diffusion" commonly refers only to this very generic model, and not the many other possibilities that might be described as anomalous. Also, a power law is, in a strict sense, the expected form only for a narrow range of rigorously defined systems, for instance when the distribution of obstacles is fractal. Nonetheless a power law can be a useful approximation for a wider range of systems.

The FCS autocorrelation function for anomalous diffusion is:

$$G(\tau) = G(0) \frac{1}{(1 - (\tau/\tau_D)^\alpha)(1 + a^{-2}(\tau/\tau_D)^\alpha)^{1/2}} + G(\infty),$$

where the anomalous exponent α is the same as above, and becomes a free parameter in the fitting.

Using FCS, the anomalous exponent has been shown to be an indication of the degree of molecular crowding (it is less than one and smaller for greater degrees of crowding)[13] .

Polydisperse diffusion

If there are diffusing particles with different sizes (diffusion coefficients), it is common to fit to a function that is the sum of single component forms:

$$G(\tau) = G(0) \sum_i \frac{\alpha_i}{(1 + (\tau/\tau_{D,i}))(1 + a^{-2}(\tau/\tau_{D,i}))^{1/2}} + G(\infty)$$

where the sum is over the number different sizes of particle, indexed by i, and α_i gives the weighting, which is related to the quantum yield and concentration of each type. This introduces new parameters, which makes the fitting more difficult as a higher dimensional space must be searched. Nonlinear least square fitting typically becomes unstable with even a small number of $\tau_{D,i}$s. A more robust fitting scheme, especially useful for polydisperse samples, is the Maximum Entropy Method[14] .

Diffusion with flow

With diffusion together with a uniform flow with velocity v in the lateral direction, the autocorrelation is[15] :

$$G(\tau) = G(0) \frac{1}{(1 + (\tau/\tau_D))(1 + a^{-2}(\tau/\tau_D))^{1/2}} \times \exp\left[-(\tau/\tau_v)^2 \times \frac{1}{1 + \tau/\tau_D}\right] + G(\infty)$$

where $\tau_v = \omega_{xy}/v$ is the average residence time if there is only a flow (no diffusion).

Chemical relaxation

A wide range of possible FCS experiments involve chemical reactions that continually fluctuate from equilibrium because of thermal motions (and then "relax"). In contrast to diffusion, which is also a relaxation process, the fluctuations cause changes between states of different energies. One very simple system showing chemical relaxation would be a stationary binding site in the measurement volume, where particles only produce signal when bound (e.g. by FRET, or if the diffusion time is much faster than the sampling interval). In this case the autocorrelation is:

$$G(\tau) = G(0) \exp(-\tau/\tau_B) + G(\infty)$$

where

$$\tau_B = (k_{on} + k_{off})^{-1}$$

is the relaxation time and depends on the reaction kinetics (on and off rates), and:

$$G(0) = \frac{1}{\langle N \rangle} \frac{k_{on}}{k_{off}} = \frac{1}{\langle N \rangle} K$$

is related to the equilibrium constant K.

Most systems with chemical relaxation also show measureable diffusion as well, and the autocorrelation function will depend on the details of the system. If the diffusion and chemical reaction are decoupled, the combined autocorrelation is the product of the chemical and diffusive autocorrelations.

Triplet State Correction

The autocorrelations above assume that the fluctuations are not due to changes in the fluorescent properties of the particles. However, for the majority of (bio)organic fluorophores--e.g. green fluorescent protein, rhodamine, Cy3 and Alexa Fluor dyes--some fraction of illuminated particles are excited to a triplet state (or other non-radiative decaying states) and then do not emit photons for a characteristic relaxation time τ_F. Typically τ_F is on the order of microseconds, which is usually smaller than the dynamics of interest (e.g. τ_D) but large enough to be measured. A

multiplicative term is added to the autocorrelation account for the triplet state. For normal diffusion:

$$G(\tau) = G(0)\frac{1 - F + Fe^{-\tau/\tau_F}}{1 - F}\frac{1}{(1 + (\tau/\tau_{D,i}))(1 + a^{-2}(\tau/\tau_{D,i}))^{1/2}} + G(\infty)$$

where F is the fraction of particles that have entered the triplet state and τ_F is the corresponding triplet state relaxation time. If the dynamics of interest are much slower than the triplet state relaxation, the short time component of the autocorrelation can simply be truncated and the triplet term is unnecessary.

Common fluorescent probes

The fluorescent species used in FCS is typically a biomolecule of interest that has been tagged with a fluorophore (using immunohistochemistry for instance), or is a naked fluorophore that is used to probe some environment of interest (e.g. the cytoskeleton of a cell). The following table gives diffusion coefficients of some common fluorophores in water at room temperature, and their excitation wavelengths.

Fluorescent dye	D (x10^{-10} m^2 s^{-1})	Excitation wavelength (nm)	Reference
Rhodamine 6G	2.8, 3.0, 4.14 ± 0.05 @ 25.00 °C	514	[16] [17] [18]
Rhodamine 110	2.7	488	[19]
Tetramethyl rhodamine	2.6	543	
Cy3	2.8	543	
Cy5	2.5, 3.7 ± 0.15 @ 25.00 °C	633	[20] [21]
carboxyfluorescein	3.2	488	
Alexa-488	1.96	488	[22]
Atto655-maleimide	4.07 ± 0.1 @ 25.00 °C	663	[23]
Atto655-carboxylicacid	4.26 ± 0.08 @ 25.00 °C	663	[24]
2′, 7′-difluorofluorescein (Oregon Green488)	4.11 ± 0.06 @ 25.00 °C	498	[25]

Variations of FCS

FCS almost always refers to the single point, single channel, temporal autocorrelation measurement, although the term "fluorescence correlation spectroscopy" out of its historical scientific context implies no such restriction. FCS has been extended in a number of variations by different researchers, with each extension generating another name (usually an acronym).

Fluorescence Cross-Correlation Spectroscopy (FCCS)

FCS is sometimes used to study molecular interactions using differences in diffusion times (e.g. the product of an association reaction will be larger and thus have larger diffusion times than the reactants individually); however, FCS is relatively insensitive to molecular mass as can be seen from the following equation relating molecular mass to the diffusion time of globular particles (e.g. proteins):

$$\tau_D = \frac{3\pi\omega_{xy}^2\eta}{2kT}(M)^{1/3}$$

where η is the viscosity of the sample and M is the molecular mass of the fluorescent species. In practice, the diffusion times need to be sufficiently different--a factor of at least **1.6**--which means the molecular masses must

differ by a factor of **4**.[26] Dual color → fluorescence cross-correlation spectroscopy (FCCS) measures interactions by cross-correlating two or more fluorescent channels (one channel for each reactant), which distinguishes interactions more sensitively than FCS, particularly when the mass change in the reaction is small.

Two- and three- photon FCS excitation

Several advantages in both spatial resolution and minimizing photodamage/photobleaching in organic and/or biological samples are obtained by two-photon or three-photon excitation FCS[27] [28] [29] [30] [31] .

FRET-FCS

Another FCS based approach to studying molecular interactions uses fluorescence resonance energy transfer (FRET) instead of fluorescence, and is called FRET-FCS.[32] With FRET, there are two types of probes, as with FCCS; however, there is only one channel and light is only detected when the two probes are very close--close enough to ensure an interaction. The FRET signal is weaker than with fluorescence, but has the advantage that there is only signal during a reaction (aside from autofluorescence).

Image Correlation Spectroscopy (ICS)

When the motion is slow (in biology, for example, diffusion in a membrane), getting adequate statistics from a single-point FCS experiment may take a prohibitively long time. More data can be obtained by performing the experiment in multiple spatial points in parallel, using a laser scanning confocal microscope. This approach has been called Image Correlation Spectroscopy (ICS)[33] . The measurements can then be averaged together.

Another variation of ICS performs a spatial autocorrelation on images, which gives information about the concentration of particles[34] . The correlation is then averaged in time.

A natural extension of the temporal and spatial correlation versions is spatio-temporal ICS (STICS) [35] . In STICS there is no explicit averaging in space or time (only the averaging inherent in correlation). In systems with non-isotropic motion (e.g. directed flow, asymmetric diffusion), STICS can extract the directional information. A variation that is closely related to STICS (by the Fourier transform) is k-space Image Correlation Spectroscopy (kICS).[36]

There are cross-correlation versions of ICS as well.[33]

Scanning FCS variations

Some variations of FCS are only applicable to serial scanning laser microscopes. Image Correlation Spectroscopy and its variations all were implemented on a scanning confocal or scanning two photon microscope, but transfer to other microscopes, like a spinning disk confocal microscope. Raster ICS (RICS)[37] , and position sensitive FCS (PSFCS)[38] incorporate the time delay between parts of the image scan into the analysis. Also, low dimensional scans (e.g. a circular ring)[39] --only possible on a scanning system--can access time scales between single point and full image measurements. Scanning path has also been made to adaptively follow particles.[40]

Spinning disk FCS, and spatial mapping

Any of the image correlation spectroscopy methods can also be performed on a spinning disk confocal microscope, which in practice can obtain faster imaging speeds compared to a laser scanning confocal microscope. This approach has recently been applied to diffusion in a spatially varying complex environment, producing a pixel resolution map of diffusion coefficient.[41] . The spatial mapping of diffusion with FCS has subsequently been extended to TIRF system.[42] Spatial mapping of dynamics using correlation techniques had been applied before, but only at sparse points[43] or at coarse resolution[35] .

Total internal reflection FCS

Total internal reflection fluorescence (TIRF) is a microscopy approach that is only sensitive to a thin layer near the surface of a coverslip, which greatly minimizes background fluorscence. FCS has been extended to that type of microscope, and is called TIR-FCS[44] . Because the fluorescence intensity in TIRF falls off exponentially with distance from the coverslip (instead of as a Gaussian with a confocal), the autocorrelation function is different.

Other fluorescent dynamical approaches

There are two main non-correlation alternatives to FCS that are widely used to study the dynamics of fluorescent species.

Fluorescence recovery after photobleaching (FRAP)

In FRAP, a region is briefly exposed to intense light, irrecoverably photobleaching fluorophores, and the fluorescence recovery due to diffusion of nearby (non-bleached) fluorophores is imaged. A primary advantage of FRAP over FCS is the ease of interpreting qualitative experiments common in cell biology. Differences between cell lines, or regions of a cell, or before and after application of drug, can often be characterized by simple inspection of movies. FCS experiments require a level of processing and are more sensitive to potentially confounding influences like: rotational diffusion, vibrations, photobleaching, dependence on illumination and fluorescence color, inadequate statistics, etc. It is much easier to change the measurement volume in FRAP, which allows greater control. In practice, the volumes are typically larger than in FCS. While FRAP experiments are typically more qualitative, some researchers are studying FRAP quantitatively and including binding dynamics.[45] A disadvantage of FRAP in cell biology is the free radical perturbation of the cell caused by the photobleaching. It is also less versatile, as it cannot measure concentration or rotational diffusion, or co-localization. FRAP requires a significantly higher concentration of fluorophores than FCS.

Particle tracking

In particle tracking, the trajectories of a set of particles are measured, typically by applying particle tracking algorithms to movies.[46] Particle tracking has the advantage that all the dynamical information is maintained in the measurement, unlike FCS where correlation averages the dynamics to a single smooth curve. The advantage is apparent in systems showing complex diffusion, where directly computing the mean squared displacement allows straightforward comparison to normal or power law diffusion. To apply particle tracking, the particles have to be distinguishable and thus at lower concentration than required of FCS. Also, particle tracking is more sensitive to noise, which can sometimes affect the results unpredictably.

- Single-molecule spectroscopic methods [47]
- FCS Classroom [48]

References

[1] Magde, D., Elson, E. L., Webb, W. W. Thermodynamic fluctuations in a reacting system: Measurement by fluorescence correlation spectroscopy,(1972) *Phys Rev Lett*, **29**,705-708.

[2] Ehrenberg, M., Rigler, R. Rotational brownian motion and fluorescence intensity fluctuations,(1974) *Chem Phys*, **4**,390-401.

[3] Elson, E. L., Magde, D. Fluorescence correlation spectroscopy I. Conceptual basis and theory,(1974) *Biopolymers*, **13**,1-27.

[4] Magde, D., Elson, E. L., Webb, W. W. Fluorescence correlation spectroscopy II. An experimental realization,(1974) *Biopolymers*, **13**,29-61.

[5] Thompson N L 1991 Topics in Fluorescence Spectroscopy Techniques vol 1, ed J R Lakowicz (New York: Plenum) pp 337–78

[6] Rigler, R, Ü. Mets1, J. Widengren and P. Kask. Fluorescence correlation spectroscopy with high count rate and low background: analysis of translational diffusion. European Biophysics Journal (1993) 22(3), 159.

[7] Eigen, M., Rigler, M. Sorting single molecules: application to diagnostics and evolutionary biotechnology,(1994) *Proc. Natl. Acad. Sci. USA*, **91**,5740-5747.

[8] Rigler, M. Fluorescence correlations, single molecule detection and large number screening. Applications in biotechnology,(1995) *J. Biotechnol.*, **41**,177-186.

[9] O. Krichevsky, G. Bonnet, "Fluorescence correlation spectroscopy: the technique and its applications," Rep. Prog. Phys. 65, 251-297 (2002).

[10] Medina, M. A., Schwille, P. Fluorescence correlation spectroscopy for the detection and study of single molecules in biology, (2002)*BioEssays*, **24**,758-764.

[11] Mayboroda, O. A., van Remoortere, A., Tanke H. J., Hokke, C. H., Deelder, A. M., A new approach for fluorescence correlation spectroscopy (FCS) based immunoassays, (2003), *J. Biotechnol.*, **107**, 185-192.

[12] Hess, S.T., and W.W. Webb. 2002. Focal volume optics and experimental artifacts in confocal fluorescence correlation spectroscopy. Biophys. J. 83:2300-2317.

[13] Banks, D. S., and C. Fradin. 2005. Anomalous diffusion of proteins due to molecular crowding. Biophys. J. 89:2960–2971.

[14] Sengupta, P., K. Garai, J. Balaji, N. Periasamy, and S. Maiti. 2003. Measuring Size Distribution in Highly Heterogeneous Systems with Fluorescence Correlation Spectroscopy. Biophys. J. 84(3):1977-1984.

[15] Kohler, R.H., P. Schwille, W.W. Webb, and M.R. Hanson. 2000. Active protein transport through plastid tubules: velocity quantified by fluorescence correlation spectroscopy. J Cell Sci 113(22):3921-3930

[16] Magde, D., Elson, E. L., Webb, W. W. Fluorescence correlation spectroscopy II. An experimental realization,(1974) *Biopolymers*, **13**,29-61.

[17] Berland, K. M. Detection of specific DNA sequences using dual-color two-photon fluorescence correlation spectroscopy. (2004),*J. Biotechnol* ,**108**(2), 127-136.

[18] Müller, C.B., Loman, A., Pacheco, V., Koberling, F., Willbold, D., Richtering, W., Enderlein, J. Precise measurement of diffusion by multi-color dual-focus fluorescence correlation spectroscopy (2008), *EPL*, **83**, 46001.

[19] Pristinski, D., Kozlovskaya, V., Sukhishvili, S. A. Fluorescence correlation spectroscopy studies of diffusion of a weak polyelectrolyte in aqueous solutions. (2005), *J. Chem. Phys.*, **122**, 014907.

[20] Widengren, J., Schwille, P., Characterization of photoinduced isomerization and back-isomerization of the cyanine dye Cy5 by fluorescence correlation spectroscopy. (2000), *J. Phys. Chem. A*, **104**, 6416-6428.

[21] Loman, A., Dertinger, T., Koberling, F., Enderlein, J. Comparison of optical saturation effects in conventional and dual-focus fluorescence correlation spectroscopy (2008), *Chem. Phys. Lett.*, **459**, 18−21.

[22] Pristinski, D., Kozlovskaya, V., Sukhishvili, S. A. Fluorescence correlation spectroscopy studies of diffusion of a weak polyelectrolyte in aqueous solutions. (2005), *J. Chem. Phys.*, **122**, 014907.

[23] Müller, C.B., Loman, A., Pacheco, V., Koberling, F., Willbold, D., Richtering, W., Enderlein, J. Precise measurement of diffusion by multi-color dual-focus fluorescence correlation spectroscopy (2008), *EPL*, **83**, 46001.

[24] Müller, C.B., Loman, A., Pacheco, V., Koberling, F., Willbold, D., Richtering, W., Enderlein, J. Precise measurement of diffusion by multi-color dual-focus fluorescence correlation spectroscopy (2008), *EPL*, **83**, 46001.

[25] Müller, C.B., Loman, A., Pacheco, V., Koberling, F., Willbold, D., Richtering, W., Enderlein, J. Precise measurement of diffusion by multi-color dual-focus fluorescence correlation spectroscopy (2008), *EPL*, **83**, 46001.

[26] Meseth, U., Wohland, T., Rigler, R., Vogel, H. Resolution of fluorescence correlation measurements. (1999) *Biophys. J.*, **76**, 1619-1631.

[27] Diaspro, A., and Robello, M. (1999). Multi-photon Excitation Microscopy to Study Biosystems. European Microscopy and Analysis., 5:5-7.

[28] Bagatolli, L.A., and Gratton, E. (2000). Two-photon fluorescence microscopy of coexisting lipid domains in giant unilamellar vesicles of binary phospholipid mixtures. Biophys J., 78:290-305.

[29] Schwille, P., Haupts, U., Maiti, S., and Webb. W.(1999). Molecular dynamics in living cells observed by fluorescence correlation spectroscopy with one- and two- photon excitation. *Biophysical Journal*, **77**(10):2251-2265.

[30] Near Infrared Microspectroscopy, Fluorescence Microspectroscopy,Infrared Chemical Imaging and High Resolution Nuclear Magnetic Resonance Analysis of Soybean Seeds, Somatic Embryos and Single Cells., Baianu, I.C. et al. 2004., In *Oil Extraction and Analysis.*, D. Luthria, Editor pp.241-273, AOCS Press., Champaign, IL.

[31] Single Cancer Cell Detection by Near Infrared Microspectroscopy, Infrared Chemical Imaging and Fluorescence Microspectroscopy.2004.I. C. Baianu, D. Costescu, N. E. Hofmann and S. S. Korban, q-bio/0407006 (July 2004) (http://arxiv.org/abs/q-bio/0407006)

[32] K. Remaut, B. Lucas, K. Braeckmans, N.N. Sanders, S.C. De Smedt and J. Demeester, FRET-FCS as a tool to evaluate the stability of oligonucleotide drugs after intracellular delivery, J Control Rel 103 (2005) (1), pp. 259–271.

[33] Wiseman, P. W., J. A. Squier, M. H. Ellisman, and K. R. Wilson. 2000. Two-photon video rate image correlation spectroscopy (ICS) and image cross-correlation spectroscopy (ICCS). J. Microsc. 200:14–25.

[34] Petersen, N. O., P. L. Ho¨ddelius, P. W. Wiseman, O. Seger, and K. E. Magnusson. 1993. Quantitation of membrane receptor distributions by image correlation spectroscopy: concept and application. Biophys. J. 65:1135–1146.

[35] Hebert, B., S. Constantino, and P. W. Wiseman. 2005. Spatio-temporal image correlation spectroscopy (STICS): theory, verification and application to protein velocity mapping in living CHO cells. Biophys. J. 88:3601–3614.

[36] Kolin, D.L., D. Ronis, and P.W. Wiseman. 2006. k-Space Image Correlation Spectroscopy: A Method for Accurate Transport Measurements Independent of Fluorophore Photophysics. Biophys. J. 91(8):3061-3075.

[37] Digman, M.A., P. Sengupta, P.W. Wiseman, C.M. Brown, A.R. Horwitz, and E. Gratton. 2005. Fluctuation Correlation Spectroscopy with a Laser-Scanning Microscope: Exploiting the Hidden Time Structure. Biophys. J. 88(5):L33-36.

[38] Skinner, J.P., Y. Chen, and J.D. Mueller. 2005. Position-Sensitive Scanning Fluorescence Correlation Spectroscopy. Biophys. J.:biophysj.105.060749.

[39] Ruan, Q., M.A. Cheng, M. Levi, E. Gratton, and W.W. Mantulin. 2004. Spatial-temporal studies of membrane dynamics: scanning fluorescence correlation spectroscopy (SFCS). Biophys. J. 87:1260–1267.

[40] A. Berglund and H. Mabuchi, "Tracking-FCS: Fluorescence correlation spectroscopy of individual particles," Opt. Express 13, 8069-8082 (2005).

[41] Sisan, D.R., R. Arevalo, C. Graves, R. McAllister, and J.S. Urbach. 2006. Spatially resolved fluorescence correlation spectroscopy using a spinning disk confocal microscope. Biophysical Journal 91(11):4241-4252.

[42] Kannan, B., L. Guo, T. Sudhaharan, S. Ahmed, I. Maruyama, and T. Wohland. 2007. Spatially resolved total internal reflection fluorescence correlation microscopy using an electron multiplying charge-coupled device camera. Analytical Chemistry 79(12):4463-4470

[43] Wachsmuth, M., W. Waldeck, and J. Langowski. 2000. Anomalous diffusion of fluorescent probes inside living cell nuclei investigated by spatially-resolved fluorescence correlation spectroscopy. J. Mol. Biol. 298(4):677-689.

[44] Lieto, A.M., and N.L. Thompson. 2004. Total Internal Reflection with Fluorescence Correlation Spectroscopy: Nonfluorescent Competitors. Biophys. J. 87(2):1268-1278.

[45] Sprague, B.L., and J.G. McNally. 2005. FRAP analysis of binding: proper and fitting. Trends in Cell Biology 15(2):84-91.

[46] http://www.physics.emory.edu/~weeks/idl/

[47] http://dx.doi.org/10.1016/j.sbi.2004.09.004

[48] http://www.fcsxpert.com/classroom

FCCS

Fluorescence cross-correlation spectroscopy (FCCS) was introduced by Eigen and Rigler in 1994 and experimentally realized by Schwille in 1997. It extends the → fluorescence correlation spectroscopy (FCS) procedure by introducing high sensitivity for distinguishing fluorescent particles which have a similar diffusion coefficient. FCCS uses two species which are independently labelled with two spectrally separated fluorescent probes. These fluorescent probes are excited and detected by two different laser light sources and detectors commonly known as green and red respectively. Both laser light beams are focused into the sample and tuned so that they overlap to form a superimposed confocal observation volume.

The normalized cross-correlation function is defined for two fluorescent species G and R which are independent green, G and red, R channels as follows:

$$G_{GR}(\tau) = 1 + \frac{<\delta I_G(t)\delta I_R(t+\tau)>}{<I_G(t)><I_R(t)>} = \frac{<I_G(t)I_R(t-\tau)>}{<I_G(t)><I_R(t)>}$$

where differential fluorescent signals δI_G at a specific time, t and δI_R at a delay time, τ later is correlated with each other.

Modeling

Cross-correlation curves are modeled according to a slightly more complicated mathematical function than applied in FCS. First of all, the effective superimposed observation volume in which the G and R channels form a single observation volume, $V_{eff,RG}$ in the solution:

$$V_{eff,RG} = \pi^{3/2}(\omega_{xy,G}^2 + \omega_{xy,R}^2)(\omega_{z,G}^2 + \omega_{z,R}^2)^{1/2}/2^{3/2}$$

where $\omega_{xy,G}^2$ and $\omega_{xy,R}^2$ are radial parameters and $\omega_{z,G}$ and $\omega_{z,R}$ are the axial parameters for the G and R channels respectively.

The diffusion time, $\tau_{D,GR}$ for a doubly (G and R) fluorescent species is therefore described as follows:

$$\tau_{D,GR} = \frac{\omega_{xy,G}^2 + \omega_{xy,R}^2}{8D_{GR}}$$

where D_{GR} is the diffusion coefficient of the doubly fluorescent particle.

The cross-correlation curve generated from diffusing doubly labelled fluorescent particles can be modelled in separate channels as follows:

$$G_G(\tau) = 1 + \frac{(<C_G>Diff_k(\tau)+<C_{GR}>Diff_k(\tau))}{V_{eff,GR}(<C_G>+<C_{GR}>)^2}$$

$$G_R(\tau) = 1 + \frac{(<C_R>Diff_k(\tau)+<C_{GR}>Diff_k(\tau))}{V_{eff,GR}(<C_R>+<C_{GR}>)^2}$$

In the ideal case, the cross-correlation function is proportional to the concentration of the doubly labeled fluorescent complex:

$$G_{GR}(\tau) = 1 + \frac{<C_{GR}>Diff_{GR}(\tau)}{V_{eff}(<C_G>+<C_{GR}>)(<C_R>+<C_{GR}>)}$$

with $Diff_k(\tau) = \dfrac{1}{(1+\frac{\tau}{\tau_{D,i}})(1+\alpha^{-2}(\frac{\tau}{\tau_{D,i}})^{1/2}}$

Contrary to FCS, the intercept of the cross-correlation curve does not yield information about the doubly labelled fluorescent particles in solution.

Polarization

Polarization (also **polarisation**) is a property of waves that describes the orientation of their oscillations. This article primarily covers the polarization of electromagnetic waves such as light, although other types of wave also exhibit polarization.

By convention, the polarization of light is described by specifying the direction of the wave's electric field. When light travels in free space, in most cases it propagates as a transverse wave—the polarization is perpendicular to the wave's direction of travel. In this case, the electric field may be oriented in a single direction (linear polarization), or it may rotate as the wave travels (circular or elliptical polarization). In the latter cases, the oscillations can rotate rightward or leftward in the direction of travel, and which of those two rotations is present in a wave is called the wave's chirality or handedness. In general the polarization of an electromagnetic (EM) wave is a complex issue. For instance in a waveguide such as an optical fiber, or for radially polarized beams in free space[1] , the description of the wave's polarization is more complicated, as the fields can have longitudinal as well as transverse components. Such EM waves are either TM or hybrid modes.

For longitudinal waves such as sound waves in fluids, the direction of oscillation is by definition along the direction of travel, so there is no polarization. In a solid medium, however, sound waves can be transverse. In this case, the polarization is associated with the direction of the shear stress in the plane perpendicular to the propagation direction. This is important in seismology.

Polarization is significant in areas of science and technology dealing with wave propagation, such as optics, seismology, telecommunications and radar science. The polarization of light can be measured with a polarimeter.

Theory

Basics: plane waves

The simplest manifestation of polarization to visualize is that of a plane wave, which is a good approximation of most light waves (a plane wave is a wave with infinitely long and wide wavefronts). For plane waves Maxwell's equations, specifically Gauss's laws impose the transversality requirement that the electric and magnetic field be perpendicular to the direction of propagation and to each other. Conventionally, when considering polarization, the electric field vector is described and the magnetic field is ignored since it is perpendicular to the electric field and proportional to it. The electric field vector of a plane wave may be arbitrarily divided into two perpendicular components labeled x and y (with z indicating the direction of travel). For a simple harmonic wave, where the amplitude of the electric vector varies in a sinusoidal manner in time, the two components have exactly the same frequency. However, these components have two other defining characteristics that can differ. First, the two components may not have the same amplitude. Second, the two components may not have the same phase, that is they may not reach their maxima and minima at the same time. Mathematically, the electric field of a plane wave can

be written as,

$$\vec{E}(\vec{r}, t) = \text{Re} \left[\left(A_x, A_y \cdot e^{i\phi}, 0 \right) e^{i(kz - \omega t)} \right]$$

or alternatively,

$$\vec{E}(\vec{r}, t) \quad \left(A_x \cdot \cos(kz - \omega t), A_y \cdot \cos(kz - \omega t + \phi), 0 \right)$$

where A_x and A_y are the amplitudes of the x and y directions and ϕ is the relative phase between the two components.

Polarization state

The shape traced out in a fixed plane by the electric vector as such a plane wave passes over it (a Lissajous figure) is a description of the **polarization state**. The following figures show some examples of the evolution of the electric field vector (blue), with time(the vertical axes), at a particular point in space, along with its x and y components (red/left and green/right), and the path traced by the tip of the vector in the plane (purple): The same evolution would occur when looking at the electric field at a particular time while evolving the point in space, along the direction opposite to propagation.
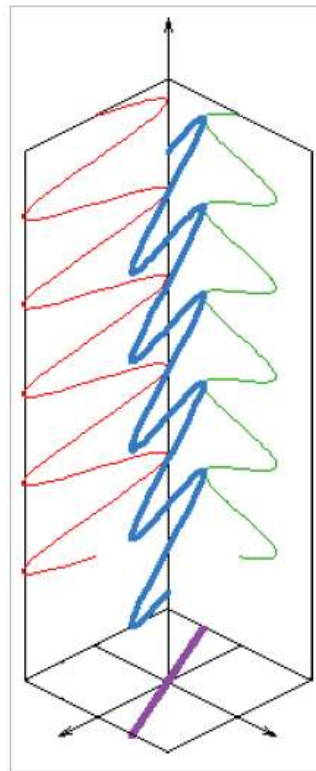
Linear
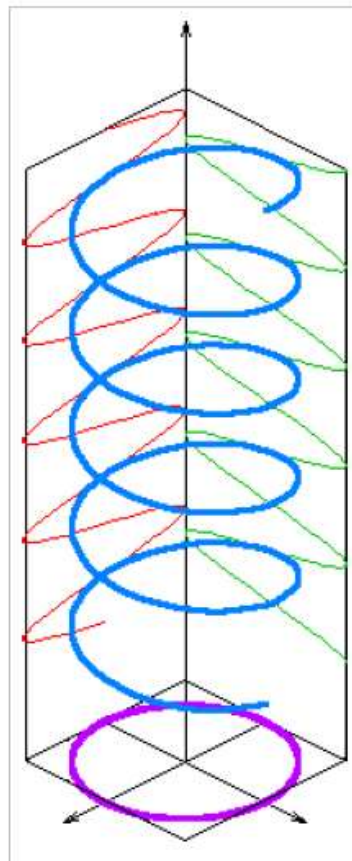
Circular
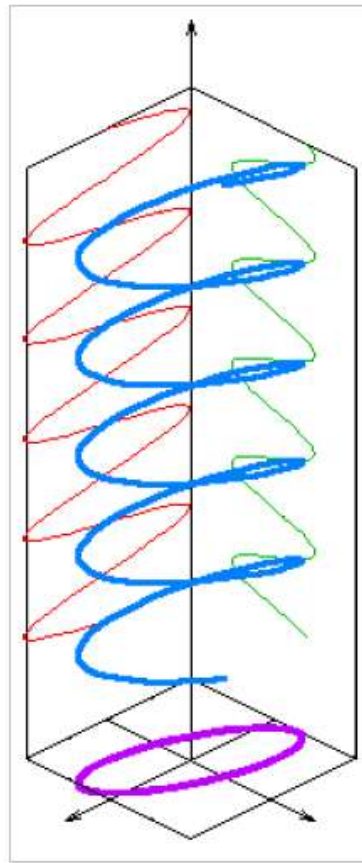
Elliptical

In the leftmost figure above, the two orthogonal (perpendicular) components are in phase. In this case the ratio of the strengths of the two components is constant, so the direction of the electric vector (the vector sum of these two components) is constant. Since the tip of the vector traces out a single line in the plane, this special case is called linear polarization. The direction of this line depends on the relative amplitudes of the two components.

In the middle figure, the two orthogonal components have exactly the same amplitude and are exactly ninety degrees out of phase. In this case one component is zero when the other component is at maximum or minimum amplitude. There are two possible phase relationships that satisfy this requirement: the x component can be ninety degrees ahead of the y component or it can be ninety degrees behind the y component. In this special case the electric vector traces out a circle in the plane, so this special case is called circular polarization. The direction the field rotates in, depends on which of the two phase relationships exists. These cases are called *right-hand circular polarization* and *left-hand circular polarization*, depending on which way the electric vector rotates.

Another case is when the two components are not in phase and either do not have the same amplitude or are not ninety degrees out of phase, though their phase offset and their amplitude ratio are constant.[2] This kind of polarization is called elliptical polarization because the electric vector traces out an ellipse in the plane (the *polarization ellipse*). This is shown in the above figure on the right.

The "Cartesian" decomposition of the electric field into x and y components is, of course, arbitrary. Plane waves of any polarization can be described instead by combining any two orthogonally polarized waves, for instance waves of opposite circular polarization. The Cartesian polarization decomposition is natural when dealing with reflection from surfaces, birefringent materials, or synchrotron radiation. The circularly polarized modes are a more useful basis for the study of light propagation in stereoisomers.

Though this section discusses polarization for idealized plane waves, all the above is a very accurate description for most practical optical experiments which use TEM modes, including Gaussian optics.

Unpolarized light

Most sources of electromagnetic radiation contain a large number of atoms or molecules that emit light. The orientation of the electric fields produced by these emitters may not be correlated, in which case the light is said to be *unpolarized*. If there is partial correlation between the emitters, the light is *partially polarized*. If the polarization is consistent across the spectrum of the source, partially polarized light can be described as a superposition of a completely unpolarized component, and a completely polarized one. One may then describe the light in terms of the degree of polarization, and the parameters of the polarization ellipse.

Parameterization

For ease of visualization, polarization states are often specified in terms of the polarization ellipse, specifically its orientation and elongation. A common parameterization uses the **azimuth angle**, ψ (the angle between the major semi-axis of the ellipse and the *x*-axis) and the **ellipticity**, ε (the major-to-minor-axis ratio), also known as the axial ratio.[3] [4] [5] [6] An ellipticity of infinity corresponds to linear polarization and an ellipticity of 1 corresponds to circular polarization. The arccotangent of the ellipticity, $\chi = \text{arccot}\,\varepsilon$ (the "**ellipticity angle**"), is also commonly used. An example is shown in the diagram to the right. An alternative to the ellipticity or ellipticity angle is the eccentricity, however unlike the azimuth angle and ellipticity angle, the latter has no obvious geometrical interpretation in terms of the Poincaré sphere (see below).
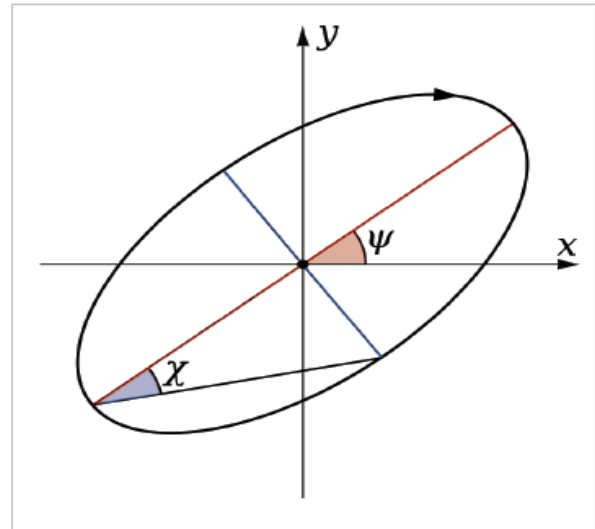

Full information on a completely polarized state is also provided by the amplitude and phase of oscillations in two components of the electric field vector in the plane of polarization. This representation was used above to show how different states of polarization are possible. The amplitude and phase information can be conveniently represented as a two-dimensional complex vector (the Jones vector):

$$\mathbf{e} = \begin{bmatrix} a_1 e^{i\theta_1} \\ a_2 e^{i\theta_2} \end{bmatrix}.$$

Here a_1 and a_2 denote the amplitude of the wave in the two components of the electric field vector, while θ_1 and θ_2 represent the phases. The product of a Jones vector with a complex number of unit modulus gives a different Jones vector representing the same ellipse, and thus the same state of polarization. The physical electric field, as the real part of the Jones vector, would be altered but the polarization state itself is independent of absolute phase. The basis vectors used to represent the Jones vector need not represent linear polarization states (i.e. be real). In general any two **orthogonal states** can be used, where an orthogonal vector pair is formally defined as one having a zero inner product. A common choice is left and right circular polarizations, for example to model the different propagation of waves in two such components in circularly birefringent media (see below) or signal paths of coherent detectors sensitive to circular polarization.

Regardless of whether polarization ellipses are represented using geometric parameters or Jones vectors, implicit in the parameterization is the orientation of the coordinate frame. This permits a degree of freedom, namely rotation about the propagation direction. When considering light that is propagating parallel to the surface of the Earth, the terms "horizontal" and "vertical" polarization are often used, with the former being associated with the first component of the Jones vector, or zero azimuth angle. On the other hand, in astronomy the equatorial coordinate system is generally used instead, with the zero azimuth (or position angle, as it is more commonly called in astronomy

Reflection of a plane wave from a surface perpendicular to the page. The p-components of the waves are in the plane of the page, while the s components are perpendicular to it.

to avoid confusion with the horizontal coordinate system) corresponding to due north. Another coordinate system frequently used relates to the plane made by the propagation direction and a vector normal to the plane of a reflecting surface. This is known as the *plane of incidence*. The rays in this plane are illustrated in the diagram to the right. The component of the electric field parallel to this plane is termed *p-like* (parallel) and the component perpendicular to this plane is termed *s-like* (from *senkrecht*, German for perpendicular). Light with a p-like electric field is said to be *p-polarized*, *pi-polarized*, *tangential plane polarized*, or is said to be a *transverse-magnetic* (TM) wave. Light with an s-like electric field is *s-polarized*, also known as *sigma-polarized* or *sagittal plane polarized*, or it can be called a *transverse-electric* (TE) wave.
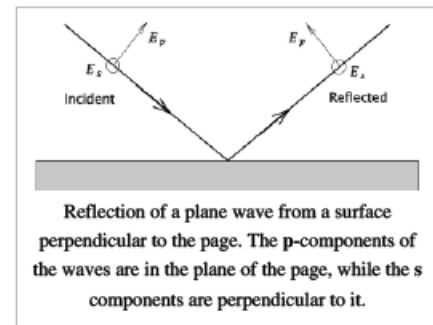
In the case of partially-polarized radiation, the Jones vector varies in time and space in a way that differs from the constant rate of phase rotation of monochromatic, purely-polarized waves. In this case, the wave field is likely stochastic, and only statistical information can be gathered about the variations and correlations between components of the electric field. This information is embodied in the **coherency matrix**:

$$\Psi = \left\langle ee^\dagger \right\rangle$$
$$- \left\langle \begin{bmatrix} e_1 e_1^* & e_1 e_2^* \\ e_2 e_1^* & e_2 e_2^* \end{bmatrix} \right\rangle$$
$$- \left\langle \begin{bmatrix} a_1^2 & a_1 a_2 e^{i(\theta_1 - \theta_2)} \\ a_1 a_2 e^{i(\theta_1 - \theta_2)} & a_2^2 \end{bmatrix} \right\rangle$$

where angular brackets denote averaging over many wave cycles. Several variants of the coherency matrix have been proposed: the Wiener coherency matrix and the spectral coherency matrix of Richard Barakat measure the coherence of a spectral decomposition of the signal, while the Wolf coherency matrix averages over all time/frequencies.

The coherency matrix contains all of the information on polarization that is obtainable using second order statistics. It can be decomposed into the sum of two idempotent matrices, corresponding to the eigenvectors of the coherency matrix, each representing a polarization state that is orthogonal to the other. An alternative decomposition is into completely polarized (zero determinant) and unpolarized (scaled identity matrix) components. In either case, the operation of summing the components corresponds to the incoherent superposition of waves from the two components. The latter case gives rise to the concept of the "degree of polarization"; i.e., the fraction of the total intensity contributed by the completely polarized component.

The coherency matrix is not easy to visualize, and it is therefore common to describe incoherent or partially polarized radiation in terms of its total intensity (*I*), (fractional) degree of polarization (*p*), and the shape parameters of the polarization ellipse. An alternative and mathematically convenient description is given by the Stokes parameters, introduced by George Gabriel Stokes in 1852. The relationship of the Stokes parameters to intensity and polarization ellipse parameters is shown in the equations and figure below.

$$S_0 = I$$

Poincaré sphere diagram
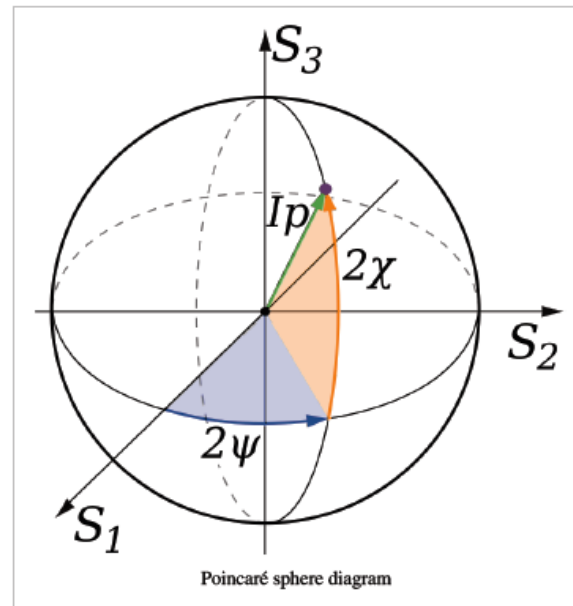
$$S_1 = Ip\cos 2\psi \cos 2\chi$$
$$S_2 = Ip\sin 2\psi \cos 2\chi$$
$$S_3 = Ip\sin 2\chi$$

Here Ip, 2ψ and 2χ are the spherical coordinates of the polarization state in the three-dimensional space of the last three Stokes parameters. Note the factors of two before ψ and χ corresponding respectively to the facts that any polarization ellipse is indistinguishable from one rotated by 180°, or one with the semi-axis lengths swapped accompanied by a 90° rotation. The Stokes parameters are sometimes denoted *I*, *Q*, *U* and *V*.

The Stokes parameters contain all of the information of the coherency matrix, and are related to it linearly by means of the identity matrix plus the three Pauli matrices:

$$\Psi = \frac{1}{2}\sum_{j=0}^{3} S_j \sigma_j, \text{ where}$$

$$\sigma_0 = \begin{bmatrix} 1 & 0 \\ 0 & 1 \end{bmatrix} \quad \sigma_1 = \begin{bmatrix} 1 & 0 \\ 0 & -1 \end{bmatrix}$$

$$\sigma_2 = \begin{bmatrix} 0 & 1 \\ 1 & 0 \end{bmatrix} \quad \sigma_3 = \begin{bmatrix} 0 & -i \\ i & 0 \end{bmatrix}$$

Mathematically, the factor of two relating physical angles to their counterparts in Stokes space derives from the use of second-order moments and correlations, and incorporates the loss of information due to absolute phase invariance.

The figure above makes use of a convenient representation of the last three Stokes parameters as components in a three-dimensional vector space. This space is closely related to the **Poincaré sphere**, which is the spherical surface occupied by completely polarized states in the space of the vector

$$\mathbf{u} = \frac{1}{S_0}\begin{bmatrix} S_1 \\ S_2 \\ S_3 \end{bmatrix}.$$

All four Stokes parameters can also be combined into the four-dimensional Stokes vector, which can be interpreted as four-vectors of Minkowski space. In this case, all physically realizable polarization states correspond to time-like, future-directed vectors.

Propagation, reflection and scattering

In a vacuum, the components of the electric field propagate at the speed of light, so that the phase of the wave varies in space and time while the polarization state does not. That is,

$$\mathbf{e}(z + \Delta z, t + \Delta t) = \mathbf{e}(z, t)e^{ik(c\Delta t - \Delta z)},$$

where k is the wavenumber and positive z is the direction of propagation. As noted above, the physical electric vector is the real part of the Jones vector. When electromagnetic waves interact with matter, their propagation is altered. If this depends on the polarization states of the waves, then their polarization may also be altered.

In many types of media, electromagnetic waves may be decomposed into two orthogonal components that encounter different propagation effects. A similar situation occurs in the signal processing paths of detection systems that record the electric field directly. Such effects are most easily characterized in the form of a complex 2×2 transformation matrix called the Jones matrix:

$$\mathbf{e}' = \mathbf{Je}.$$

In general the Jones matrix of a medium depends on the frequency of the waves.

For propagation effects in two orthogonal modes, the Jones matrix can be written as

$$\mathbf{J} = \mathbf{T}\begin{bmatrix} g_1 & 0 \\ 0 & g_2 \end{bmatrix}\mathbf{T}^{-1},$$

where g_1 and g_2 are complex numbers representing the change in amplitude and phase caused in each of the two propagation modes, and $\mathbf{T}$ is a unitary matrix representing a change of basis from these propagation modes to the linear system used for the Jones vectors. For those media in which the amplitudes are unchanged but a differential phase delay occurs, the Jones matrix is unitary, while those affecting amplitude without phase have Hermitian Jones matrices. In fact, since *any* matrix may be written as the product of unitary and positive Hermitian matrices, any sequence of linear propagation effects, no matter how complex, can be written as the product of these two basic types of transformations.
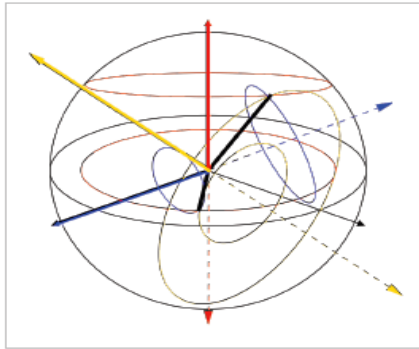
Paths taken by vectors in the Poincaré sphere under birefringence. The propagation modes (rotation axes) are shown with red, blue, and yellow lines, the initial vectors by thick black lines, and the paths they take by colored ellipses (which represent circles in three dimensions).

Media in which the two modes accrue a differential delay are called *birefringent*. Well known manifestations of this effect appear in optical wave plates/retarders (linear modes) and in Faraday rotation/optical rotation (circular modes). An easily visualized example is one where the propagation modes are linear, and the incoming radiation is linearly polarized at a 45° angle to the modes. As the phase difference starts to appear, the polarization becomes elliptical, eventually changing to purely circular polarization (90° phase difference), then to elliptical and eventually linear polarization (180° phase) with an azimuth angle perpendicular to the original direction, then through circular again (270° phase), then elliptical with the original azimuth angle, and finally back to the original linearly polarized state (360° phase) where the cycle begins anew. In general the situation is more complicated and can be characterized as a rotation in the Poincaré sphere about the axis defined by the propagation modes (this is a consequence of the isomorphism of SU(2) with SO(3)). Examples for linear (blue), circular (red), and elliptical (yellow) birefringence are shown in the figure on the left. The total intensity and degree of polarization are unaffected. If the path length in the birefringent medium is sufficient, plane waves will exit the material with a significantly different propagation direction, due to refraction. For example, this is the case with macroscopic

crystals of calcite, which present the viewer with two offset, orthogonally polarized images of whatever is viewed through them. It was this effect that provided the first discovery of polarization, by Erasmus Bartholinus in 1669. In addition, the phase shift, and thus the change in polarization state, is usually frequency dependent, which, in combination with dichroism, often gives rise to bright colors and rainbow-like effects.

Media in which the amplitude of waves propagating in one of the modes is reduced are called *dichroic*. Devices that block nearly all of the radiation in one mode are known as *polarizing filters* or simply "polarizers". In terms of the Stokes parameters, the total intensity is reduced while vectors in the Poincaré sphere are "dragged" towards the direction of the favored mode. Mathematically, under the treatment of the Stokes parameters as a Minkowski 4-vector, the transformation is a scaled Lorentz boost (due to the isomorphism of SL(2,C) and the restricted Lorentz group, SO(3,1)). Just as the Lorentz transformation preserves the proper time, the quantity det $\Psi = S_0^2 - S_1^2 - S_2^2 - S_3^2$ is invariant within a multiplicative scalar constant under Jones matrix transformations (dichroic and/or birefringent).

In birefringent and dichroic media, in addition to writing a Jones matrix for the net effect of passing through a particular path in a given medium, the evolution of the polarization state along that path can be characterized as the (matrix) product of an infinite series of infinitesimal steps, each operating on the state produced by all earlier matrices. In a uniform medium each step is the same, and one may write

$$\mathbf{J} = Je^{\mathbf{D}},$$

where J is an overall (real) gain/loss factor. Here **D** is a traceless matrix such that α**De** gives the derivative of **e** with respect to z. If **D** is Hermitian the effect is dichroism, while a unitary matrix models birefringence. The matrix **D** can be expressed as a linear combination of the Pauli matrices, where real coefficients give Hermitian matrices and imaginary coefficients give unitary matrices. The Jones matrix in each case may therefore be written with the convenient construction

$$\mathbf{J_b} = J_b e^{\beta\sigma \cdot \hat{\mathbf{n}}} \quad \text{and} \quad \mathbf{J_r} = J_r e^{\phi i\sigma \cdot \hat{\mathbf{m}}},$$

where σ is a 3-vector composed of the Pauli matrices (used here as generators for the Lie group SL(2,C)) and **n** and **m** are real 3-vectors on the Poincaré sphere corresponding to one of the propagation modes of the medium. The effects in that space correspond to a Lorentz boost of velocity parameter 2β along the given direction, or a rotation of angle 2ϕ about the given axis. These transformations may also be written as biquaternions (quaternions with complex elements), where the elements are related to the Jones matrix in the same way that the Stokes parameters are related to the coherency matrix. They may then be applied in pre- and post-multiplication to the quaternion representation of the coherency matrix, with the usual exploitation of the quaternion exponential for performing rotations and boosts taking a form equivalent to the matrix exponential equations above. (*See Quaternion rotation*)

In addition to birefringence and dichroism in extended media, polarization effects describable using Jones matrices can also occur at (reflective) interface between two materials of different refractive index. These effects are treated by the Fresnel equations. Part of the wave is transmitted and part is reflected, with the ratio depending on angle of incidence and the angle of refraction. In addition, if the plane of the reflecting surface is not aligned with the plane of propagation of the wave, the polarization of the two parts is altered. In general, the Jones matrices of the reflection and transmission are real and diagonal, making the effect similar to that of a simple linear polarizer. For unpolarized light striking a surface at a certain optimum angle of incidence known as Brewster's angle, the reflected wave will be completely *s*-polarized.

Certain effects do not produce linear transformations of the Jones vector, and thus cannot be described with (constant) Jones matrices. For these cases it is usual instead to use a 4×4 matrix that acts upon the Stokes 4-vector. Such matrices were first used by Paul Soleillet in 1929, although they have come to be known as Mueller matrices. While every Jones matrix has a Mueller matrix, the reverse is not true. Mueller matrices are frequently used to study the effects of the scattering of waves from complex surfaces or ensembles of particles.

Polarization in nature, science, and technology

Polarization effects in everyday life

Light reflected by shiny transparent materials is partly or fully polarized, except when the light is normal (perpendicular) to the surface. It was through this effect that polarization was first discovered in 1808 by the mathematician Etienne Louis Malus. A polarizing filter, such as a pair of polarizing sunglasses, can be used to observe this effect by rotating the filter while looking through it at the reflection off of a distant horizontal surface. At certain rotation angles, the reflected light will be reduced or eliminated. Polarizing filters remove light polarized at 90° to the filter's polarization axis. If two polarizers are placed atop one another at 90° angles to one another, there is minimal light transmission.

Effect of a polarizer on reflection from mud flats. In the picture on the left, the polarizer is rotated to transmit the reflections as well as possible; by rotating the polarizer by 90° (picture on the right) almost all specularly reflected sunlight is blocked.

The effects of a polarizing filter on the sky in a photograph. The picture on the right uses the filter.

Polarization by scattering is observed as light passes through the atmosphere. The scattered light produces the brightness and color in clear skies. This partial polarization of scattered light can be used to darken the sky in photographs, increasing the contrast. This effect is easiest to observe at sunset, on the horizon at a 90° angle from the setting sun. Another easily observed effect is the drastic reduction in brightness of images of the sky and clouds reflected from horizontal surfaces (see Brewster's angle), which is the main reason polarizing filters are often used in sunglasses. Also frequently visible through polarizing sunglasses are rainbow-like patterns caused by color-dependent birefringent effects, for example in toughened glass (e.g., car windows) or items made from transparent plastics. The role played by polarization in the operation of liquid crystal displays (LCDs) is also frequently apparent to the wearer of polarizing sunglasses, which may reduce the contrast or even make the display unreadable.

The photograph on the right was taken through polarizing sunglasses and through the rear window of a car. Light from the sky is reflected by the windshield of the other car at an angle, making it mostly horizontally polarized. The rear window is made of tempered glass. Stress in the glass, left from its heat treatment, causes it to alter the polarization of light passing through it, like a wave plate. Without this effect, the sunglasses would block the horizontally

Polarizing sunglasses reveal stress in car window (see text for explanation.)

polarized light reflected from the other car's window. The stress in the rear window, however, changes some of the horizontally polarized light into vertically polarized light that can pass through the glasses. As a result, the regular pattern of the heat treatment becomes visible.

Biology

Many animals are apparently capable of perceiving some of the components of the polarization of light, e.g. linear horizontally-polarized light. This is generally used for navigational purposes, since the linear polarization of sky light is always perpendicular to the direction of the sun. This ability is very common among the insects, including bees, which use this information to orient their communicative dances. Polarization sensitivity has also been observed in species of octopus, squid, cuttlefish, and mantis shrimp. In the latter case, one species measures all six orthogonal components of polarization, and is believed to have optimal polarization vision.[7] The rapidly changing, vividly colored skin patterns of cuttlefish, used for communication, also incorporate polarization patterns, and mantis shrimp are known to have polarization selective reflective tissue. Sky polarization was thought to be perceived by pigeons, which was assumed to be one of their aids in homing, but research indicates this is a popular myth.[8]

The naked human eye is weakly sensitive to polarization, without the need for intervening filters. Polarized light creates a very faint pattern near the center of the visual field, called Haidinger's brush. This pattern is very difficult to see, but with practice one can learn to detect polarized light with the naked eye.

Geology

The property of (linear) birefringence is widespread in crystalline minerals, and indeed was pivotal in the initial discovery of polarization. In mineralogy, this property is frequently exploited using polarization microscopes, for the purpose of identifying minerals. See pleochroism.

Chemistry

Polarization is principally of importance in chemistry due to → circular dichroism and "optical rotation" (circular birefringence) exhibited by optically active (chiral) molecules. It may be measured using polarimetry.

The term 'polarization' may also refer to the through-bond (inductive or resonant effect) or through-space influence of a nearby functional group on the electronic properties (e.g. dipole moment) of a covalent bond or atom. This concept is based on the formation of an electric dipole within a molecule, which is generally not related to the polarization of electromagnetic waves.

Polarized light does interact with anisotropic materials, which is the basis for birefringence. This is usually seen in crystalline materials and is especially useful in geology (see above). The polarized light is 'double refracted', as the refractive index is different for horizontally and vertically polarized light in these materials. This is to say, the polarizability of anisotropic materials is not equivalent in all directions. This anisotropy causes changes in the polarization of the incident beam, and is easily observable using cross-polar microscopy or polarimetry. The optical rotation of chiral compounds (as opposed to achiral compounds that form anisotropic crystals), is derived from circular birefringence. Like linear birefringence described above, circular birefringence is the 'double refraction' of circular polarized light.[9]

Astronomy

In many areas of astronomy, the study of polarized electromagnetic radiation from outer space is of great importance. Although not usually a factor in the thermal radiation of stars, polarization is also present in radiation from coherent astronomical sources (e.g. hydroxyl or methanol masers), and incoherent sources such as the large radio lobes in active galaxies, and pulsar radio radiation (which may, it is speculated, sometimes be coherent), and is also imposed upon starlight by scattering from interstellar dust. Apart from providing information on sources of radiation and scattering, polarization also probes the interstellar magnetic field via Faraday rotation. The polarization

of the cosmic microwave background is being used to study the physics of the very early universe. Synchrotron radiation is inherently polarised.

Technology

Technological applications of polarization are extremely widespread. Perhaps the most commonly encountered examples are liquid crystal displays and polarized sunglasses.

All radio transmitting and receiving antennas are intrinsically polarized, special use of which is made in radar. Most antennas radiate either horizontal, vertical, or circular polarization although elliptical polarization also exists. The electric field or E-plane determines the polarization or orientation of the radio wave. Vertical polarization is most often used when it is desired to radiate a radio signal in all directions such as widely distributed mobile units. AM and FM radio uses vertical polarization. Television uses horizontal polarization. Alternating vertical and horizontal polarization is used on satellite communications (including television satellites), to allow the satellite to carry two separate transmissions on a given frequency, thus doubling the number of customers a single satellite can serve.

In engineering, the relationship between strain and birefringence motivates the use of polarization in characterizing the distribution of stress and strain in prototypes. Electronically controlled birefringent devices are used in combination with polarizing filters as modulators in fiber optics. Polarizing filters are also used in photography. They can deepen the color of a blue sky and eliminate reflections from windows and standing water.

Strain in Glass
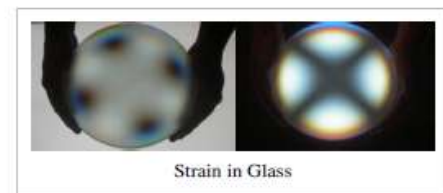
Sky polarization has been exploited in the "sky compass", which was used in the 1950s when navigating near the poles of the Earth's magnetic field when neither the sun nor stars were visible (e.g. under daytime cloud or twilight). It has been suggested, controversially, that the Vikings exploited a similar device (the "sunstone") in their extensive expeditions across the North Atlantic in the 9th–11th centuries, before the arrival of the magnetic compass in Europe in the 12th century. Related to the sky compass is the "polar clock", invented by Charles Wheatstone in the late 19th century.

Polarization is also used for some 3D movies, in which the images intended for each eye are either projected from two different projectors with orthogonally oriented polarizing filters or from a single projector with time multiplexed polarization (a fast alternating polarization device for successive frames). Filter glasses with similarly oriented polarized filters ensure that each eye receives only the correct image. Typical stereoscopic projection displays use linear polarization encoding, because it is not very expensive and offers high contrast. In environments where the viewer is moving, such as in simulators, circular polarization is sometimes used. This makes the channel separation insensitive to the viewing orientation. The 3-D effect only works on a silver screen since it maintains polarization, whereas the scattering in a normal projection screen would void the effect.

Art

Several visual artists have worked with polarized light and birefringent materials to create colorful, sometimes changing images. One example is contemporary artist Austine Wood Comarow, whose "Polage" art works have been exhibited at the Museum of Science, Boston,[10] the New Mexico Museum of Natural History and Science in Albuquerque, NM, and the Cité des Sciences et de l'Industrie (the City of Science and Industry) in Paris.[11] [12] The artist works by cutting hundreds of small pieces of cellophane and other birefringent films and laminating them between plane polarizing filters.

3-D films make use of polarized light and polarization filters in order to generate the 3D effect.

Notes and references

- *Principles of Optics*, 7th edition, M. Born & E. Wolf, Cambridge University, 1999, ISBN 0-521-64222-1.
- *Fundamentals of polarized light: a statistical optics approach*, C. Brosseau, Wiley, 1998, ISBN 0-471-14302-2.
- *Polarized Light, second edition*, Dennis Goldstein, Marcel Dekker, 2003, ISBN 0-8247-4053-X
- *Field Guide to Polarization*, Edward Collett, SPIE Field Guides vol. **FG05**, SPIE, 2005, ISBN 0-8194-5868-6.
- *Polarization Optics in Telecommunications*, Jay N. Damask, Springer 2004, ISBN 0-387-22493-9.
- *Optics*, 4th edition, Eugene Hecht, Addison Wesley 2002, ISBN 0-8053-8566-5.
- *Polarized Light in Nature*, G. P. Können, Translated by G. A. Beerling, Cambridge University, 1985, ISBN 0-521-25862-6.
- *Polarised Light in Science and Nature*, D. Pye, Institute of Physics, 2001, ISBN 0-7503-0673-4.
- *Polarized Light, Production and Use*, William A. Shurcliff, Harvard University, 1962.
- *Ellipsometry and Polarized Light*, R. M. A. Azzam and N. M. Bashara, North-Holland, 1977, ISBN 0-444-87016-4
- *Secrets of the Viking Navigators—How the Vikings used their amazing sunstones and other techniques to cross the open oceans*, Leif Karlsen, One Earth Press, 2003.

[1] Dorn, R. and Quabis, S. and Leuchs, G. (dec 2003). "Sharper Focus for a Radially Polarized Light Beam". *Physical Review Letters* **91** (23,): 233901-+.
[2] Subrahmanyan Chandrasekhar (1960) Radiative transfer, p.27
[3] Merrill Ivan Skolnik (1990) *Radar Handbook*, Fig. 6.52, sec. 6.60.
[4] Hamish Meikle (2001) *Modern Radar Systems*, eq. 5.83.
[5] T. Koryu Ishii (Editor), 1995, *Handbook of Microwave Technology. Volume 2, Applications*, p. 177.
[6] John Volakis (ed) 2007 *Antenna Engineering Handbook, Fourth Edition*, sec. 26.1. Note: in contrast with other authors, this source initially defines ellipticity reciprocally, as the minor-to-major-axis ratio, but then goes on to say that "Although [it] is less than unity, when expressing ellipticity in decibels, the minus sign is frequently omitted for convenience", which essentially reverts back to the definition adopted by other authors.
[7] Sonja Kleinlogel, Andrew White (2008). "The secret world of shrimps: polarisation vision at its best". *PLoS ONE* **3**: e2190. doi: 10.1371/journal.pone.0002190 (http://dx.doi.org/10.1371/journal.pone.0002190).
[8] "No evidence for polarization sensitivity in the pigeon electroretinogram", J. J. Vos Hzn, M. A. J. M. Coemans & J. F. W. Nuboer, *The Journal of Experimental Biology*, 1995.
[9] Hecht, Eugene (1998). *Optics* (3rd ed.). Reading, MA: Addison Wesley Longman.
[10] http://www.youtube.com/watch?v=UEU-aoFHIRk
[11] " Austine Studios Polarized Light Art (http://www.austine.com/aboutaustine.shtml)". . Retrieved January 31, 2009.
[12] Mann, James (2005). *Austine Wood Comarow: Paintings in Polarized Light*. Las Vegas, NV: Wasabi Pub.. ISBN 0-9768198-0-5.

Optical rotatory dispersion

Optical rotatory dispersion is the variation in the optical rotation of a substance with a change in the wavelength of light. Optical rotatory dispersion can be used to find the absolute configuration of metal complexes. For example when plane polarized white light from an overhead projector is passed through a cylinder of sucrose solution a spiral rainbow is observed perpendicular to the cylinder. When white light passes through a polarizer, the extent of rotation of light depends on its wavelength. Short wavelengths are rotated more than longer wavelengths. Because the wavelength of light determines its color, the variation of color with distance through the tube is observed. This dependence of specific rotation on wavelength is called optical rotatory dispersion.

See also

- → Circular dichroism

Circular dichroism

Circular dichroism (CD) is the differential absorption of left- and right-handed circularly polarized light.[1]

A CD Spectrometer is an instrument that records this phenomenon as a function of wavelength. Modern instruments, however, can generally also record CD as a function of temperature or chemical environment, at several wavelengths.

This phenomenon is exhibited in the absorption bands of an optically active molecule. CD can be used to help determine the structure of macromolecules (including the secondary structure of proteins and the handedness of DNA).

CD was discovered by the French physicist Aimé Cotton in 1896.

Basic information

Circular polarization

Linearly polarized light is polarized in a certain direction (that is, the magnitude of its electric field vector oscillates only in one plane, similar to a sine wave). In circularly polarized light, the electric field vector has a constant length, but rotates about its propagation direction. Hence it forms a helix in space while propagating. If this is a left-handed helix, the light is referred to as left circularly polarized, and vice versa for a right-handed helix. See the external links for a demonstrative animation of the different types of electromagnetic waves.

Interaction of circularly polarized light with matter

The electric field of a light beam causes a linear displacement of charge when interacting with a molecule, whereas the magnetic field of it causes a circulation of charge. These two motions combined result in a helical displacement when light impinges on a molecule (both field vectors in the same place are of the same direction, but at different moments of time). Since circularly polarized light itself is "chiral", it interacts differently with chiral molecules. That is, the two types of circularly polarized light are absorbed to different extents. In a CD experiment, equal amounts of left and right circularly polarized light of a selected wavelength are alternately radiated into a (chiral) sample. One of the two polarizations is absorbed more than the other one, and this wavelength-dependent difference of absorption is measured, yielding the CD spectrum of the sample.

Due to the interaction with the molecule, the electric field vector of the light traces out an elliptical path after passing through the sample.

Delta absorbance

At a given wavelength,

$$\Delta A = A_L - A_R$$

where ΔA is the difference between absorbance of left circularly polarized (LCP) and right circularly polarized (RCP) light (this is what is usually measured).

Molar circular dichroism

It can also be expressed, by applying Beer's law, as:

$$\Delta A = (\epsilon_L - \epsilon_R)Cl$$

where

ε$_L$ and ε$_R$ are the molar extinction coefficients for LCP and RCP light,

C is the molar concentration

l is the path length in centimeters (cm).

Then

$$\Delta\epsilon = \epsilon_L - \epsilon_R$$

is the molar circular dichroism. This intrinsic property is what is usually meant by the circular dichroism of the substance.

Application to biological molecules

In general, this phenomenon will be exhibited in absorption bands of any optically active molecule. As a consequence, circular dichroism is exhibited by biological molecules, because of their dextrorotary and levorotary components. Even more important is that a secondary structure will also impart a distinct CD to its respective molecules. Therefore, the alpha helix of proteins and the double helix of nucleic acids have CD spectral signatures representative of their structures.

CD is closely related to the → optical rotatory dispersion (ORD) technique, and is generally considered to be more advanced. CD is measured in or near the absorption bands of the molecule of interest, while ORD can be measured far from these bands. CD's advantage is apparent in the data analysis. Structural elements are more clearly distinguished since their recorded bands do not overlap extensively at particular wavelengths as they do in ORD. In principle these two spectral measurements can be interconverted through an integral transform (Kramers–Kronig_relation), if all the absorptions are included in the measurements.

The far-UV (ultraviolet) CD spectrum of proteins can reveal important characteristics of their secondary structure. CD spectra can be readily used to estimate the fraction of a molecule that is in the alpha-helix conformation, the beta-sheet conformation, the beta-turn conformation, or some other (e.g. random coil) conformation.[2] [3] These fractional assignments place important constraints on the possible secondary conformations that the protein can be in. CD cannot, in general, say where the alpha helices that are detected are located within the molecule or even completely predict how many there are. Despite this, CD is a valuable tool, especially for showing changes in conformation. It can, for instance, be used to study how the secondary structure of a molecule changes as a function of temperature or of the concentration of denaturing agents, e.g. Guanidinium hydrochloride or urea. In this way it can reveal important thermodynamic information about the molecule (such as the enthalpy and Gibbs free energy of denaturation) that cannot otherwise be easily obtained. Anyone attempting to study a protein will find CD a valuable tool for verifying that the protein is in its native conformation before undertaking extensive and/or expensive experiments with it. Also, there are a number of other uses for CD spectroscopy in protein chemistry not related to alpha-helix fraction estimation.

The near-UV CD spectrum (>250 nm) of proteins provides information on the tertiary structure. The signals obtained in the 250-300 nm region are due to the absorption, dipole orientation and the nature of the surrounding environment of the phenylalanine, tyrosine, cysteine (or S-S disulfide bridges) and tryptophan amino acids. Unlike in far-UV CD, the near-UV CD spectrum cannot be assigned to any particular 3D structure. Rather, near-UV CD spectra provide structural information on the nature of the prosthetic groups in proteins, e.g., the heme groups in hemoglobin and cytochrome c.

Visible CD spectroscopy is a very powerful technique to study metal–protein interactions and can resolve individual d-d electronic transitions as separate bands. CD spectra in the visible light region are only produced when a metal ion is in a chiral environment, thus, free metal ions in solution are not detected. This has the advantage of only observing the protein-bound metal, so pH dependence and stoichiometries are readily obtained. Optical activity in transition metal ion complexes have been attributed to configurational, conformational and the vicinal effects. Klewpatinond and Viles (2007) have produced a set of empirical rules for predicting the appearance of visible CD spectra for Cu^{2+} and Ni^{2+} square-planar complexes involving histidine and main-chain coordination.

CD gives less specific structural information than X-ray crystallography and protein NMR spectroscopy, for example, which both give atomic resolution data. However, CD spectroscopy is a quick method that does not require large amounts of proteins or extensive data processing. Thus CD can be used to survey a large number of solvent conditions, varying temperature, pH, salinity, and the presence of various cofactors.

CD → spectroscopy is usually used to study proteins in solution, and thus it complements methods that study the solid state. This is also a limitation, in that many proteins are embedded in membranes in their native state, and solutions containing membrane structures are often strongly scattering. CD is sometimes measured in thin films.

Experimental limitations

CD has also been studied in carbohydrates, but with limited success due to the experimental difficulties associated with measurement of CD spectra in the vacuum ultraviolet (VUV) region of the spectrum (100-200 nm), where the corresponding CD bands of unsubstituted carbohydrates lie. Substituted carbohydrates with bands above the VUV region have been successfully measured.

Measurement of CD is also complicated by the fact that typical aqueous buffer systems often absorb in the range where structural features exhibit differential absorption of circularly polarized light. Phosphate, sulfate, carbonate, and acetate buffers are generally incompatible with CD unless made extremely dilute e.g. in the 10-50 mM range. The TRIS buffer system should be completely avoided when performing far-UV CD. Borate and Onium compounds are often used to establish the appropriate pH range for CD experiments. Some experimenters have substituted fluoride for chloride ion because fluoride absorbs less in the far UV, and some have worked in pure water. Another, almost universal, technique is to minimize solvent absorption by using shorter path length cells when working in the far UV, 0.1 mm path lengths are not uncommon in this work.

In addition to measuring in aqueous systems, CD, particularly far-UV CD, can be measured in organic solvents e.g. ethanol, methanol, trifluoroethanol (TFE). The latter has the advantage to induce structure formation of proteins, inducing beta-sheets in some and alpha helices in others, which they would not show under normal aqueous conditions. Most common organic solvents such as acetonitrile, THF, chloroform, dichloromethane are however, incompatible with far-UV CD.

It may be of interest to note that the protein CD spectra used in secondary structure estimation are related to the π to π*orbital absorptions of the amide bonds linking the amino acids. These absorption bands lie partly in the *so-called* vacuum ultraviolet (wavelengths less than about 200 nm). The wavelength region of interest is actually inaccessible in **air** because of the strong absorption of light by oxygen at these wavelengths. In practice these spectra are measured not in vacuum but in an oxygen-free instrument (filled with pure nitrogen gas).

Once oxygen has been eliminated, perhaps the second most important technical factor in working below 200 nm is to design the rest of the optical system to have low losses in this region. Critical in this regard is the use of aluminized mirrors whose coatings have been optimized for low loss in this region of the spectrum.
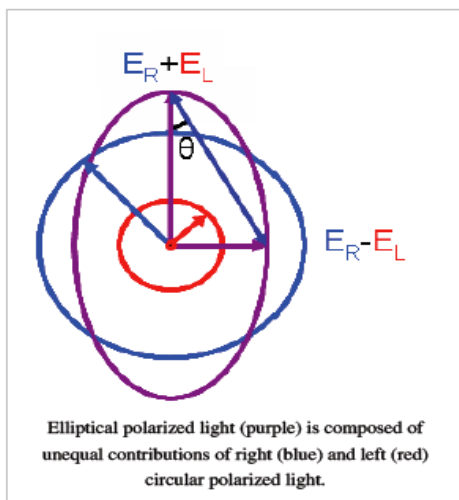
The usual light source in these instruments is a high pressure, short-arc xenon lamp. Ordinary xenon arc lamps are unsuitable for use in the low UV. Instead specially constructed lamps with envelopes made from high-purity synthetic fused silica must be used.

Light from synchrotron sources has a much higher flux at short wavelengths, and has been used to record CD down to 160 nm. Recently the CD spectrometer at the electron storage ring facility ISA at the University of Aarhus in Denmark was used to record solid state CD spectra down to 120 nm.

At the quantum mechanical level, the information content of circular dichroism and optical rotation are identical.

Molar ellipticity

Although ΔA is usually measured, for historical reasons most measurements are reported in degrees of ellipticity. Molar circular dichroism and molar ellipticity, [θ], are readily interconverted by the equation:

Elliptical polarized light (purple) is composed of
unequal contributions of right (blue) and left (red)
circular polarized light.

$$[\theta] = 3298.2 \Delta\epsilon .$$

This relationship is derived by defining the → ellipticity of the polarization as:

$$tan\theta = \frac{E_R - E_L}{E_R + E_L}$$

where

E_R and E_L are the magnitudes of the electric field vectors of the right-circularly and left-circularly polarized light, respectively.

When E_R equals E_L (when there is no difference in the absorbance of right- and left-circular polarized light), θ is 0° and the light is linearly polarized. When either E_R or E_L is equal to zero (when there is complete absorbance of the circular polarized light in one direction), θ is 45° and the light is circularly polarized.

Generally, the circular dichroism effect is small, so tanθ is small and can be approximated as θ in radians. Since the intensity or irradiance, I, of light is proportional to the square of the electric-field vector, the ellipticity becomes:

$$\theta(radians) = \frac{(I_R^{1/2} - I_L^{1/2})}{(I_R^{1/2} + I_L^{1/2})}$$

Then by substituting for I using Beer's Law in natural logarithm form:

$$I = I_0 e^{-A \ln 10}$$

The ellipticity can now be written as:

$$\theta(radians) = \frac{(e^{\frac{-A_R}{2} \ln 10} - e^{\frac{-A_L}{2} \ln 10})}{(e^{\frac{-A_R}{2} \ln 10} + e^{\frac{-A_L}{2} \ln 10})} = \frac{e^{\Delta A \frac{\ln 10}{2}} - 1}{e^{\Delta A \frac{\ln 10}{2}} + 1}$$

Since ΔA<<1, this expression can be approximated by expanding the exponentials in a Taylor series to first-order and then discarding terms of ΔA in comparison with unity and converting from radians to degrees:

$$\theta(degrees) = \Delta A \left(\frac{\ln 10}{4}\right) \left(\frac{180}{\pi}\right)$$

The linear dependence of solute concentration and pathlength is removed by defining molar ellipticity as,

$$[\theta] = \frac{100\theta}{Cl}$$

Then combining the last two expression with Beer's Law, molar ellipticity becomes:

$$[\theta] = 100\Delta\epsilon \left(\frac{ln\,10}{4}\right)\left(\frac{180}{\pi}\right) = 3298.2\Delta\epsilon$$

- Circular Dichroism explained [5]
- Circular Dichroism at UMDNJ [6] - a good site for information on structure estimation software
- Electromagnetic waves [7] - Animated electromagnetic waves. The Emanim program is a teaching resource for helping students understand the nature of electromagnetic waves and their interaction with birefringent and dichroic samples
- An Introduction to Circular Dichroism [8]

References

[1] P. Atkins and J. de Paula (2005). *Elements of Physical Chemistry, 4th ed.*. Oxford University Press.

[2] Whitmore L, Wallace BA (2008). "Protein secondary structure analyses from circular dichroism spectroscopy: methods and reference databases". *Biopolymers* **89** (5): 392–400. doi: 10.1002/bip.20853 (http://dx.doi.org/10.1002/bip.20853). PMID 17896349 (http://www.ncbi.nlm.nih.gov/pubmed/17896349).

[3] Greenfield NJ (2006). "Using circular dichroism spectra to estimate protein secondary structure". *Nature protocols* **1** (6): 2876–90. doi: 10.1038/nprot.2006.202 (http://dx.doi.org/10.1038/nprot.2006.202). PMID 17406547 (http://www.ncbi.nlm.nih.gov/pubmed/17406547).

[4] http://books.google.co.uk/books?hl=en&id=THeKGC99hJcC

[5] http://www.ap-lab.com/circular_dichroism.htm

[6] http://www2.umdnj.edu/cdrwjweb/index.htm#software

[7] http://www.enzim.hu/~szia/cddemo/edemo1.htm

[8] http://www.photophysics.com/circulardichroism.php

Further reading

1. Alison Rodger and Bengt Nordén, *Circular Dichroism and Linear Dichroism* [4] (1997) Oxford University Press, Oxford, UK. ISBN 019855897X.

2. Fasman, G.D., *Circular Dichroism and the Conformational Analysis of Biomolecules* (1996) Plenum Press, New York.

3. Hecht, E., *Optics* 3rd Edition (1998) Addison Wesley Longman, Massachusetts.

4. Klewpatinond, M. and Viles, J.H. (2007) Empirical rules for rationalising visible circular dichroism of Cu^{2+} and Ni^{2+} histidine complexes: Applications to the prion protein. FEBS Letters 581, 1430-1434.

Vibrational circular dichroism

Vibrational circular dichroism (VCD) → spectroscopy is basically → circular dichroism spectroscopy in the infrared and near infrared ranges[1] . Because VCD is sensitive to the mutual orientation of distinct groups in a molecule, it provides three-dimensional structural information. Thus, it is a powerful technique as VCD spectra of enantiomers can be simulated using *ab initio* calculations, thereby allowing the identification of absolute configurations of small molecules in solution from VCD spectra. Among such quantum computations of VCD spectra resulting from the chiral properties of small organic molecules are those based on density functional theory (DFT) and gauge-invariant atomic orbitals (GIAO). As a simple example of the experimental results that were obtained by VCD are the spectral data obtained within the carbon-hydrogen (C-H) stretching region of 21 amino acids in heavy water solutions. Measurements of vibrational optical activity (VOA) have thus numerous applications, not only for small molecules, but also for large and complex biopolymers such as muscle proteins (myosin, for example) and DNA.

Vibrational modes
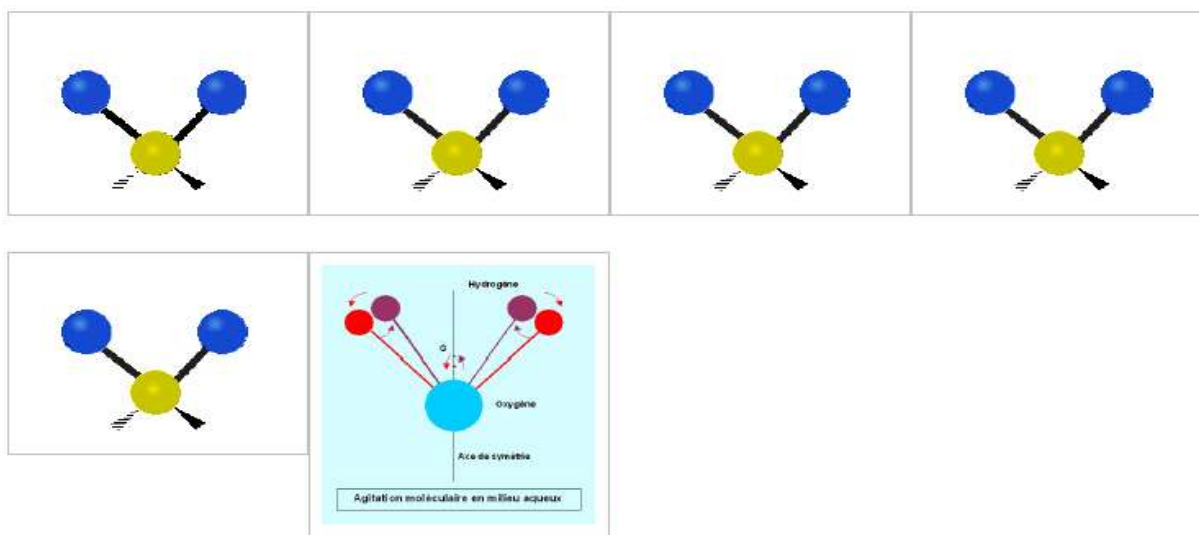
VCD of peptides and proteins

Extensive VCD studies have been reported for both polypeptides and several proteins in solution[2] [3] [4] ; several recent reviews were also compiled[5] [6] [7] [8] . An extensive but not comprehensive VCD publications list is also provided in the "References" section. The published reports over the last 22 years have established VCD as a powerful technique with improved results over those previously obtained by visible/UV circular dichroism (CD) or → optical rotatory dispersion (ORD) for proteins and nucleic acids.

Amino acid and polypeptide structures
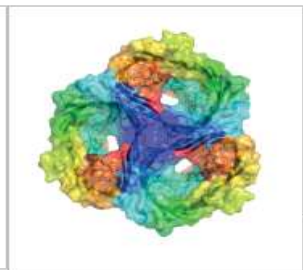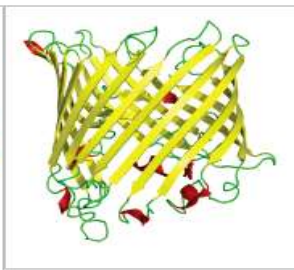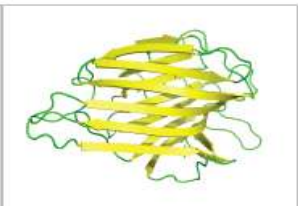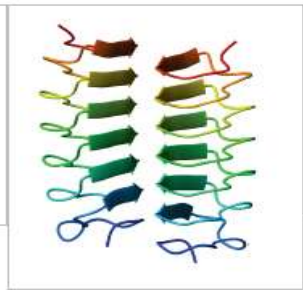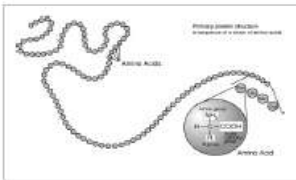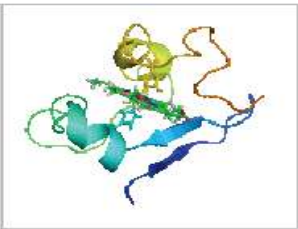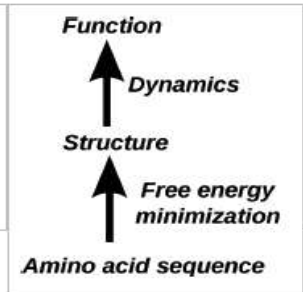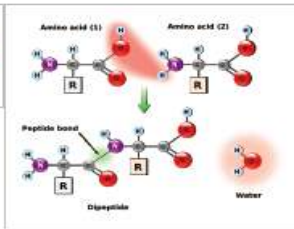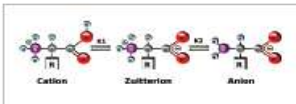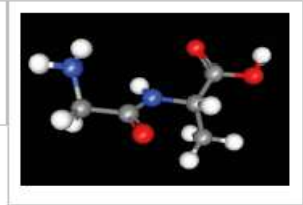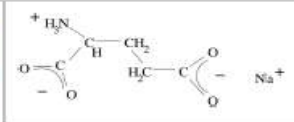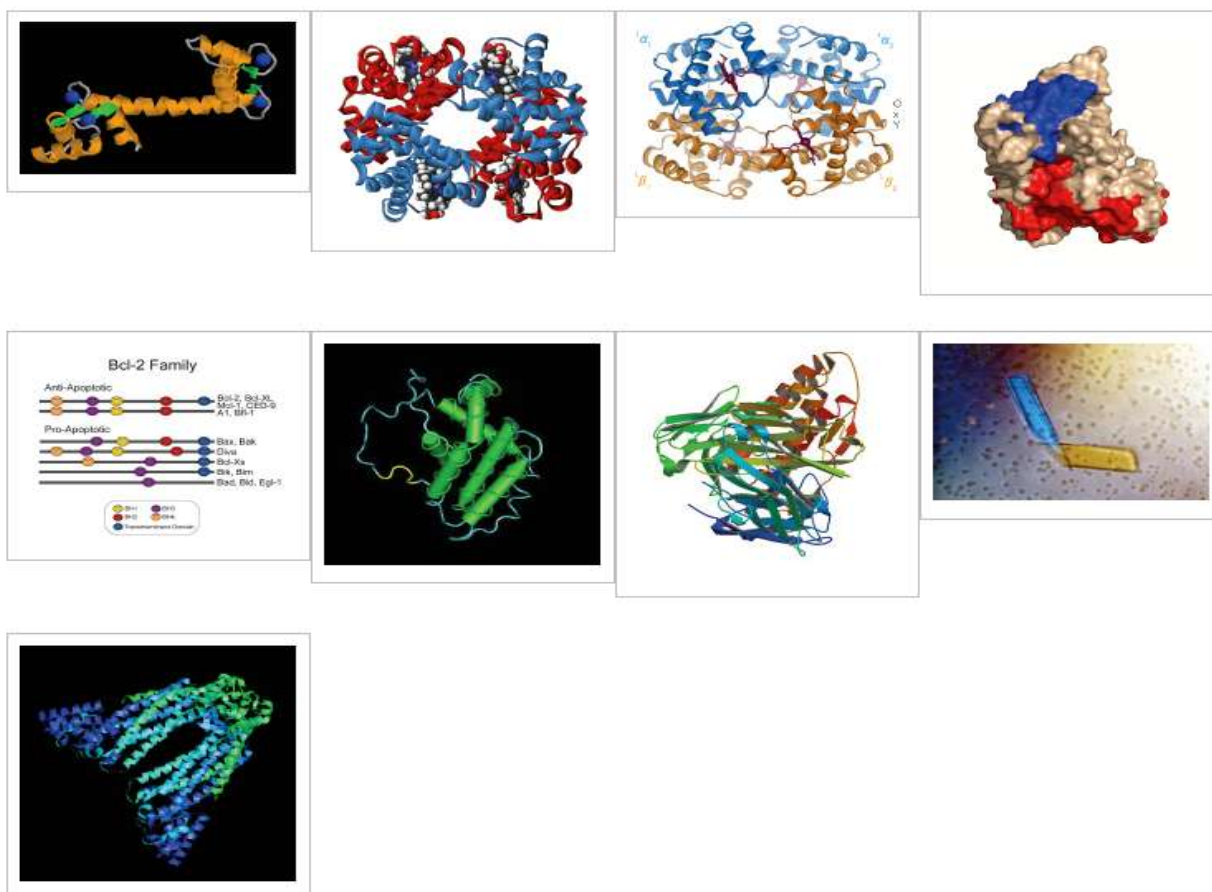
VCD of nucleic acids

VCD spectra of nucleotides, synthetic polynucleotides and several nucleic acids, including DNA, have been reported and assigned in terms of the type and number of helices present in A-, B-, and Z- DNA.

VCD Instrumentation

For biopolymers such as proteins and nucleic acids, the difference in absorbance between the levo- and dextro-configurations is five orders of magnitude smaller than the corresponding (unpolarized) absorbance. Therefore, VCD of biopolymers requires the use of very sensitive, specially built instrumentation as well as time-averaging over relatively long intervals of time even with such sensitive VCD spectrometers. Most CD instruments produce left- and right- circularly polarized light which is then either sine-wave or square-wave modulated, with subsequent phase-sensitive detection and lock-in amplification of the detected signal. In the case of FT-VCD, a photo-elastic modulator (PEM) is employed in conjunction with an FT-IR interferometer set-up. An example is that of a Bomem model MB-100 FT-IR interferometer equipped with additional polarizing optics/ accessories needed for recording VCD spectra. A parallel beam emerges through a side port of the interferometer which passes first through a wire grid linear polarizer and then through an octagonal-shaped ZnSe crystal PEM which modulates the polarized beam at a fixed, lower frequency such as 37.5 kHz. A mechanically stressed crystal such as ZnSe exhibits birefringence when stressed by an adjacent piezoelectric transducer. The linear polarizer is positioned close to, and at 45 degrees, with

respect to the ZnSe crystal axis. The polarized radiation focused onto the detector is doubly modulated, both by the PEM and by the interferometer setup. A very low noise detector, such as MCT (HgCdTe), is also selected for the VCD signal phase-sensitive detection. Quasi-complete commercial FT-VCD instruments are also available from a few manufacturers but these are quite expensive and also have to be still considered as being at the prototype stage. To prevent detector saturation an appropriate, long wave pass filter is placed before the very low noise MCT detector, which allows only radiation below 1750 cm^{-1} to reach the MCT detector; the latter however measures radiation only down to 750 cm^{-1}. FT-VCD spectra accumulation of the selected sample solution is then carried out, digitized and stored by an in-line computer. Published reviews that compare various VCD methods are also available.[9] [10]
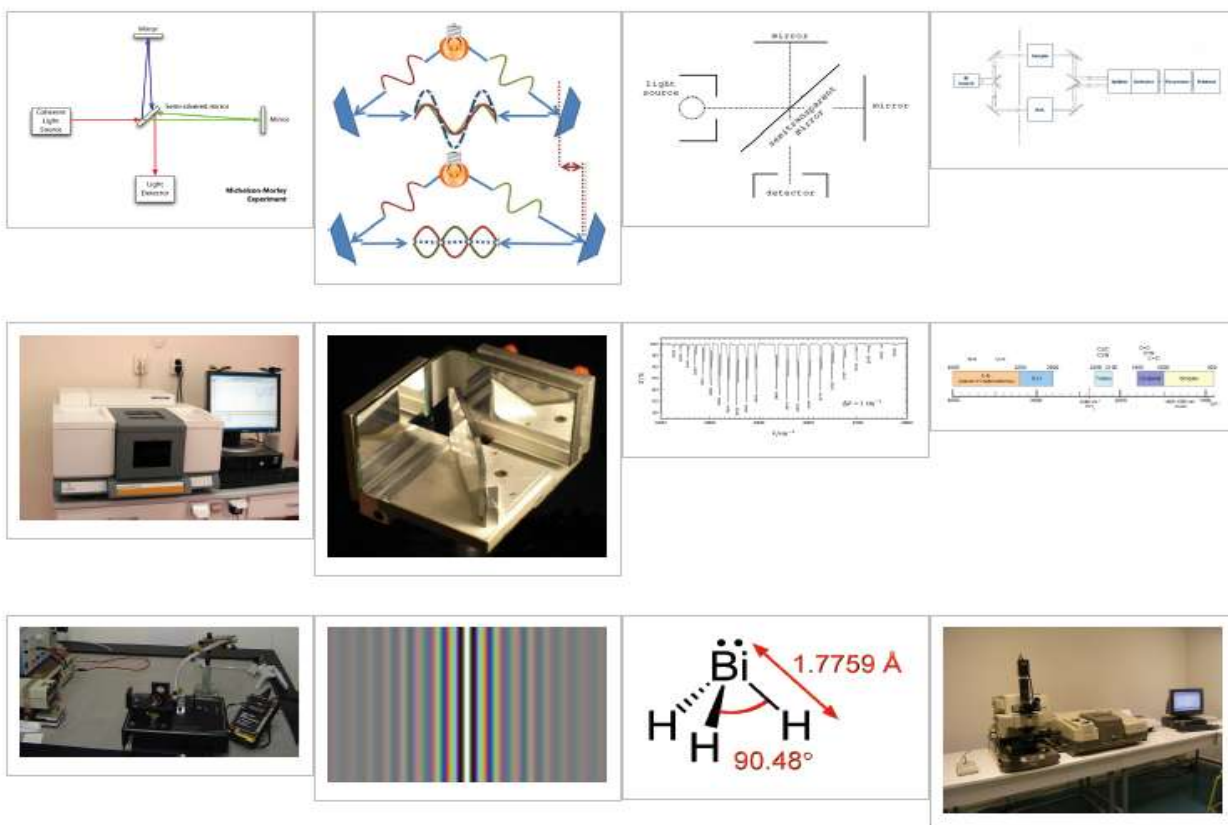
Magnetic VCD

VCD spectra have also been reported in the presence of an applied external magnetic field[11]. This method can enhance the VCD spectral resolution for small molecules[12] [13] [14] [15] [16].

Raman optical activity (ROA)

ROA is a technique complementary to VCD especially useful in the 50—1600 cm^{-1} spectral region; it is considered as the technique of choice for determining optical activity for photon energies less than 600 cm^{-1}.

References

Peptides and proteins

- Huang R, Wu L, McElheny D, Bour P, Roy A, Keiderling TA. Cross-Strand Coupling and Site-Specific Unfolding Thermodynamics of a Trpzip beta-Hairpin Peptide Using (13)C Isotopic Labeling and IR Spectroscopy. *The journal of physical chemistry. B*. 2009 Apr;113(16):5661-74.
- "Vibrational Circular Dichroism of Poly alpha-Benzyl-L-Glutamate," R. D. Singh, and T. A. Keiderling, Biopolymers, 20, 237-40 (1981).
- "Vibrational Circular Dichroism of Polypeptides II. Solution Amide II and Deuteration Results," A. C. Sen and T. A. Keiderling, Biopolymers, 23, 1519-32 (1984).
- "Vibrational Circular Dichroism of Polypeptides III. Film Studies of Several alpha-Helical and ß-Sheet Polypeptides," A. C. Sen and T. A. Keiderling, Biopolymers, 23, 1533-46 (1984).
- "Vibrational Circular Dichroism of Polypeptides IV. Film Studies of L-Alanine Homo Oligopeptides," U. Narayanan, T. A. Keiderling, G. M. Bonora, and C. Toniolo, *Biopolymers* 24, 1257-63 (1985).
- "Vibrational Circular Dichroism of Polypeptides, T. A. Keiderling, S. C. Yasui, A. C. Sen, C. Toniolo, G. M. Bonora, in Peptides Structure and Function, Proceedings of the 9th American Peptide Symposium," ed. C. M. Deber, K. Kopple, V. Hruby; Pie rce Chemical: Rockford, IL; 167-172 (1985).
- "Vibrational Circular Dichroism of Polypeptides V. A Study of 310 Helical-Octapeptides" S. C. Yasui, T. A. Keiderling, G. M. Bonora, C. Toniolo, Biopolymers 25, 79-89 (1986).
- "Vibrational Circular Dichroism of Polypeptides VI. Polytyrosine alpha-helical and Random Coil Results," S. C. Yasui and T. A. Keiderling, Biopolymers 25, 5-15 (1986).
- "Vibrational Circular Dichroism of Polypeptides VII. Film and Solution Studies of alpha-forming Homo-Oligopeptides," U. Narayanan, T. A. Keiderling, G. M. Bonora, C. Toniolo, *Journal of the American Chemical Society*, 108, 2431-2437 (1986).
- "Vibrational Circular Dichroism of Polypeptides VIII. Poly Lysine Conformations as a Function of pH in Aqueous Solution," S. C. Yasui, T. A. Keiderling, Journal of the American Chemical Society, 108, 5576-5581 (1986).
- "Vibrational Circular Dichroism of Polypeptides IX. A Study of Chain Length Dependence for 310-Helix Formation in Solution." S. C. Yasui, T. A. Keiderling, F. Formaggio, G. M. Bonora, C. Toniolo, Journal of the American Chemical Society 108, 4988-499 3 (1986).
- "Vibrational Circular Dichroism of Biopolymers." T. A. Keiderling, *Nature*, 322, 851-852 (1986).
- "Vibrational Circular Dichroism of Polypeptides X. A Study of alpha-Helical Oligopeptides in Solution." S. C. Yasui, T. A. Keiderling, R. Katachai, Biopolymers 26, 1407-1412 (1987).
- "Vibrational Circular Dichroism of Polypeptides XI. Conformation of Poly(L-Lysine(Z)-L-Lysine(Z)-L-1-Pyrenylalanine) and Poly(L-Lysine(Z)-L-Lysine(Z)-L-1-Napthylala-nine) in Solution" S. C. Yasui, T. A. Keiderling, and M. Sisido, *Macromolecules* 20, 2 403-2406 (1987).
- "Vibrational Circular Dichroism of Biopolymers" T. A. Keiderling, S. C. Yasui, A. C. Sen, U. Narayanan, A. Annamalai, P. Malon, R. Kobrinskaya, L. Yang, in "F.E.C.S. Second International Conference on Circular

Dichroism, Conference Proceedings," ed. M. Kajtar, L. Eötvös Univ., Budapest, 1987, p. 155-161.

- "Vibrational Circular Dichroism of Poly-L-Proline and Other Helical Poly-peptides," R. Kobrinskaya, S. C. Yasui, T. A. Keiderling, in "Peptides: Chemistry and Biology, Proceedings of the 10th American Peptide Symposium," ed. G. R. Marshall, ESCOM, L eiden, 1988, p. 65-67.

- "Vibrational Circular Dichroism of Polypeptides with Aromatic Side Chains," S. C. Yasui, T. A. Keiderling, in "Peptides: Chemistry and Biology, Proceedings of the 10th American Peptide Symposium," ed. G. R. Marshall, ESCOM, Leiden, 1988, p. 90-92.

- "Vibrational Circular Dichroism of Polypeptides XII. Re-evaluation of the Fourier Transform Vibrational Circular Dichroism of Poly-gamma-Benzyl-L-Glutamate," P. Malon, R. Kobrinskaya, T. A. Keiderling, Biopolymers 27, 733-746 (1988).

- "Vibrational Circular Dichroism of Biopolymers," T. A. Keiderling, S. C. Yasui, U. Narayanan, A. Annamalai, P. Malon, R. Kobrinskaya, L. Yang, in *Spectroscopy of Biological Molecules New Advances* ed. E. D. Schmid, F. W. Schneider, F. Siebert, p. 73-76 (1988).

- "Vibrational Circular Dichroism of Polypeptides and Proteins," S. C. Yasui, T. A. Keiderling, *Mikrochimica Acta*, II, 325-327, (1988).

- "(1R,7R)-7-Methyl-6,9,-Diazatricyclo[6,3,0,01,6]Tridecanne-5,10-Dione, A Tricyclic Spirodilactam Containing Non-planar Amide Groups: Synthesis, NMR, Crystal Structure, Absolute Configuration, Electronic and Vibrational Circular Dichroism" P. Malon, C . L. Barness, M. Budesinsky, R. K. Dukor, D. van der Helm, T. A. Keiderling, Z. Koblicova, F. Pavlikova, M. Tichy, K. Blaha, Collections of Czechoslovak Chemical Communications 53, 2447-2472 (1988).

- "Vibrational Circular Dichroism of Poly Glutamic Acid" R. K. Dukor, T. A. Keiderling, in *Peptides 1988* (ed. G. Jung, E. Bayer) Walter de Gruyter, Berlin (1989) pp 519–521.

- "Biopolymer Conformational Studies with Vibrational Circular Dichroism" T. A. Keiderling, S. C. Yasui, P. Pancoska, R. K. Dukor, L. Yang, SPIE Proceeding 1057, ("Biomolecular Spectroscopy," ed. H. H. Mantsch, R. R. Birge) 7-14 (1989).

- "Vibrational Circular Dichroism. Comparison of Techniques and Practical Considerations" T. A. Keiderling, in "Practical Fourier Transform Infrared Spectroscopy. Industrial and Laboratory Chemical Analysis," ed. J. R. Ferraro, K. Krishnan (Academic Press, San Diego, 1990) p. 203-284.

- "Vibrational Circular Dichroism Study of Unblocked Proline Oligomers," R. K. Dukor, T. A. Keiderling, V. Gut, *International Journal of Peptide and Protein Research*, 38, 198-203 (1991).

- "Reassessment of the Random Coil Conformation. Vibrational CD Study of Proline Oligopeptides and Related Polypeptides" R. K. Dukor and T. A. Keiderling, Biopolymers 31 1747-1761 (1991).

- "Vibrational CD of the Amide II band in Some Model Polypeptides and Proteins" V. P. Gupta, T. A. Keiderling, Biopolymers 32 239-248 (1992).

- "Vibrational Circular Dichroism of Proteins Polysaccharides and Nucleic Acids" T. A. Keiderling, Chapter 8 in *Physical Chemistry of Food Processes, Vol. 2 Advanced Techniques, Structures and Applications.*, eds. I.C. Baianu, H. Pessen, T. Kumosinski, Van Norstrand—Reinhold, New York (1993), pp 307–337.

- "Structural Studies of Biological Macromolecules using Vibrational Circular Dichroism" T. A. Keiderling, P. Pancoska, Chapter 6 in Advances in Spectroscopy Vol. 21, *Biomolecular Spectroscopy Part B* eds. R. E. Hester, R. J. H. Clarke, John W iley Chichester (1993) pp 267–315.

- "Ab Initio Simulations of the Vibrational Circular Dichroism of Coupled Peptides" P. Bour and T. A. Keiderling, Journal of the American Chemical Society 115 9602-9607 (1993).

- "Ab initio Simulations of Coupled Peptide Vibrational Circular Dichroism" P. Bour, T. A. Keiderling in "Fifth International Conference on The Spectroscopy of Biological Molecules" Th. Theophanides, J. Anastassopoulou, N. Fotopoulos (Eds), Kluwen Aca demic Publ., Dortrecht, 1993, p. 29-30.

- "Vibrational Circular Dichroism Spectroscopy of Peptides and Proteins" T. A. Keiderling, in "Circular Dichroism Interpretations and Applications," K. Nakanishi, N. Berova, R. Woody, Eds., VCH Publishers, New York, (1994)

pp 497–521.

- "Conformational Study of Sequential Lys-Leu Based Polymers and Oligomers using Vibrational and Electronic Circular Dichroism Spectra" V. Baumruk, D. Huo, R. K. Dukor, T. A. Keiderling, D. LeLeivre and A. Brack Biopolymers 34, 1115-1121 (1994).
- "Vibrational Optical Activity of Oligopeptides" T. B. Freedman, L. A. Nafie, T. A. Keiderling *Biopolymers* (Peptide Science) 37 (ed. C. Toniolo) 265-279 (1995).
- "Characterization of ß-bend ribbon spiral forming peptides using electronic and vibrational circular dichroism" G. Yoder, T. A. Keiderling, F. Formaggio, M. Crisma, C. Toniolo Biopolymers 35, 103-111 (1995).
- "Vibrational Circular Dichroism as a Tool for Determination of Peptide Secondary Structure" P. Bour, T. A. Keiderling, P. Malon, in "Peptides 1994 (Proceedings of the 23rd European Peptide Symposium,1994," (H.L.S. Maia, ed.), Escom, Le iden 1995, p. 517-518.
- "Helical Screw Sense of homo-oligopeptides of C-alpha-methylated alpha-amino acids as Determined with Vibrational Circular Dichroism." G. Yoder, T. A. Keiderling, M. Crisma, F. Formaggio, C. Toniolo, J. Kamphuis, Tetrahedron Assymmetry 6, 687 -690 (1995).
- "Conformational Study of Linear Alternating and Mixed D- and L-Proline Oligomers Using Electronic and Vibrational CD and Fourier Transform IR." W. Mästle, R. K. Dukor, G. Yoder, T. A. Keiderling *Biopolymers* 36, 623-631 (1995).
- Review: "Vibrational Circular Dichroism Applications to Conformational Analysis of Biomolecules" T. A. Keiderling in *Circular Dichroism and the Conformational Analysis of Biomolecules* ed. G. D. Fasman, Plenum, New York (1996) p. 555-585.
- "Mutarotation studies of Poly L-Proline using FT-IR, Electronic and Vibrational Circular Dichroism" R. K. Dukor, T. A. Keiderling, Biospectroscopy 2, 83-100 (1996).
- "Vibrational Circular Dichroism Applications in Proteins and Peptides" T. A. Keiderling, Proceedings of the NATO ASI in Biomolecular Structure and Dynamics, Loutrakii Greece, May 1996, Ed. G. Vergoten (delayed second volume to 1998).
- "Transfer of Molecular Property Tensors in Cartesian Coordinates: A new algorithm for simulation of vibrational spectra" Petr Bour, Jana Sopkova, Lucie Bednarova, Petr Malon, T. A. Keiderling, *Journal of Computational Chemistry* 18, 6 46-659 (1997).
- "Vibrational Circular Dichroism Characterization of Alanine-Rich Peptides." Gorm Yoder and Timothy A. Keiderling, "Spectroscopy of Biological Molecules: Modern Trends," Ed. P. Carmona, R. Navarro, A. Hernanz, Kluwer Acad. Pub., Netherlands (1997) p p. 27-28.
- "Ionic strength effect on the thermal unfolding of alpha-spectrin peptides." D. Lusitani, N. Menhart, T.A. Keiderling and L. W. M. Fung. *Biochemistry* 37(1998)16546-16554.
- "In search of the earliest events of hCGb folding: structural studies of the 60-87 peptide fragment" S. Sherman, L. Kirnarsky, O. Prakash, H. M. Rogers, R.A.G.D. Silva, T.A. Keiderling, D. Smith, A.M. Hanly, F. Perini, and R.W. Ruddon, American Pep tide Symposium Proceedings, 1997.
- "Cold Denaturation Studies of (LKELPKEL)n Peptide Using Vibrational Circular Dichroism and FT-IR". R. A. G. D. Silva, Vladimir Baumruk, Petr Pancoska, T. A. Keiderling, Eric Lacassie, and Yves Trudelle, American Peptide Symposium Proceedings, 1997.
- "Simulations of oligopeptide vibrational CD. Effects of isotopic labeling." Petr Bour, Jan Kubelka,T. A. Keiderling Biopolymers 53, 380-395 (2000).
- "Site specific conformational determination in thermal unfolding studies of helical peptides using vibrational circular dichroism with isotopic substitution" R. A. G. D. Silva, Jan Kubelka, Petr Bour, Sean M. Decatur, Timothy A. Keiderling, *Proceedings of the National Academy of Sciences* (PNAS:USA) 97, 8318-8323 (2000).
- "Folding studies on the human chorionic gonadotropin b -subunit using optical spectroscopy of peptide fragments" R. A. G. D. Silva, S. A. Sherman, F. Perini, E. Bedows, T. A. Keiderling, Journal of the American Chemical Society, 122, 8623-8630 (2000).

- "Peptide and Protein Conformational Studies with Vibrational Circular Dichroism and Related Spectroscopies", Timothy A. Keiderling, (Revised and Expanded Chapter) In Circular Dichroism: Principles and Applications, 2nd Edition. (Eds. K. Nakanishi, N. Berova and R. A. Woody, John Wiley & Sons, New York (2000) p. 621-666.
- "Conformation studies with Optical Spectroscopy of peptides taken from hairpin sequences in the Human Chorionic Gonadotropin " R. A. G. D. Silva, S. A. Sherman, E. Bedows, T. A. Keiderling, Peptides for the New Millenium, Proceedings of the 16th American Peptide Symposium, (June, 1999 Minneapolis, MN) Ed.G. B. Fields, J. P. Tam, G. Barany, Kluwer Acad. Pub., Dordrecht,(2000) p. 325-326.
- "Analysis of Local Conformation within Helical Peptides via Isotope-Edited Vibrational Spectroscopy." S. M. Decatur, T. A. Keiderling, R. A. G. D.Silva, and P. Bour, Peptides for the New Millenium, Proceedings of the 16th American Peptide Symposium, (June, 1999 Minneapolis, MN) Ed. Ed.G. B. Fields, J. P. Tam, G. Barany, Kluwer Acad. Pub., Dordrecht, (2000) p. 414-416.
- "The anomalous infrared amide I intensity distribution in C-13 isotopically labeled peptide beta-sheets comes from extended, multiple stranded structures. An *Ab Initio* study." Jan Kubelka and T. A. Keiderling , *Journal of the American Chemical Society.* 123, 6142-6150 (2001).
- "Vibrational Circular Dichroism of Peptides and Proteins: Survey of Techniques, Qualitative and Quantitative Analyses, and Applications" Timothy A. Keiderling, Chapter in Infrared and Raman Spectroscopy of Biological Materials, Ed. Bing Yan and H.-U. Gremlich, Marcel Dekker, New York (2001) p. 55-100.
- "Chirality in peptide vibrations. Ab initio computational studies of length, solvation, hydrogen bond, dipole coupling and isotope effects on vibrational CD. " Jan Kubelka, Petr Bour, R. A. Gangani D. Silva, Sean M. Decatur, Timothy A. Keiderling, ACS Symposium Series 810, ["Chirality: Physical Chemistry," (Ed. Janice Hicks) American Chemical Society, Washington, DC] (2002), pp. 50–64.
- "Spectroscopic Characterization of Selected b-Sheet Hairpin Models", J. Hilario, J. Kubelka, F. A. Syud, S. H. Gellman, and T. A. Keiderling. Biopolymers (Biospectroscopy) 67: 233-236 (2002)
- " Discrimination between peptide 3_{10}- and alpha-helices. Theoretical analysis of the impact of alpha-methyl substitution on experimental spectra " Jan Kubelka, R. A. Gangani D. Silva, and T. A. Keiderling, *Journal of the American Chemical Society*, 124, 5325-5332 (2002).
- "*Ab Initio* Quantum Mechanical Models of Peptide Helices and their Vibrational Spectra" Petr Bour, Jan Kubelka and T. A. Keiderling, Biopolymers 65, 45-59 (2002).
- "Discriminating 3_{10}- from alpha-helices. Vibrational and electronic CD and IR Absorption study of related Aib-contining oligopeptides" R. A. Gangani D. Silva, Sritana Yasui, Jan Kubelka, Fernando Formaggio, Marco Crisma, Claudio Toniolo, and Timothy A. Keiderling, Biopolymers 65, 229-243 (2002).
- "Spectroscopic characterization of Unfolded peptides and proteins studied with infrared absorption and vibrational circular dichroism spectra" T. A. Keiderling and Qi Xu, Advances in Protein Chemistry Volume 62, [Unfolded Proteins, Dedicated to John Edsall, Ed.: George Rose, Academic Press:New York] (2002), pp. 111–161.
- "Protein and Peptide Secondary Structure and Conformational Determination with Vibrational Circular Dichroism " Timothy A. Keiderling, *Current Opinions in Chemical Biology* (Ed. Julie Leary and Mark Arnold) 6, 682-688 (2002).
- Review: Conformational Studies of Peptides with Infrared Techniques. Timothy A. Keiderling and R. A. G. D. Silva, in Synthesis of Peptides and Peptidomimetics, Ed. M. Goodman and G. Herrman, Houben-Weyl, Vol 22Eb, Georg Thiem Verlag, New York (2002) pp. 715–738, (written and accepted in 2000).
- "Spectroscopic Studies of Structural Changes in Two beta-Sheet Forming Peptides Show an Ensemble of Structures That Unfold Non-Cooperatively" Serguei V. Kuznetsov, Jovencio Hilario, T. A. Keiderling, Anjum Ansari, *Biochemistry*, 42 :4321-4332, (2003).
- "Optical spectroscopic investigations of model beta-sheet hairpins in aqueous solution" Jovencio Hilario, Jan Kubelka, T. A. Keiderling, *Journal of the American Chemical Society* 125, 7562-7574 (2003).

- "Synthesis and conformational study of homopeptides based on (S)-Bin, a C2-symmetric binapthyl-derived Caa-disubstituted glycine with only axial chirality" J.-P. Mazaleyrat, K. Wright, A. Gaucher, M. Wakselman, S. Oancea, F. Formaggio, C. Toniolo, V. Setnicka, J. Kapitan, T. A. Keiderling, Tetrahedron Asymmetry, 14, 1879-1893 (2003).
- "Empirical modeling of the peptide amide I band IR intensity in water solution," Petr Bour, Timothy A. Keiderling, *Journal of Chemical Physics*, 119, 11253-11262 (2003)
- "The Nature of Vibrational Coupling in Helical Peptides: An Isotope Labeling Study" by R. Huang, J. Kubelka, W. Barber-Armstrong, R. A. G. D Silva, S. M. Decatur, and T. A. Keiderling, *Journal of the American Chemical Society*, 126, 2346-2354 (2004).
- "The Complete Chirospectroscopic Signature of the Peptide 3_{10} Helix in Aqueous Solution" Claudio Toniolo, Fernando Formaggio, Sabrina Tognon, Quirinus B. Broxterman, Bernard Kaptein, Rong Huang, Vladimir Setnicka, Timothy A. Keiderling, Iain H. McColl, Lutz Hecht, Laurence D. Barron, Biopolymers 75, 32-45 (2004).
- "Induced axial chirality in the biphenyl core for the Ca-tetrasubstituted a-amino acid residue Bip and subsequent propagation of chirality in (Bip)n/Val oligopeptides" J.-P. Mazaleyrat, K. Wright, A. Gaucher, N. Toulemonde, M. Wakselman, S. Oancea, C. Peggion, F. Formaggio, V. Setnicka, T. A. Keiderling, C. Toniolo, *Journal of the American Chemical Society* 126; 12874-12879 (2004).
- *Ab initio* modeling of amide I coupling in anti-parallel b-sheets and the effect of the 13C isotopic labeling on vibrational spectra" Petr Bour, Timothy A. Keiderling, *Journal of Physical Chemistry B*, 109, 5348-5357 (2005)
- Solvent Effects on IR And VCD Spectra of Helical Peptides: Insights from Ab Initio Spectral Simulations with Explicit Water" Jan Kubelka and Timothy A. Keiderling, Journal of Physical Chemistry B 109, 8231-8243 (2005)
- IR Study of Cross-Strand Coupling in a beta-Hairpin Peptide Using Isotopic Labels., Vladimir Setnicka, Rong Huang, Catherine L. Thomas, Marcus A. Etienne, Jan Kubelka, Robert P. Hammer, Timothy A. Keiderling *Journal of the American Chemical Society* 127, 4992-4993 (2005).
- Vibrational spectral simulation for peptides of mixed secondary structure: Method comparisons with the trpzip model hairpin. Petr Bour and Timothy A. Keiderling, *Journal of Physical Chemistry B* 109, 232687-23697 (2005).
- Isotopically labeled peptides provide site-resolved structural data with infrared spectra. Probing the structural limit of optical spectroscopy, Timothy A. Keiderling, Rong Huang, Jan Kubelka, Petr Bour, Vladimir Setnicka, Robert P. Hammer, Marcus *A. Etienne, R. A. Gangani D. Silva, Sean M. Decatur Collections Symposium Series, 8, 42-49 (2005)—["Biologically Active Peptides" IXth Conference, Prague Czech Republic, April 20-22, 2005.

Nucleic acids and polynucleotides

- "Application of Vibrational Circular Dichroism to Synthetic Polypeptides and Polynucleic Acids" T. A. Keiderling, S. C. Yasui, R. K. Dukor, L. Yang, Polymer Preprints 30, 423-424 (1989).
- "Vibrational Circular Dichroism of Polyribonucleic Acids. A Comparative Study in Aqueous Solution." A. Annamalai and T. A. Keiderling, *Journal of the American Chemical Society*, 109, 3125-3132 (1987).
- "Conformational phase transitions (A-B and B-Z) of DNA and models using vibrational circular dichroism" L. Wang, L. Yang, T. A. Keiderling in *Spectroscopy of Biological Molecules.*, eds. R. E. Hester, R. B. Girling, Special Publication 94 Roya l Society of Chemistry, Cambridge (1991) p. 137-38.
- "Vibrational Circular Dichroism of Proteins Polysaccharides and Nucleic Acids" T. A. Keiderling, Chapter 8 in *Physical Chemistry of Food Processes, Vol. 2 Advanced Techniques, Structures and Applications* eds. I. C. Baianu, H. Pessen, T. Kumosinski, Van Norstrand—Reinhold, New York (1993) pp. 307–337.
- "Structural Studies of Biological Macromolecules using Vibrational Circular Dichroism" T. A. Keiderling, P. Pancoska, Chapter 6 in Advances in Spectroscopy Vol. 21, "Biomolecular Spectroscopy Part B" ed. R. E. Hester, R. J. H. Clarke, John W iley Chichester (1993) pp 267–315.

- "Detection of Triple Helical Nucleic Acids with Vibrational Circular Dichroism," L. Wang, P. Pancoska, T. A. Keiderling in "Fifth International Conference on The Spectroscopy of Biological Molecules" Th. Theophanides, J. Anastassopoulou, N. Fotopoul os (Eds), Kluwen Academic Publ., Dortrecht, 1993, p. 81-82.
- "Helical Nature of Poly (dI-dC) ◆ Poly (dI-dC). Vibrational Circular Dichroism Results" L. Wang and T. A. Keiderling Nucleic Acids Research 21 4127-4132 (1993).
- "Detection and Characterization of Triple Helical Pyrimidine-Purine-Pyrimidine Nucleic Acids with Vibrational Circular Dichroism" L. Wang, P. Pancoska, T. A. Keiderling, Biochemistry 33 8428-8435 (1994).
- "Vibrational Circular Dichroism of A-, B- and Z- form Nucleic Acids in the PO2- Stretching Region" L. Wang, L. Yang, T. A. Keiderling, Biophysical Journal 67, 2460-2467 (1994).
- "Studies of multiple stranded RNA and DNA with FTIR, vibrational and electronic circular dichroism," Zhihua Huang, Lijiang Wang and Timothy A. Keiderling, in Spectrosopy of Biological Molecules, Ed. J. C. Merlin, Kluwer Acad. Pub., Dordrecht, 1995, pp . 321-322.
- "Vibrational Circular Dichroism Applications to Conformational Analysis of Biomolecules" T. A. Keiderling in "Circular Dichroism and the Conformational Analysis of Biomolecules" ed G. D. Fasman, Plenum, New York (1996) pp. 555–598.
- "Vibrational Circular Dichroism Techniques and Application to Nucleic Acids" T. A. Keiderling, In "Biomolecular Structure and Dynamics", NATO ASI series, Series E: Applied Sciences- Vol.342, Eds: G. Vergoten and T. Theophanides, Kluwer Academ ic Publishers, Dordrecht, The Netherlands,pp. 299–317 (1997).

See also

- → Circular dichroism
- Birefringence
- → Optical rotatory dispersion
- IR spectroscopy
- → Polarization
- Proteins
- Nucleic Acids
- DNA
- Molecular models of DNA
- DNA structure
- Protein structure
- Amino acids
- Density functional theory
- Quantum chemistry
- Raman optical activity (ROA)

References

[1] http://planetphysics.org/?op=getobj;from=objects;id=410 Principles of IR and NIR Spectroscopy

[2] *"Vibrational Circular Dichroism of Polypeptides XII. Re-evaluation of the Fourier Transform Vibrational Circular Dichroism of Poly-gamma-Benzyl-L-Glutamate," P. Malon, R. Kobrinskaya, T. A. Keiderling, Biopolymers 27, 733-746 (1988).

[3] *"Vibrational Circular Dichroism of Biopolymers," T. A. Keiderling, S. C. Yasui, U. Narayanan, A. Annamalai, P. Malon, R. Kobrinskaya, L. Yang, in *Spectroscopy of Biological Molecules New Advances* ed. E. D. Schmid, F. W. Schneider, F. Siebert, p. 73-76 (1988).

[4] *"Vibrational Circular Dichroism of Polypeptides and Proteins," S. C. Yasui, T. A. Keiderling, *Mikrochimica Acta*, II, 325-327, (1988).

[5] *"Vibrational Circular Dichroism of Proteins Polysaccharides and Nucleic Acids" T. A. Keiderling, Chapter 8 in *Physical Chemistry of Food Processes, Vol. 2 Advanced Techniques, Structures and Applications.*, eds. I.C. Baianu, H. Pessen, T. Kumosinski, Van Norstrand--Reinhold, New York (1993), pp 307-337.

[6] "Spectroscopic characterization of Unfolded peptides and proteins studied with infrared absorption and vibrational circular dichroism spectra" T. A. Keiderling and Qi Xu, Advances in Protein Chemistry Volume 62, [Unfolded Proteins, Dedicated to John Edsall, Ed.: George Rose, Academic Press:New York] (2002), pp. 111-161.

[7] *"Protein and Peptide Secondary Structure and Conformational Determination with Vibrational Circular Dichroism " Timothy A. Keiderling, *Current Opinions in Chemical Biology* (Ed. Julie Leary and Mark Arnold) 6, 682-688 (2002).

[8] *Review: Conformational Studies of Peptides with Infrared Techniques. Timothy A. Keiderling and R. A. G. D. Silva, in Synthesis of Peptides and Peptidomimetics, Ed. M. Goodman and G. Herrman, Houben-Weyl, Vol 22Eb, Georg Thiem Verlag, New York (2002) pp. 715-738, (written and accepted in 2000).

[9] "Polarization Modulation Fourier Transform Infrared Spectroscopy with Digital SignalProcessing: Comparison of Vibrational Circular Dichroism Methods." Jovencio Hilario, DavidDrapcho, Raul Curbelo, Timothy A. Keiderling, Applied Spectroscopy 55, 1435-1447(2001)--

[10] "Vibrational circular dichroism of biopolymers. Summary of methods and applications.", Timothy A. Keiderling, Jan Kubelka, Jovencio Hilario, in *Vibrational spectroscopy of polymers and biological systems*, Ed. Mark Braiman, Vasilis Gregoriou, Taylor&Francis, Atlanta (CRC Press, Boca Raton, FL) (2006) pp. 253-324 (originally written in 2000, updated in 2003)

[11] "Observation of Magnetic Vibrational Circular Dichroism," T. A. Keiderling, Journal of Chemical Physics, 75, 3639-41 (1981).

[12] "Vibrational Spectral Assignment and Enhanced Resolution Using Magnetic Vibrational Circular Dichroism," T. R. Devine and T. A. Keiderling, *Spectrochimica Acta*, 43A, 627-629 (1987).

[13] "Magnetic Vibrational Circular Dichroism with an FTIR" P. V. Croatto, R. K. Yoo, T. A. Keiderling, SPIE Proceedings 1145 (7th International Conference on FTS, ed. D. G. Cameron) 152-153 (1989).

[14] "Direct Measurement of the Rotational g-Value in the Ground State of Acetylene by Magnetic Vibrational Circular Dichroism." C. N. Tam and T. A. Keiderling, Chemical Physics Letters, 243, 55-58 (1995).

[15] . "Ab initio calculation of the vibrational magnetic dipole moment" P. Bour, C. N. Tam, T. A. Keiderling, Journal of Physical Chemistry 99, 17810-17813 (1995)

[16] "Rotationally Resolved Magnetic Vibrational Circular Dichroism. Experimental Spectra and Theoretical Simulation for Diamagnetic Molecules." P. Bour, C. N. Tam, B. Wang, T. A. Keiderling, *Molecular Physics* 87, 299-318, (1996).

Microwave spectroscopy

Rotational spectroscopy or microwave spectroscopy studies the absorption and emission of electromagnetic radiation (typically in the microwave region of the electromagnetic spectrum) by molecules associated with a corresponding change in the rotational quantum number of the molecule. The use of microwaves in spectroscopy essentially became possible due to the development of microwave technology for RADAR during World War II. Rotational spectroscopy is only really practical in the gas phase where the rotational motion is quantized. In solids or liquids the rotational motion is usually quenched due to collisions.

Rotational spectrum from a molecule (to first order) requires that the molecule have a dipole moment and that there be a difference between its center of charge and its center of mass, or equivalently a separation between two unlike charges. It is this dipole moment

Part of the rotational-vibrational spectrum of HCl Gas, showing the presence of P- and R- branches. Frequency is on the x-axis, and transmittance on the y-axis.

that enables the electric field of the light (microwave) to exert a torque on the molecule causing it to rotate more quickly (in excitation) or slowly (in de-excitation). Diatomic molecules such as dioxygen (O_2), dihydrogen (H_2), etc. do not have a dipole moment and hence no purely rotational spectrum. However, electronic excitations can lead to asymmetric charge distributions and thus provide a net dipole moment to the molecule. Under such circumstances, these molecules will exhibit a rotational spectrum.

Amongst the diatomic molecules, carbon monoxide (CO) has one of the simplest rotational spectra. As for tri-atomic molecules, hydrogen cyanide (HC≡N) has a simple rotational spectrum for a linear molecule and hydrogen isocyanide (HN=C:) for a non-linear molecule. As the number of atoms increases the spectrum becomes more complex as lines due to different transitions start overlapping.

Understanding the rotational spectrum

In quantum mechanics the free rotation of a molecule is quantized, that is the rotational energy and the angular momentum can only take certain fixed values; what these values are is simply related to the moment of inertia, I, of the molecule. In general for any molecule, there are three moments of inertia: I_A, I_B and I_C about three mutually orthogonal axes A, B, and C with the origin at the center of mass of the system. A linear molecule is a special case in this regard. These molecules are cylindrically symmetric and one of the moment of inertia (I_A, which is the moment of inertia for a rotation taking place along the axis of the molecule) is negligible (i.e. $I_A \ll I_B = I_C$).
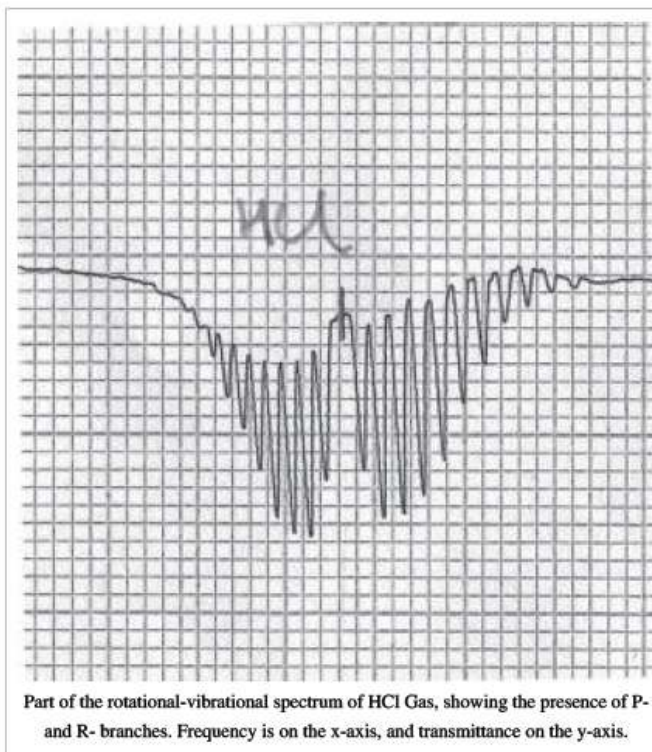
Classification of molecules based on rotational behavior

The general convention is to define the axes such that the axis A has the smallest moment of inertia (and hence the highest rotational frequency) and other axes such that $I_A \leq I_B \leq I_C$. Sometimes the axis A may be associated with the symmetric axis of the molecule, if any. If such is the case, then I_A need not be the smallest moment of inertia. To avoid confusion, we will stick with the former convention for the rest of the article. The particular pattern of energy levels (and hence of transitions in the rotational spectrum) for a molecule is determined by its symmetry. A convenient way to look at the molecules is to divide them into four different classes (based on the symmetry of their structure). These are,

1. Linear molecules (or linear rotors)
2. Symmetric tops (or symmetric rotors)
3. Spherical tops (or spherical rotors) and
4. Asymmetric tops

Dealing with each in turn:

1. *Linear molecules:*

   - As mentioned earlier, for a linear molecule $I_A \ll I_B = I_C$. For most of the purposes, I_A is taken to be zero. For a linear molecule, the separation of lines in the rotational spectrum can be related directly to the moment of inertia of the molecule, and for a molecule of known atomic masses, can be used to determine the bond lengths (structure) directly. For diatomic molecules this process is trivial, and can be made from a single measurement of the rotational spectrum. For linear molecules with more atoms, rather more work is required, and it is necessary to measure molecules in which more than one isotope of each atom have been substituted (effectively this gives rise to a set of simultaneous equations which can be solved for the bond lengths).
   - Examples of linear molecules: dioxygen (O=O), carbon monoxide (O≡C*), hydroxy radical (OH), carbon dioxide (O=C=O), hydrogen cyanide (HC≡N), carbonyl sulfide (O=C=S), chloroethyne (HC≡CCl), acetylene (HC≡CH)

2. *Symmetric tops:*

   - A symmetric top is a molecule in which two moments of inertia are the same. As a matter of historical convenience, spectroscopists divide molecules into two classes of symmetric tops, *Oblate symmetric tops* (saucer or disc shaped) with $I_A = I_B < I_C$ and *Prolate symmetric tops* (rugby football, or cigar shaped) with $I_A < I_B = I_C$. The spectra look rather different, and are instantly recognizable. As for linear molecules, the structure of *symmetric tops* (bond lengths and bond angles) can be deduced from their spectra.
   - Examples of symmetric tops:
     - Oblate: benzene (C_6H_6), cyclobutadiene (C_4H_4), ammonia (NH_3)
     - Prolate: chloromethane (CH_3Cl), propyne ($CH_3C≡CH$)

3. *Spherical tops:*

   - A spherical top molecule, can be considered as a special case of *symmetric tops* with equal moment of inertia about all three axes ($I_A = I_B = I_C$).
   - Examples of spherical tops: phosphorus tetramer (P_4), carbon tetrachloride (CCl_4), nitrogen tetrahydride (NH_4), ammonium ion (NH_4^+), sulfur hexafluoride (SF_6)

4. *Asymmetric tops:*

   - As you would have guessed a molecule is termed an asymmetric top if all three moments of inertia are different. Most of the larger molecules are asymmetric tops, even when they have a high degree of symmetry. Generally for such molecules a simple interpretation of the spectrum is not normally possible. Sometimes asymmetric tops have spectra that are similar to those of a linear molecule or a symmetric top, in which case the molecular structure must also be similar to that of a linear molecule or a symmetric top. For the most general case, however, all that can be done is to fit the spectra to three different moments of inertia. If the

molecular formula is known, then educated guesses can be made of the possible structure, and from this guessed structure, the moments of inertia can be calculated. If the calculated moments of inertia agree well with the measured moments of inertia, then the structure can be said to have been determined. For this approach to determining molecular structure, isotopic substitution is invaluable.
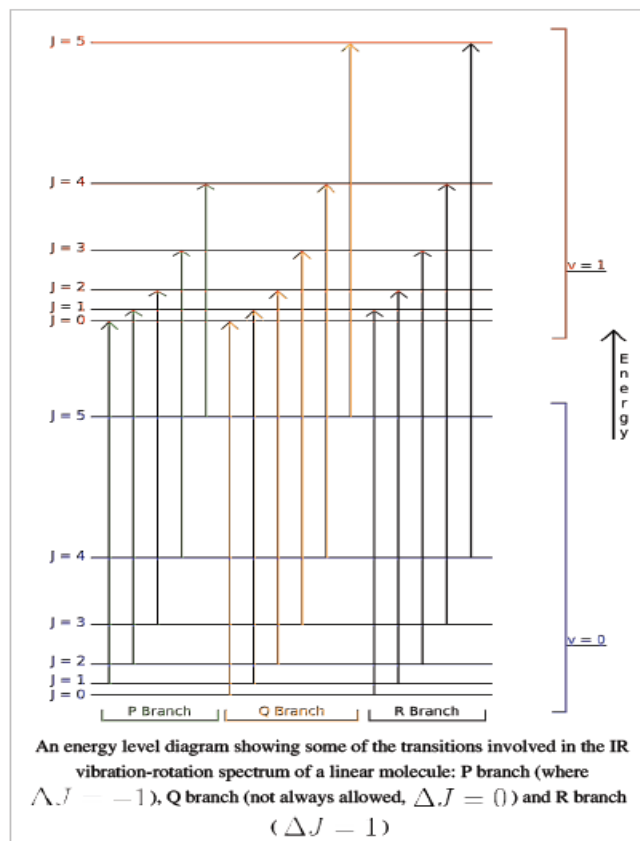
- Examples of asymmetric tops: anthracene ($C_{14}H_{10}$), water (H_2O), nitrogen dioxide (NO_2)

Structure of rotational spectrum

- **Linear molecules**

These molecules have two degenerate modes of rotation ($I_B = I_C$, $I_A = 0$). Since we cannot distinguish between the two modes, we need only one rotational quantum number (J) to describe the rotational motion of the molecule.

The rotational energy levels ($F(J)$) of the molecule based on rigid rotor model can be expressed as,

An energy level diagram showing some of the transitions involved in the IR vibration-rotation spectrum of a linear molecule: P branch (where $\Delta J = -1$), Q branch (not always allowed, $\Delta J = 0$) and R branch ($\Delta J = 1$)

$$F(J) = \tilde{B}_e J(J+1) \qquad J = 0, 1, 2, \ldots$$

where $\tilde{B}_e$ is the rotational constant of the molecule and is related to the moment of inertia of the molecule $I_B = I_C$ by,

$$\tilde{B}_e = \frac{h}{8\pi^2 c I_B}$$

Selection rules dictate that during emission or absorption the rotational quantum number has to change by unity i.e. $\Delta J = J' - J'' = \pm 1$. Thus the locations of the lines in a rotational spectrum will be given by,

$$\tilde{\nu}_{J' \leftarrow J''} = F(J') - F(J'') = 2\tilde{B}_e (J'' + 1) \qquad J'' = 0, 1, 2, \ldots$$

where J'' denotes the lower energy level and J' denotes higher energy level involved in the transition. The height of the lines is determined by the distribution of the molecules in the different levels and the probability of transition

between two energy levels.

We observe that, for a rigid rotor, the transition lines are equally spaced in the wavenumber space. However, this is not always the case, except for the rigid rotor model. For non-rigid rotor model, we need to consider changes in the moment of inertia of the molecule. Two primary reasons for this are,

- **Centrifugal distortion:**

When a molecule rotates, the centrifugal force pulls the atoms apart. As a result, the moment of inertia of the molecule increases, thus decreasing $\tilde{B}_e$. To account for this a centrifugal distortion correction term is added to the rotational energy levels of the molecule.

$$F(J) = \tilde{B}_e J(J+1) - \tilde{D}_e J^2 (J+1)^2 \qquad J = 0, 1, 2, \ldots$$

where $\tilde{D}_e$ is the centrifugal distortion constant.

Accordingly the line spacing for the rotational mode changes to,

$$\tilde{\nu}_{J' \leftrightarrow J''} = 2\tilde{B}_e (J''+1) - 4\tilde{D}_e (J''+1)^3 \qquad J'' = 0, 1, 2, \ldots$$

- **Effect of vibration on rotation:**

A molecule is always in vibration. As the molecule vibrates, its moment of inertia changes. Further there is a fictitious force, Coriolis coupling, between the vibrational motion of the nuclei in the rotating (non-inertial) frame. However, as long as the vibrational quantum number does not change (i.e. the molecule is in only one state of vibration), the effect of vibration on rotation is not important, because the time for vibration is much shorter than the time required for rotation. The Coriolis coupling is often negligible, too, if one is interested in low vibrational and rotational quantum numbers only.

- **Symmetric Top**

The rotational motion of a symmetric top molecule can be described by two independent rotational quantum numbers (since two axes have equal moments of inertia, the rotational motion about these axes requires only one rotational quantum number for complete description). Instead of defining the two rotational quantum numbers for two independent axes, we associate one of the quantum number (J) with the total angular momentum of the molecule and the other quantum number (K) with the angular momentum of the axis which has different moment of inertia (i.e. axis C for oblate symmetric top and axis A for prolate symmetric tops). The rotational energy $F(J, K)$ of such a molecule, based on rigid rotor assumptions can be expressed in terms of the two previously defined rotational quantum numbers as follows,

$$F(J, K) = \tilde{B} J(J+1) + \left(\tilde{A} - \tilde{B}\right) K^2 \qquad J = 0, 1, 2, \ldots \quad \text{and} \quad K = -J, -J+1, \ldots, -1, 0, 1, \ldots, J-1$$

where $\tilde{B} = \dfrac{h}{8\pi^2 c I_B}$ and $\tilde{A} = \dfrac{h}{8\pi^2 c I_A}$ for a *prolate* symmetric top molecule or $\tilde{A} = \dfrac{h}{8\pi^2 c I_C}$ for an *oblate* molecule.

Selection rule for these molecules provide the guidelines for possible transitions. Accordingly,

$$\Delta J = +1 \quad \text{and} \quad \Delta K = 0.$$

This is so because K is associated with the axis about which the molecule is symmetric and hence has no net dipole moment in that direction. Thus there is no interaction of this mode with the light particles (photon).

This gives the transition wavenumbers of,

$$\tilde{\nu}_{J' \leftrightarrow J'', K} = F(J', K) - F(J'', K) = 2\tilde{B}(J''+1) \qquad J'' = 0, 1, 2, \ldots$$

which is the same as in the case of a linear molecule.

In case of non-rigid rotors, the first order centrifugal distortion correction is given by,

$$F(J, K) = \tilde{B} J(J+1) + \left(\tilde{A} - \tilde{B}\right) K^2 - \tilde{D}_J J^2 (J+1)^2 - \tilde{D}_{JK} J(J+1) K^2 - D_K K^4 \qquad J = 0, 1, 2, \ldots$$

The suffixes on the centrifugal distortion constant D indicate the rotational mode involved and are not a function of the rotational quantum number. The location of the transition lines on a spectrum is given by,

$$\tilde{\nu}_{J' \leftrightarrow J'', K} = F\left(J', K\right) - F\left(J'', K\right) = 2\tilde{B}\left(J'' + 1\right) - 4D_J\left(J'' + 1\right)^3 - 2D_{JK}\left(J'' + 1\right)K^2 \qquad J'' = 0.1$$

- **Spherical Tops**

Unlike other molecules, spherical top molecules have no net dipole moment, and hence they do not exhibit a pure rotational spectrum.

- **Asymmetric Tops**

The spectrum for these molecules usually involves many lines due to three different rotational modes and their combinations. The following analysis is valid for the general case and collapses to the various special cases described above in the appropriate limit.

From the moments of inertia one can define an asymmetry parameter κ as

$$\kappa = \frac{2B - A - C}{A - C}$$

which varies from -1 for a prolate symmetric top to 1 for an oblate symmetric top.

One can define a scaled rotational Hamiltonian dependent on J and κ. The (symmetric) matrix representation of this Hamiltonian is banded, zero everywhere but the main diagonal and the second subdiagonal. The Hamiltonian can be formulated in six different settings, dependent on the mapping of the principal axes to lab axes and handedness. For the most asymmetric, right-handed representation the diagonal elements are, for $|k| \leq J$

$$H_{k,k}(\kappa) = \kappa k^2$$

and the second off-diagonal elements (independent of κ) are

$$H_{k,k+2}(\kappa) = \sqrt{[J(J+1) - (k+1)(k+2)][J(J+1) - k(k+1)]}/2.$$

Diagonalising H yields a set of $2J + 1$ scaled rotational energy levels $E_k(\kappa)$. The rotational energy levels of the asymmetric rotor for total angular momentum J are then given by

$$\frac{A+C}{2}J(J+1) - \frac{A-C}{2}E_k(\kappa)$$

Hyperfine interactions:

In addition to the main structure that is observed in microwave spectra due to the rotational motion of the molecules, a whole host of further interactions are responsible for small details in the spectra, and the study of these details provides a very deep understanding of molecular quantum mechanics. The main interactions responsible for small changes in the spectra (additional splittings and shifts of lines) are due to magnetic and electrostatic interactions in the molecule. The particular strength of such interactions differs in different molecules, but in general, the order of these effects (in decreasing significance) is:

1. *electron spin - electron spin interaction* (this occurs in molecules with two or more unpaired electrons, and is a magnetic-dipole / magnetic-dipole interaction)
2. *electron spin - molecular rotation* (the rotation of a molecule corresponds to a magnetic dipole, which interacts with the magnetic dipole moment of the electron)
3. *electron spin - nuclear spin interaction* (the interaction between the magnetic dipole moment of the electron and the magnetic dipole moment of the nuclei (if present)).
4. *electric field gradient - nuclear electric quadrupole interaction* (the interaction between the electric field gradient of the electron cloud of the molecule and the electric quadrupole moments of nuclei (if present)).
5. *nuclear spin - nuclear spin interaction* (nuclear magnetic moments interacting with one another).

These interactions give rise to the characteristic energy levels that are probed in "magnetic resonance" spectroscopy such as NMR and ESR, where they represent the "zero field splittings" which are always present.

Experimental determination of the spectrum

→ Fourier transform infrared (FTIR) spectroscopy can be used to experimentally study rotational spectra. Typically spectra at these wavelengths involve rovibrational excitation, i.e., excitation of both a vibrational and a rotational mode of a molecule.

Traditionally, microwave spectra were determined using a simple arrangement in which low pressure gas was introduced to a section of waveguide between a microwave source (of variable frequency) and a microwave detector. The spectrum was obtained by sweeping the frequency of the source while detecting the intensity of the transmitted radiation. This experimental arrangement has a major difficulty related to the propagation of microwave radiation through waveguides. The physical size of the waveguide restricts the frequency of the radiation that can be transmitted through it. For a given waveguide size (such as X-band) there is a cutoff frequency, and microwave radiation with smaller frequencies (longer wavelengths) cannot be propagated through the waveguide. Additionally, as the frequency is increased, additional modes of propagation become possible, which correspond to different velocities of the radiation propagating down the waveguide (this can be envisaged as the radiation bouncing down the guide, at different angles of reflection). the net result of these considerations is that each size of waveguide is only useful over a rather narrow range of frequencies and must be physically swapped out for a different size of waveguide once this frequency range is exceeded.

More recently, microwave spectra have often been obtained using Fourier Transform Microwave Spectroscopy - a technique invented by

Within the last two years, a further development of Fourier Transform Microwave Spectroscopy has occurred, which may well introduce a new renaissance into microwave spectroscopy. This is the use of "Chirped Pulses" to provide an electromagnetic wave that has as its Fourier Transform a very wide range of microwave frequencies. (see University of Virginia, Chemistry Department website).

Applications

Microwave spectroscopy is commonly used in physical chemistry to determine the structure of small molecules (such as ozone, methanol, or water) with high precision. Other common techniques for determining molecular structure, such as X-ray crystallography don't work very well for some of these molecules (especially the gases) and are not as precise. However, microwave spectroscopy is not useful for determining the structures of large molecules such as proteins.

Microwave spectroscopy is one of the principal means by which the constituents of the universe are determined from the earth. It is particularly useful for detecting molecules in the interstellar medium (ISM). One of the early surprises in interstellar chemistry was the existence in the ISM of long chain carbon molecules. It was in attempting to research such molecules in the laboratory that Harry Kroto was led to the laboratory of Rick Smalley and Robert Curl, where it was possible to vaporize carbon under enormous energy conditions. This collaborative experiment led to the discovery of C_{60}, buckminsterfullerene, which led to the award of the 1996 Nobel prize in chemistry to Kroto, Smalley and Curl.

References

- *Microwave Spectroscopy*, Townes and Schawlow, Dover;
- *Molecular Rotation Spectra*, Harry Kroto, Dover;
- *Rotational Spectroscopy of Diatomic molecules*, Brown and Carrington;
- *Quantum Mechanics*, Mcquarrie, Donald A.

See also

- → Spectroscopy
- Rigid rotor
- Rovibronic excitation
- Vibrational spectroscopy
- → Infrared spectroscopy

Further Reading

[1] http://hyperphysics.phy-astr.gsu.edu/HBASE/molecule/rotrig.html

EXAFS

X-ray Absorption Spectroscopy (XAS) includes both **Extended X-Ray Absorption Fine Structure** (EXAFS) and **X-ray Absorption Near Edge Structure** (XANES). XAS is the measurement of the x-ray absorption coefficient ($\mu(E)$ in the equations below) of a material as a function of energy. X-rays of a narrow energy resolution are shone on the sample and the incident and transmitted x-ray intensity is recorded as the incident x-ray energy is incremented. The number of x-rays that are transmitted through a sample (I_t) is equal to the number of x-rays shone on the sample (I_0) multiplied by a decreasing exponential that depends of the type of atoms in the sample, the absorption coefficient μ, and the thickness of the sample x.

$$I_t = I_0 e^{-\mu x}$$

The absorption coefficient is obtained by taking the log ratio of the incident x-ray intensity to the transmitted x-ray intensity.

$$\mu = \frac{-ln(I_t/I_0)}{x}$$

When the incident x-ray energy matches the binding energy of an electron of an atom within the sample, the number of x-rays absorbed by the sample increases dramatically, causing a drop in the transmitted x-ray intensity. This results in an absorption edge. Each element on the periodic table has a set of unique absorption edges corresponding to different binding energies of its electrons. This gives XAS element selectivity. XAS spectra are most often collected at synchrotrons. Because X-rays are highly penetrating, XAS samples can be gases, solids or liquids. And because of the brilliance of Synchrotron X-ray sources the concentration of the absorbing element can be as low as a few ppm.

EXAFS spectra are displayed as graphs of the absorption coefficient of a given material versus energy, typically in a 500 − 1000 eV range beginning before an absorption edge of an element in the sample. The x-ray absorption coefficient is usually normalized to unit step height. This is done by regressing a line to the region before and after the absorption edge, subtracting the pre-edge line from the entire data set and dividing by the absorption step height,

which is determined by the difference between the pre-edge and post-edge lines at the value of E0 (on the absorption edge).

The normalized absorption spectra are often called XANES spectra. These spectra can be used to determine the average oxidation state of the element in the sample. The XANES spectra are also sensitive to the coordination environment of the absorbing atom in the sample. Finger printing methods have been used to match the XANES spectra of an unknown sample to those of known "standards". Linear combination fitting of several different standard spectra can give an estimate to the amount of each of the known standard spectra within an unknown sample.

X-ray absorption spectra are produced over the range of $200 - 35{,}000$ eV. The dominant physical process is one where the absorbed photon ejects a core photoelectron from the absorbing atom, leaving behind a core hole. The atom with the core hole is now excited. The ejected photoelectron's energy will be equal to that of the absorbed photon minus the binding energy of the initial core state. The ejected photoelectron interacts with electrons in the surrounding non-excited atoms.

If the ejected photoelectron is taken to have a wave-like nature and the surrounding atoms are described as point scatterers, it is possible to imagine the backscattered electron waves interfering with the forward-propagating waves. The resulting interference pattern shows up as a modulation of the measured absorption coefficient, thereby causing the oscillation in the EXAFS spectra. A simplified plane-wave single-scattering theory has been used for interpretation of EXAFS spectra for many years, although modern methods (like FEFF, GNXAS) have shown that curved-wave corrections and multiple-scattering effects can not be neglected. The photelectron scattering amplitude in the low energy range (5-200 eV) of the phoelectron kinetic energy become much larger so that multiple scattering events become dominant in the NEXAFS (or XANES) spectra.

The wavelength of the photoelectron is dependent on the energy and phase of the backscattered wave which exists at the central atom. The wavelength changes as a function of the energy of the incoming photon. The phase and amplitude of the backscattered wave are dependent on the type of atom doing the backscattering and the distance of the backscattering atom from the central atom. The dependence of the scattering on atomic species makes it possible to obtain information pertaining to the chemical coordination environment of the original absorbing (centrally excited) atom by analyzing these EXAFS data.

Experimental considerations

Since EXAFS requires a tunable x-ray source, data are always collected at synchrotrons, often at beamlines which are especially optimized for the purpose. The utility of a particular synchrotron to study a particular solid depends on the brightness of the x-ray flux at the absorption edges of the relevant elements.

Applications

XAS is an interdisciplinary technique and its unique properties, as compared to x-ray diffraction, have been exploited for understanding the details of local structure in:

- glass, amorphous and liquid systems
- solid solutions
- Doping and ionic implantation materials for electronics
- local distortions of crystal lattices
- organometallic compounds
- metalloproteins
- metal clusters
- vibrational dynamics
- ions in solutions

Example of Significance

EXAFS is, like NEXAFS/XANES, a highly sensitive technique with elemental specificity. As such, EXAFS is an extremely useful way to determine the chemical state of practically important species which occur in very low abundance or concentration. Frequent use of EXAFS occurs in environmental chemistry, where scientists try to understand the propagation of pollutants through an ecosystem. EXAFS can be used along with accelerator mass spectrometry in forensic examinations, particularly in nuclear non-proliferation applications.

For an example of an EXAFS study of uranium chemistry in glass see [1], and for a general study of trivalent lanthanides and actinides in chloride containing aqueous media can be read at [2]

See also

- X-ray absorption spectroscopy
- XANES
- NEXAFS
- SEXAFS

History

A very detailed, balanced and informative account about the history of EXAFS (originally called Kossel's structures) is given in the paper "A History of the X-ray Absorption Fine Structure} by R. Stumm von Bordwehr", Ann. Phys. Fr. vol. 14, 377-466 (1989) (author's name is C. Brouder).

Relevant Websites

- International XAFS Society [3]
- FEFF Project, University of Washington, Seattle [4]
- GNXAS project and XAS laboratory, Università di Camerino [5]
- EXAFS theory Introduction [6]
- Community web site for XAFS [7]

Books

- B.-K. Teo, *EXAFS: basic principles and data analysis*, Springer 1986
- *X-ray Absorption: principles, applications and techniques of EXAFS, SEXAFS and XANES*, a cura di D.C. Koeningsberger, R. Prins, Wiley 1988

Book Chapters

- Kelly, S.D., Hesterberg, D., and Ravel, B., *Analysis of Soils and Minerals Using X-ray Absorption Spectroscopy* in Methods of Soil Analysis, Part 5 -Mineralogical Methods, (A.L. Ulery and L.R. Drees, Eds.) p. 367. Soil Science Society of America, Madison, WI, USA, 2008.

Papers

- J.J. Rehr and R.C. Albers, "Theoretical approaches to X-ray absorption fine structure", *Reviews of Modern Physics* 72 (2000), 621-654
- A. Filipponi, A. Di Cicco and C.R. Natoli, "X-ray absorption spectroscopy and n-body distribution functions in condensed matter", *Physical Review* B 52/21 (1995) 15122-15148
- F. de Groot, "High-resolution X-ray emission and X-ray absorption spectroscopy", *Chemical Reviews* 101 (2001) 1779-1808
- F.W. Lytle, "The EXAFS family tree: a personal history of the development of extended X-ray absorption fine structure", [8]
- Dale E. Sayers, Edward A. Stern, and Farrel W. Lytle, New Technique for Investigating Noncrystalline Structures: Fourier Analysis of the Extended X-Ray—Absorption Fine Structure, [9]Phys. Rev. Lett. 27, 1204–1207 (1971).
- A. Kodre, I. Arčon, Proceedings of 36th International Conference on Microelectronics, Devices and Materials, MIDEM, Postojna, Slovenia, October 28-20, (2000), p. 191-196

References

[1]   http://www.osti.gov/bridge/servlets/purl/459339-8dNh9T/webviewable/459339.pdf

[2]   http://www-ssrl.slac.stanford.edu/pubs/activity_rep/ar98/2525-edelstein.pdf

[3]   http://www.i-x-s.org/

[4]   http://leonardo.phys.washington.edu/feff/

[5]   http://gnxas.unicam.it

[6]   http://srs.dl.ac.uk/xrs/Theory/theory.html

[7]   http://xafs.org/XAFS

[8]   http://www.exafsco.com/techpapers/index.html

[9]   http://dx.doi.org/10.1103/PhysRevLett.27.1204

Neutron spectroscopy

Inelastic neutron scattering is an experimental technique commonly used in condensed matter research to study atomic and molecular motion as well as magnetic and crystal field excitations. It distinguishes itself from other neutron scattering techniques by resolving the change in kinetic energy that occurs when the collision between neutrons and the sample is an inelastic one. Results are generally communicated as the dynamic structure factor (also called inelastic scattering law) $S(q,\omega)$, sometimes also as the dynamic susceptibility $\chi(q,\omega)$ where the scattering vector q is the difference between incoming and outgoing wave vector, and $\hbar\omega$ is the energy change experienced by the sample (negative that of the scattered neutron). When results are plotted as function of ω, they can often be interpreted in the same way as spectra obtained by conventional → spectroscopic techniques; insofar as inelastic neutron scattering can be seen as a special spectroscopy.

Inelastic scattering experiments normally require a monochromatization of the incident or outgoing beam and an energy analysis of the scattered neutrons. This can be done either through time-of-flight techniques (neutron time-of-flight scattering) or through Bragg reflection from single crystals (neutron triple-axis spectroscopy, neutron backscattering). Monochromatization is not needed in echo techniques (→ neutron spin echo, neutron resonance spin echo), which use the quantum mechanical phase of the neutrons in addition to their amplitudes.

Generic layout of an inelastic neutron scattering experiment
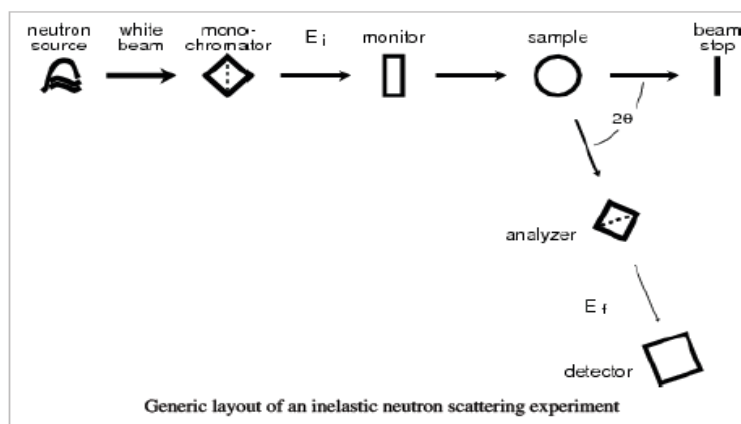
Types of Inelastic Neutron Scattering

- neutron triple-axis scattering
- neutron time-of-flight scattering
- neutron backscattering
- → neutron spin echo

Further Information

Literature:

- G L Squires *Introduction to the Theory of Thermal Neutron Scattering* Dover 1997 (reprint?)

External links

- Joachim Wuttke: Introduction to Inelastic Crystal Spectrometers [1]

References

[1] http://iffwww.iff.kfa-juelich.de/~wuttke/doku/lib/exe/fetch.php?id=spheres%3Aprinciple&cache=cache&media=spheres:np9v05.pdf

Neutron spin echo

Neutron spin echo spectroscopy is an → inelastic neutron scattering technique invented by Ferenc Mezei in the 1970's, and developed in collaboration with John Hayter. In recognition of this work and in other areas, Mezei was awarded the first Walter Haelg Prize [1] in 1999.

The spin-echo spectrometer possesses an extremely high energy resolution (roughly one part in 100,000). Additionally, it measures the density-density correlation (or intermediate scattering function) $F(Q,t)$ as a function of momentum transfer Q and time. Other neutron scattering techniques measure the dynamic structure factor, which then must be converted to $F(Q,t)$ by a Fourier transform, which is difficult in practice. Because of these advantages over other neutron scattering techniques, NSE is an ideal method to observe [2] internal dynamic modes in materials such as a polymer blend, alkane chain, or microemulsion. The extraordinary power of NSE spectrometry was further demonstrated recently [3] by the direct observation of coupled internal protein domain dynamics in the protein Taq polymerase, allowing the visualization of protein nanomachinery in motion.

Technical details

The technique of neutron spin echo exploits the neutron's intrinsic angular momentum, or spin, to access extremely high-resolution inelastic scattering windows.

The core of a neutron spin echo instrument is a *symmetric* field integral around the sample position, and a spin flipper (or the sample itself) to reverse the spin direction, so that any loss in polarisation at the detector position can be directly attributed to inelastic scattering processes in the sample.

Because of the interference of the wavevectors associated with the spin up and spin down quantum states of the neutron, the measured neutron polarisation is proportional to the sample's correlation function *in real time*. This makes it a very useful and intuitive technique for the high-resolution study of low-energy excitations in materials.

In soft matter research the structure of macromolecular objects is often investigated by small angle neutron scattering, SANS. The exchange of hydrogen with deuterium in some of the molecules creates scattering contrast between even equal chemical species. The SANS diffraction pattern --if interpreted in real space-- corresponds to a snapshot picture of the molecular arrangement. Neutron spin echo instruments can analyze the inelastic broadening of the SANS intensity and thereby analyze the motion of the macromolecular objects. A coarse analogy would be a photo with a certain opening time instead of the SANS like snapshot. The opening time corresponds to the Fourier time which depends on the setting of the NSE spectrometer, it is proportional to the magnetic field (integral) and to the third power of the neutron wavelength. Values up to several hundreds of nanoseconds are available. Note that the spatial resolution of the scattering experiment is in the nanometer range, which means that a time range of e.g. 100ns corresponds to effective molecular motion velocities of 1 nm/100ns = 1cm/s. This may be compared to the typical neutron velocity of 200..1000 m/s used in these type of experiments.

Existing Spectrometers

- IN11 [4] (Institut Laue-Langevin,ILL [5], Grenoble, France)
- IN15 [6] (Institut Laue-Langevin,ILL [5], Grenoble, France)
- J-NSE (Juelich Centre for Neutron Science JCNS [7], Juelich, Germany, hosted by FRMII [8], Munich (Garching), Germany)
- NG5-NSE (NIST CNRF [9], Gaithersburg, USA)
- RESEDA (FRM II Munich FRMII [8], Munich, Germany)
- V5/SPAN (Hahn-Meitner Institut [10], Berlin, Germany)
- C2-2 (ISSP [11], Tokai, Japan)

See also

- Biological small-angle scattering
- Larmor precession
- Neutron resonance spin echo
- Neutron scattering
- NMR
- Protein domain
- SAXS
- Soft matter
- Spin echo

References

[1] http://neutron.neutron-eu.net/n_ensa/Prize

[2] B. Farago (2006). "Neutron spin echo study of well organized soft matter systems". *Physica B: Condensed matter* **385-386**: 688-691. doi: 10.1016/j.physb.2006.05.292 (http://dx.doi.org/10.1016/j.physb.2006.05.292).

[3] Bu Z, Biehl R, Monkenbusch M, Richter D, Callaway DJE (2005). "Coupled protein domain motion in Taq polymerase revealed by neutron spin-echo spectroscopy.". *Proc Natl Acad Sci U S A* **102** (49): 17646-17651. doi: 10.1073/pnas.0503388102 (http://dx.doi.org/10.1073/pnas.0503388102). PMID 16306270 (http://www.ncbi.nlm.nih.gov/pubmed/16306270).

[4] http://www.ill.eu/in11/

[5] http://www.ill.fr

[6] http://www.ill.eu/in15/

[7] http://www.jcns.info

[8] http://wwwnew.frm2.tum.de

[9] http://www.ncnr.nist.gov

[10] http://www.hmi.de

[11] http://www.issp.u-tokyo.ac.jp

Plasma spectroscopy

Plasma oscillations, also known as "**Langmuir waves**" (after Irving Langmuir), are rapid oscillations of the electron density in conducting media such as plasmas or metals. The frequency only depends weakly on the wavelength. The quasiparticle resulting from the quantization of these oscillations is the plasmon.

Langmuir waves were discovered by American physicists Irving Langmuir and Lewi Tonks in the 1920s. They are parallel in form to Jeans instability waves, which are caused by gravitational instabilities in a static medium.

Explanation

Consider a neutral plasma, consisting of a gas of positively charged ions and negatively charged electrons. If one displaces by a tiny amount all of the electrons with respect to the ions, the Coulomb force pulls back, acting as a restoring force.

'Cold' electrons

If the electrons are cold, it is possible to show that the charge density oscillates at the *plasma frequency*

$$\omega_{pe} = \sqrt{\frac{4\pi n_e e^2}{m^*}} \text{ (cgs units)} = \sqrt{\frac{n_e e^2}{m^* \varepsilon_0}} \text{ (SI units)} \left[s^{-1} \right],$$ where n_e is the density of electrons, e is the electric

charge, m^* is the effective mass of the electron, and ϵ_0 is the permittivity of free space. Note that the above formula is derived under the approximation that the ion mass is infinite. This is generally a good approximation, as the electrons are so much lighter than ions. (One must modify this expression in the case of electron-positron plasmas, often encountered in astrophysics). Since the frequency is independent of the wavelength, these oscillations have an infinite phase velocity and zero group velocity.

'Warm' electrons

If warm electrons are considered with an electron thermal speed $v_{e,th} = \sqrt{\frac{k_B T_e}{m_e}}$, the electron pressure acts as a

restoring force as well as the electric field and the oscillations propagate with frequency and wavenumber related by

$$\omega^2 = \omega_{pe}^2 + 3k^2 v_{e,th}^2,$$

called the Bohm-Gross dispersion relation. If the spatial scale is large compared to the Debye length, the oscillations are only weakly modified by the pressure term, but at small scales the pressure term dominates and the waves become dispersionless with a speed of $\sqrt{3} \cdot v_{e,th}$. For such waves, however, the electron thermal speed is comparable to the phase velocity, i.e.,

$$v \sim v_{ph} \stackrel{\text{def}}{=} \frac{\omega}{k},$$

so the plasma waves can accelerate electrons that are moving with speed nearly equal to the phase velocity of the wave. This process often leads to a form of collisionless damping, called Landau damping. Consequently, the large-k portion in the dispersion relation is difficult to observe and seldom of consequence.

In a bounded plasma, fringing electric fields can result in propagation of plasma oscillations, even when the electrons are cold.

In a metal or semiconductor, the effect of the ions' periodic potential must be taken into account. This is usually done by using the electrons' effective mass in place of *m*.

See also

- Waves in plasmas
- plasmon
- Surface plasmon resonance
- Upper hybrid oscillation, in particular for a discussion of the modification to the mode at propagation angles oblique to the magnetic field
- In 2006, plasma physicists at the Universities of Texas and Michigan were able to photograph Langmuir waves, generated by a 30 TW laser pulse, for the first time.[1]
- Electron wake

References

- Longair, Malcolm S., "Galaxy Formation", 1998.

[1] Fastest waves ever photographed (http://www.eurekalert.org/pub_releases/2006-10/aps-fwe_1102706.php)